

Electronic Thesis and Dissertation Repository

7-28-2016 12:00 AM

Structural Analysis of TPR Ligand Complexes of STIP1 Implicated in Alzheimer's Disease

Andrzej Maciejewski
The University of Western Ontario

Supervisor
Choy, Wing-Yiu
The University of Western Ontario Joint Supervisor
Prado, Marco
The University of Western Ontario

Graduate Program in Biochemistry
A thesis submitted in partial fulfillment of the requirements for the degree in Doctor of Philosophy
© Andrzej Maciejewski 2016

Follow this and additional works at: <https://ir.lib.uwo.ca/etd>

 Part of the [Biochemistry Commons](#)

Recommended Citation

Maciejewski, Andrzej, "Structural Analysis of TPR Ligand Complexes of STIP1 Implicated in Alzheimer's Disease" (2016). *Electronic Thesis and Dissertation Repository*. 3998.
<https://ir.lib.uwo.ca/etd/3998>

This Dissertation/Thesis is brought to you for free and open access by Scholarship@Western. It has been accepted for inclusion in Electronic Thesis and Dissertation Repository by an authorized administrator of Scholarship@Western. For more information, please contact wlsadmin@uwo.ca.

Abstract

Amyloid-beta oligomers (A β O) induce neurological dysfunction in part through the cellular prion protein (PrP^C) resulting in deregulation of Ca²⁺ homeostasis in Alzheimer's disease (AD). Stress inducible phosphoprotein 1 (STIP1), a cochaperone of Hsp70 and Hsp90, protects neurons from A β O-induced cell death. As well, STIP1 interacts with the Ca²⁺ sensor S100A1, which is an important biomarker upregulated in AD and regulates STIP1 and other cochaperone association with Hsp70 and Hsp90. While the molecular details of STIP1-Hsp complexes are well studied, little information is available concerning alternate STIP1 binding partners. Here, we investigated the structural details of STIP1 binding to PrP^C and S100A1.

We showed that residues located in a short region of PrP (90-110) mediate A β O binding and refined the main interaction to residues 91-100. We identified that STIP1 binds to PrP through multiple domains (DP1, TPR1 and TPR2A) and that the interactions with TPR1 and TPR2A effectively block A β O binding to PrP^C and cell death. The DP1 domain interacted with the flexible N-terminal (residues 23-95), while TPR1 and TPR2A interacts with the C-terminal (residues 90-231) of PrP. NMR spectroscopy revealed that the TPR domains interact with PrP competitively through distinct regions, with the TPR2A binding site overlapping with Hsp90. Our data suggest PrP, STIP1 and Hsp90 may form a ternary complex, which may influence A β O toxicity in cells.

In contrast to PrP complex formation, S100A1 binding to STIP1 is Ca²⁺ dependent and mediated through the TPR (TPR1, TPR2A and TPR2B) domains of STIP1. Each TPR binds asymmetrically to a single S100A1 dimer resulting in a

stoichiometry of three S100A1 dimers binding a single STIP1 molecule. S100A1 bound each TPR through a common interface spanning α -helix IV; however, with different binding affinities. Our findings provide novel structural insights regarding STIP1 complexes with PrP^C and S100A1.

Keywords

Alzheimer's disease, neurotoxicity, cochaperone, neuronal cell death, S100A1, stress-inducible phosphoprotein 1, prion protein, nuclear magnetic resonance spectroscopy, neurodegeneration, amyloid- β

Co-Authorship Statement

Chapter 2: Structural characterization of STIP1 domains

The enclosed chapter contains excerpts from the published work of Maciejewski, A., Prado, M. A. and Choy, W. Y. (2012) (1)H, (1)(5)N and (1)(3)C backbone resonance assignments of the TPR1 and TPR2A domains of mouse STIP1. *Biomol NMR Assign.* **7**, 305-310. Maciejewski, A. performed the experiments and data analysis. Maciejewski, A., Prado, M. A. and Choy, W. Y. wrote and revised the manuscript.

Chapter 3: Domains of STIP1 responsible for regulating the PrP^C-dependent amyloid- β oligomer toxicity

The following work is from the published manuscript Maciejewski, A., Ostapchenko, V. G., Beraldo, F. H., Prado, V. F., Prado, M. A. and Choy, W. Y. (2016) Domains of STIP1 responsible for regulating the PrPC-dependent amyloid-beta oligomer toxicity. *Biochem J.* **473**, 2119-2130.

Maciejewski, A. performed the experiments and analyzed the data. Maciejewski, A., Ostapchenko, V.G., Beraldo, F. H., Prado, V.F., Prado, M. A. and Choy, W. Y. assisted in experimental design and discussion of results. Maciejewski, A., Prado, M. A. and Choy, W. Y. wrote the manuscript.

Chapter 4: Structural details of STIP1 complex with S100A1

This chapter contains unpublished work from a manuscript in preparation. Maciejewski, A. performed the experiments and data analysis. Maciejewski, A., Prado, M. A. and Choy, W. Y. helped revise the enclosed chapter.

Dedication

To my family

Acknowledgments

Thank you to my supervisors Dr. James Wing-Yiu Choy and Dr Marco Antonio Maximo Prado for their continued support and insightful comments and suggestions throughout the years. Your expertise in your diverse and respective fields provided a broad range of ways to approach a problem and expanded the scope of this thesis.

I would like to thank my advisory committee Dr. David Litchfield and Dr. Lars Konermann for their helpful suggestions and discussions regarding the following work.

Thank you to all past and present members of the Choy and Prado laboratories for your assistance and making the work environment an enjoyable one. I would like to extend my sincerest thanks to Anne Brickenden for her assistance through her extensive knowledge in laboratory techniques. As well, as for her continued support during numerous experimental setbacks and difficult times.

Table of Contents

Abstract.....	i
Co-Authorship Statement.....	iii
Dedication.....	iv
Acknowledgments.....	v
List of Tables.....	x
List of Figures.....	xi
List of Abbreviations.....	xiii
1 Introduction.....	1
1.1 Protein aggregation and neurological disorders.....	1
1.2 Amyloid precursor protein (APP) processing.....	3
1.3 Amyloid- β oligomers and toxicity.....	5
1.4 Cellular prion protein (PrP ^C).....	8
1.5 Hsp70 and Hsp90 chaperones.....	15
1.6 Stress-inducible phosphoprotein 1 (STIP1).....	15
1.7 STIP1 as a signaling molecule.....	21
1.8 S100A1.....	25
1.9 Scope of thesis.....	29
1.10References.....	31
2 Structural characterization of STIP1 domains.....	45
2.1 Introduction.....	45
2.2 Materials and Methods.....	48
2.2.1 Protein expression and purification.....	48
2.2.2 Circular dichroism (CD) Spectropolarimetry.....	49

2.2.3	Analytical Ultracentrifugation – Sedimentation Equilibrium and Gel Filtration Chromatography	49
2.2.4	Backbone amide NMR Resonance Assignments.....	50
2.2.5	HSP90 chemical shift mapping.....	51
2.3	Results.....	51
2.3.1	Structural analysis of STIP1	51
2.3.2	Assignment of structural domains of STIP1.....	54
2.3.3	Monomeric state of STIP1 and TPR2A.....	61
2.3.4	Stability of TPR1 and TPR2A	63
2.3.5	Hsp90 binding to TPR2A	66
2.4	Discussion	68
2.5	References	71
3	Domains of STIP1 responsible for regulating the PrP ^C -dependent amyloid- β oligomer toxicity.....	76
3.1	Introduction	76
3.2	Materials and methods	78
3.2.1	Protein expression and purification.....	78
3.2.2	NMR spectroscopy	80
3.2.3	Protein-protein binding assay	81
3.2.4	Surface plasmon resonance (SPR)	82
3.2.5	Primary neuronal culture	82
3.2.6	Cell death and viability assay	83
3.2.7	A β O binding to primary hippocampal neurons	83
3.3	Results.....	84
3.3.1	Mapping of A β O interface on PrP	84
3.3.2	Identification of STIP1 binding domains of PrP.....	87

3.3.3	TPR1 and TPR2A prevent A β O binding to PrP	90
3.3.4	TPR1 and TPR2A inhibit A β O binding and toxicity in neurons.....	92
3.3.5	Mapping of TPR1 and TPR2A interfaces mediating PrP binding.....	94
3.4	Discussion	98
3.5	References	104
4	Structural details of STIP1 complex with S100A1	110
4.1	Introduction	110
4.2	Materials and methods	112
4.2.1	Protein purification.....	112
4.2.2	Analytical ultracentrifugation – sedimentation equilibrium.....	114
4.2.3	Isothermal titration calorimetry (ITC).....	115
4.2.4	Nuclear magnetic resonance (NMR) spectroscopy.....	115
4.3	Results.....	116
4.3.1	Multiple S100A1 dimers bind to STIP1 with different affinities	116
4.3.2	STIP1 binds to three S100A1 dimers.....	121
4.3.3	S100A1 shares a common interface when binding each TPR domain....	123
4.4	Discussion	127
4.5	References	132
5	Summary	135
5.1	Structural characterization of STIP1 domains.....	136
5.2	Mapping of A β O interface on PrP	137
5.3	Domains of STIP1 participating in PrP binding.....	138
5.4	Domains of STIP1 that inhibit PrP-A β O toxicity	139
5.5	Regions of TPR1 and TPR2A involved in PrP binding.....	140
5.6	Molecular details of STIP1 interaction with S100A1.....	141

5.7 Future directions	143
5.8 Conclusions	144
5.9 References	146
Curriculum Vitae.....	151

List of Tables

Table 1. Thermodynamic parameters of TPR domains of STIP1 binding to S100A1... 119

List of Figures

Figure 1.1. Sequential cleavage of the amyloid precursor protein (APP).....	4
Figure 1.2. Structure of cellular prion protein (PrP ^C).....	11
Figure 1.3. Structural schematic of stress-inducible phosphoprotein 1 (STIP1).....	17
Figure 1.4. STIP1 signaling pathway through PrP ^C at the cellular membrane.	23
Figure 1.5. Ribbon diagram of apo-S100A1 (left) (PDB: 1K2H) and Ca ²⁺ -bound S100A1 (right) (PDB: 1ZFS).	27
Figure 2.1. ¹ H- ¹⁵ N HSQC of full-length STIP1 indicates NMR spectroscopy of full-length protein is unfeasible due to lack of backbone amide resonances.	53
Figure 2.2. (A) ¹ H- ¹⁵ N HSQC spectrum and backbone assignment of ¹⁵ N/ ¹³ C labeled TPR1 domain of STIP1.	56
Figure 2.3. (A) ¹ H- ¹⁵ N HSQC spectrum and backbone assignment of ¹⁵ N/ ¹³ C labeled TPR2A domain of STIP1.....	57
Figure 2.4. (A) ¹ H- ¹⁵ N HSQC spectrum and backbone assignment of ¹⁵ N/ ¹³ C labeled TPR2B domain of STIP1.....	58
Figure 2.5. (A) ¹ H- ¹⁵ N HSQC spectrum and backbone assignment of ¹⁵ N/ ¹³ C labeled DP2 domain of STIP1.	59
Figure 2.6. (A) ¹ H- ¹⁵ N HSQC spectrum and backbone assignment of ¹⁵ N/ ¹³ C labeled DP1 domain of STIP1.	60
Figure 2.7. TPR2A behaves as a monomer in solution.	62
Figure 2.8. TPR1 domain is predominately α -helical and demonstrates increased stability at neutral pH.....	64

Figure 2.9. TPR2A domain is predominately α -helical and demonstrates increased stability at neutral pH.	65
Figure 2.10. Chemical shift mapping of Hsp90 C-terminal peptide binding to TPR2A agrees with the solved crystal structure for the complex.....	67
Figure 3.1. NMR reveals A β O associate with PrP residues 90-110.	86
Figure 3.2. DP1, TPR1 and TPR2A associate with PrP.....	89
Figure 3.3. TPR1 and TPR2A, but not DP1, inhibit A β O binding to PrP(23-231) in vitro.	91
Figure 3.4. STIP1, TPR1 and TPR2A inhibit A β O binding and toxicity in primary mouse hippocampal neurons.....	93
Figure 3.5. NMR indicates distinct regions of TPR1 and TPR2A interact with PrP(23-231).....	95
Figure 3.6. Hsp90 inhibits STIP1 rescue of primary mouse hippocampal neurons against A β O induced cell death.	97
Figure 4.1. STIP1 binds multiple S100A1 dimers in a Ca ²⁺ -dependent manner.....	117
Figure 4.2. The TPR domains of STIP1 bind a single S100A1 dimer with various affinities.	120
Figure 4.3. A single STIP1 molecule binds three S100A1 dimers simultaneously.....	122
Figure 4.4. TPR domains of STIP1 share a common binding interface on S100A1.	124
Figure 4.5. Graphical representations of chemical shift changes observed in ¹ H- ¹⁵ N spectra of ¹⁵ N-labelled (A)TPR1, (B) TPR2A or (C) TPR2B in the presence of S100A1.	126

List of Abbreviations

4E-BP - eIF4E-binding proteins

$\alpha 7$ nAChR - $\alpha 7$ nicotinic acetylcholine receptor

A β - amyloid beta

A β O - amyloid beta oligomers

AD – Alzheimer's disease

ADDL - amyloid beta derived diffusible ligand

Ala - alanine

ALS - amyotrophic lateral sclerosis

APP – amyloid precursor protein

Asn - asparagine

Asp - aspartate

ATP - adenosine triphosphate

AUC - Analytical ultracentrifugation

BACE1- beta secretase 1

BSA - bovine serum albumin

BSE - bovine spongiform encephalopathy

Ca²⁺ - calcium

CD - circular dichroism

CDK5-p25 - cyclin dependant kinase 5-p25

CHIP - C terminus of HSC70-Interacting Protein

CJD - Creutzfeldt-Jakob disease

CK2 - casein kinase 2

CNS - central nervous system

CWD - chronic wasting disease

Cyp40 - cyclophilin 40

DSS - dimethyl-2-sila-pentane-5-sulfonic acid

DTT - dithiothreitol

eEF2 - eukaryotic translation elongation factor 2

EGFR - epidermal growth factor receptor

EOAD – early onset Alzheimer’s disease

ERK1/2 - Extracellular signal-regulated kinase 1/2

FFI - fatal familial insomnia

FKBP52 - FK506-binding protein

GA - geldanamycin

Gly - glycine

GPI - glycoposphatidylinositol

GSK3 β - glycogen synthase kinase 3 beta

GSS - Gertzmann-Straussler-Scheinker syndrome

His - histidine

HOP - hsp organizing protein

HRP -horse radish peroxidase

HSC - hematopoietic stem cells

HSF-1 heat shock factor 1

Hsp - heat shock protein

Hsp40 - heat shock protein 40

Hsp70 - heat shock protein 70

Hsp90 - heat shock protein 90

HSQC - heteronuclear single quantum coherence

IPTG - isopropyl β -D-1-thiogalactopyranoside

ITC - isothermal titration calorimetry

LB - Luria broth

Leu - leucine

LOAD – late onset Alzheimer’s disease

LTD - long term depression

LTP - long term potentiation

Lys- lysine

MEM - Minimum Essential Media

mGluR5 - metabotropic glutamate receptor 5

NFT – neurofibrillary tangles

NLS- nuclear localization signal

NMDA - N-methyl-D-aspartate

NMR - nuclear magnetic resonance

OPD - o-phenylenediamine

OR - octapeptide region

PIAS1- protein inhibitor of activated STAT 1

PP5 - protein phosphatase 5

PrP^C - cellular prion protein

PrP^{Sc} - scrapie prion protein

PS1 - presenilin 1

PS2 - presenilin 2

RAGE - receptor for advanced glycation products

RAGE- receptor for advanced glycation endproducts

RNAi -ribonucleic acid interference

RU -resonance units

SDS-PAGE - sodium dodecyl sulfate polyacrylamide gel electrophoresis

SPR -surface plasmon resonance

SSP - secondary structure propensity

STIP1 - stress inducible phosphoprotein 1

TEV- tobacco etch virus

Thr - threonine

TPR - tetratricopeptide repeat

Trp - tryptophan

Val - valine

1 Introduction

1.1 Protein aggregation and neurological disorders

Protein aggregation into amorphous bodies is a common mechanism shared by most neurodegenerative diseases. Proteins that coalesce into abnormal intracellular or extracellular fibrils and inclusion bodies within specific brain regions generally characterize disease pathology [1]. Huntington's disease, prion diseases, amyotrophic lateral sclerosis (ALS), Parkinson's and Alzheimer's disease (AD) all involve formation of abnormally folded proteins that accumulate as insoluble aggregates extracellularly or in the cytoplasm.

Alzheimer's disease is predominately a late-onset neurodegenerative disorder and the most prevalent form of dementia. The disease typically is diagnosed in patients 65 and older and results in a progressive loss of memory and executive function, confusion, agitation and behavioral abnormalities. AD afflicts approximately 24 million people worldwide and the rate of incidence is expected to increase exponentially with an aging population [2, 3]. Alzheimer's disease cases are segregated into 2 subtypes based on age of onset. Early-onset AD (EOAD) patients range from 30-65 years and form the minority of cases (1-6%), while late-onset AD (LOAD) cases are characterized in individuals 65 years old and over [3]. AD is a multi-factorial disorder with multiple genetic and environmental factors affecting disease predisposition.

The neuropathology of AD is defined by the accumulation of two insoluble filaments; intraneuronal neurofibrillary tangles (NFT) and extracellular amyloid plaques [4, 5].

NFTs are composed of the hyperphosphorylated microtubule associated protein tau while amyloid plaques are the result of accumulation and self-aggregation of the amyloid-beta ($A\beta$) peptide into larger macromolecular assemblies. Tau and $A\beta$ act separately and interdependently to promote synaptic dysfunction and neuronal cell death [6].

The functional link between $A\beta$ and tau was first described in *in vivo* mouse models of tau and $A\beta$ deposition. Injection of preformed $A\beta$ fibrils into P301L mutant tau transgenic mice, which develop a non-Alzheimer's tauopathy, frontotemporal dementia with parkinsonism linked to chromosome 17, resulted in a five-fold increase in NFT accumulation at the site of injection [7]. Additionally, crosses of τ_{P301L} mice with the familial EOAD causative mutation (K670N/M671L) in the amyloid precursor protein (APP) resulted in accelerated tau deposition with no change in plaque burden compared to either parental mouse line alone [8]. These studies suggest $A\beta$ can exacerbate NFT formation without affecting amyloid deposition.

Numerous protein kinases have been implicated to functionally connect $A\beta$ to tau hyperphosphorylation at the molecular level. GSK3 β , ERK1/2 and Cdk5-p25 have been described to phosphorylate tau at Ser/Thr-Pro sites and are stimulated by $A\beta$ treatment [9-12]. Interestingly, recent studies suggest the non-receptor tyrosine kinase, Fyn, hyperphosphorylates tau in response to activation by $A\beta$ oligomer ($A\beta O$) through molecular complexes that include the cellular prion protein (PrP^C), metabotropic glutamate 5 (mGluR5) and N-methyl-D-aspartate (NMDA) receptors [12-15]. Thus, current models postulate $A\beta$ accumulation upstream of tau hyperphosphorylation in AD.

1.2 Amyloid precursor protein (APP) processing

The amyloid precursor protein (APP) is a single-pass transmembrane protein with a large ectodomain. Eight isoforms are generated by alternative splicing though the 695 amino acid isoform is predominately expressed in the central nervous system (CNS) [16]. The major proteolytic APP pathway involves sequential cleavage of APP by α and γ secretase complexes generating non-amyloidogenic fragments sAPP α and intracellular fragment that are associated with synaptic plasticity and neuronal protection (Figure 1.1) [17, 18]. Alternatively, sequential proteolytic processing by the β and γ secretases results in a heterogeneous population of peptide variants (A β 43, A β 42, A β 40, A β 38 and A β 37) with various propensities to self-associate into larger amyloidogenic species [19, 20]. The predominant peptide products are A β 40 and A β 42, with the former being the major species in the normal state. In AD the ratio of A β 42: A β 40 increases with A β 42 becoming the main proteolytic product [21]. A β 42 possesses enhanced amyloidogenic properties and the shift towards A β 42 production is characteristic of AD. Thus, AD results increased APP processing by the amyloidogenic pathway and failure to clear the resultant toxic fragments [22].

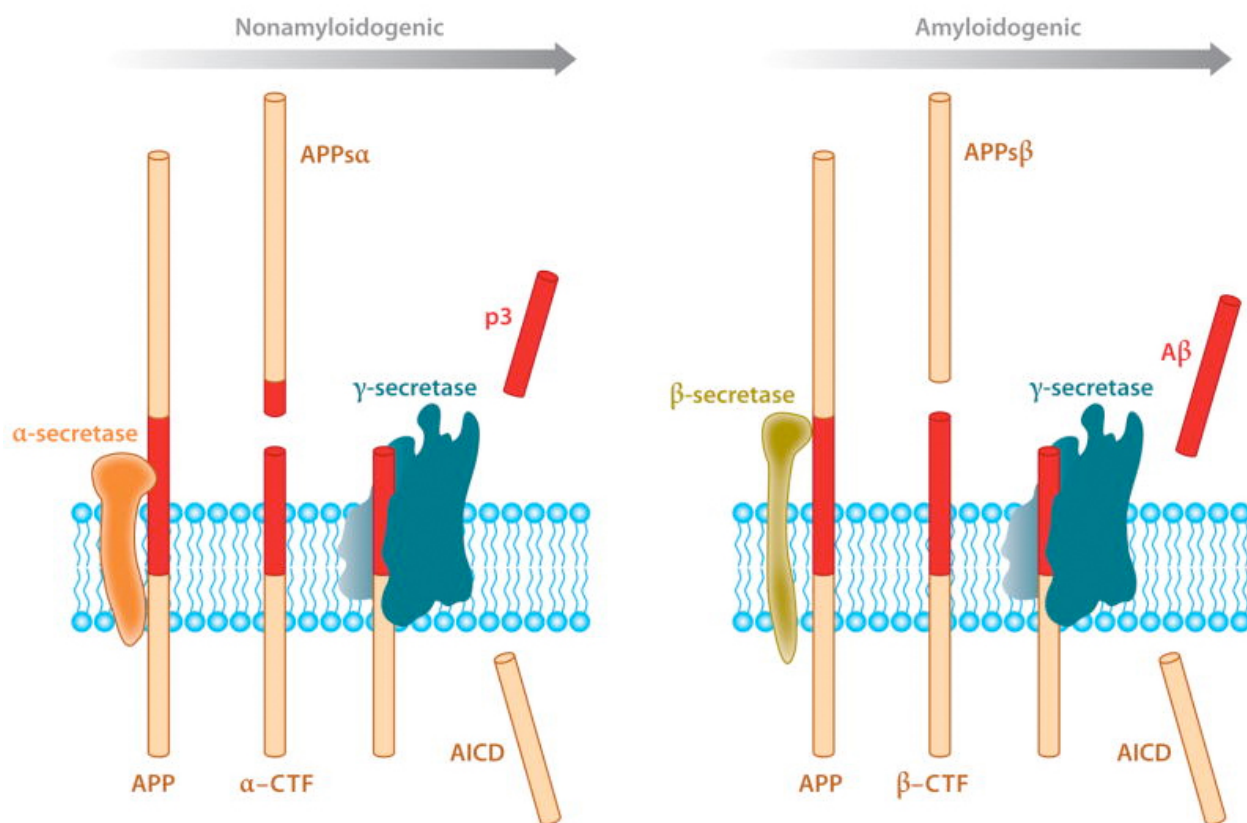


Figure 1.1. Sequential cleavage of the amyloid precursor protein (APP).

APP is processed by two mechanisms. In the non-amyloidogenic pathway, APP is initially cleaved by α -secretase followed by γ -secretase resulting in production of a soluble ectodomain (APPs α) and an intracellular fragment. Amyloidogenic processing involves sequential cleavage by β -secretase followed by γ -secretase resulting in the formation of A β peptide and a soluble APPs β fragment. Both processes generate intracellular C-terminal fragments (AICD). This figure was adapted from [22].

In the amyloidogenic pathway, the transmembrane aspartic protease BACE1 functions as the β -secretase, initially cleaving the ectodomain of APP generating a membrane anchored β - C-terminal fragment (β -CTF) (Figure 1.1). The γ -secretase is a multiprotein complex composed of presenilin 1 (PS1) or presenilin 2 (PS2), nicastrin (Nct), Aph-1 and Pen-2, which plays a functional role in the proteolytic processing of transmembrane proteins [22]. Mutations in PS1, PS2 and APP have been linked as causative mutations of autosomal dominant familial AD [3]. The γ -secretase cleaves the intramembranous fragment at one of several locations in the intramembrane helix generating the various length $A\beta$ peptides. $A\beta_{40}$ and $A\beta_{42}$ are the most commonly generated, with the latter increased in EOAD associated mutations. $A\beta_{42}$ has been classically viewed as the more toxic species and demonstrates a greater propensity for self-association into oligomers, protofibrils, fibrils and ultimately, the characteristic amyloid plaques seen in AD.

1.3 Amyloid- β oligomers and toxicity

While amyloid plaques are a hallmark of AD neuropathology, studies have been unable to demonstrate a relationship between amyloid plaque load and neuronal death, synaptotoxicity or disease severity [23]. Neuronal death is observed in regions far removed from plaques and cases have been reported of non-demented individuals with high plaque burden [24-26]. These studies suggest an alternative species is primarily responsible for synaptic dysfunction in AD. The identification of small diffusible $A\beta$ oligomers ($A\beta O$) provides a rationale for these discrepancies. $A\beta O$ are prefibrillar intermediates which are potent neurotoxins [27]. Robust correlations are observed

between soluble A β O concentrations and disease severity, thus the field considers soluble A β O as the predominant neurotoxin in AD [28, 29].

A β polymerization follows a complex and multifaceted pathway generating a range of buffer-soluble oligomers (i.e. dimers, trimers, tetramers, dodecamers and high molecular weight oligomers) during fibril formation [20]. Atomic force and electron microscopies revealed them to be 10-15 nm spherical shaped structures [30]. A β O are potent neurotoxins thought to trigger synaptic dysfunction, neuronal cell death and dementia [30]. The current paradigm in AD suggests these soluble oligomeric species are the primary pathological unit and not the amyloid plaques, which characterize the disease.

Toxicity is thought to depend on size and aggregation state; however, due to the diverse oligomeric and structural heterogeneity of A β O, the toxic species and their relative potency is poorly defined [20]. The diversity of synthetic and natural A β O has complicated the interpretation and reproducibility of studies [31]. SDS-stable dimers and trimers are secreted in culture and are found in human diseased brain extracts, which inhibit long-term potentiation (LTP) [32]. LTP is an electrophysiological mechanism underlying learning and memory formation and is compromised in AD. Larger species (nonamers and dodecamers) have also been observed to correlate with memory deficits in an APP transgenic mouse model [33]. As well, larger assemblies over 100 kDa have been found in AD brain suggesting a diverse range of sizes of A β O are associated with disease [34].

Synthetic preparations of A β O_s have been employed to elucidate disease mechanisms *in vitro* and in an attempt to better standardize A β O preparations [35]. Synthetic A β O, also referred to as A β -derived diffusible ligands (ADDLs) mimic A β O induced deficiencies including robust binding to neurons, inhibition of LTP, synaptotoxicity and neuronal cell death [27]. Antibodies generated against synthetic ADDLs derived oligomers cross-reacted with AD brain tissue, demonstrating synthetic ADDL conformations are generated *in vivo* and are relevant in studies of AD [36].

Multiple molecular mechanisms have been implicated to contribute to A β O toxicity. A β O association with the plasma membrane results in increased intracellular calcium concentrations and excitotoxicity in neurons [37]. A β O have been found to compromise the integrity of the plasma cell membrane, disrupting intracellular calcium homeostasis [38, 39]. A β O_s insert themselves into lipid bilayers leading to pore formation or lipid bilayer defects resulting in ion deregulation [40]. Rapid increases in intracellular Ca²⁺ promote further deficits, such as increases in radical formation and oxidative stress [41]. Elevation of intracellular Ca²⁺ concentrations by compromising its cellular membrane integrity may contribute to the potent neurotoxicity of A β O_s and neurodegeneration in AD.

Alternatively, binding of A β O_s to the cell surface through endogenous cellular receptors may result in aberrant signaling, synaptic dysfunction and neuronal cell death. Indeed, a number of amyloid-protein interactions have been described between native neuronal receptors or co-receptors/scaffold proteins resulting in detrimental effects [42]. These include α 7 nicotinic acetylcholine receptor (α 7nAChR), receptor for advance

glycation end products (RAGE), ephrin type B receptor 2 and paired immunoglobulin – like receptor B [43]. Receptors in glutamatergic transmission have garnered tremendous interest in A β O toxicity. Glutamate is a portent neurotransmitter essential in memory formation and synaptic plasticity [44]. In particular, the N-methyl-D-aspartate (NMDA) receptor and metabotropic glutamate receptors (mGluR) have been demonstrated to be susceptible to deregulation by A β O resulting in Ca²⁺ influx and synaptotoxicity [45, 46]. A β O were shown to depolarize neurons, disrupt glutamatergic transmission, inhibit LTP, promote LTD and excitotoxicity [47, 48].

A β O have been demonstrated to activate NMDA receptors through the NR2B subunit and inhibit LTP [49]. Interestingly, the cellular prion protein (PrP^C) has been identified as a coreceptor for NMDA, mGluR5 receptors and A β Os [12, 13]. A β O binding to PrP^C induces NMDA and mGluR5 activation resulting in Fyn kinase activation, thus potentially coupling A β O toxicity to hyperphosphorylation of tau protein in AD [12, 13].

1.4 Cellular prion protein (PrP^C)

The cellular prion protein (PrP^C) is the pathological unit of several progressive and fatal neurodegenerative diseases termed prion diseases. These include Creutzfeldt-Jakob disease (CJD), kuru, fatal familial insomnia (FFI) and Gertzmann-Straussler-Scheinker syndrome (GSS) in humans, scrapie in goats and sheep, chronic wasting disease (CWD) in deer and elk and bovine spongiform encephalopathy (BSE) in cattle [50]. Conversion of the normal PrP^C to an alternate β -sheet and protease resistant conformer (PrP^{Sc}) is thought to be behind the etiology of prion diseases [51, 52]. PrP^{Sc} conversion can occur sporadically or be promoted by mutations within the PrP^C gene [53]. PrP^{Sc} particles are

transmissible, promoting conversion of endogenous PrP^C to the pathogenic conformer and initiating progressive neurodegeneration in the host.

PrP^C knockout mice are resistant to prion infection while, for the most part, maintaining normal neurological function [54, 55]. Subtle neurological phenotypes have been identified including slight deficiencies in synaptic transmission, LTP, circadian rhythms, spatial learning and increased susceptibility to seizures [56-58]. As well, lower levels of anxiety and increases in locomotor activity have been observed in particular backgrounds of PrP-null mice [59]. Ablation of PrP^C was also noted to result in a chronic demyelinating polyneuropathy [60].

PrP^C is a carboxy-terminal glycosylphosphatidylinositol (GPI) anchored protein located on the outer leaflet of the cellular plasma membrane (Figure 1.2) [61]. A 22 amino acid N-terminal signaling peptide targets the nascent protein to the lumen of the endoplasmic reticulum, where the signaling peptide is cleaved and the protein undergoes post-translational modification [62]. The mature protein is trafficked to the cellular membrane through the Golgi apparatus and undergoes endocytosis and cycling from the cell membrane and intracellular compartment. Pulse-chase experiments indicate the half-life of PrP^C is about 1.5-2 hrs, demonstrating the protein undergoes rapid recycling [63]. Internalization of PrP^C is dependant on the N-terminal region of PrP^C and the initial basic cluster 'KKRPK' [64, 65].

Mature PrP^C contains flexible disordered N-terminal spanning residues 23-124 and a structurally conserved globular C-terminal (Figure 1.2) [66, 67]. The disordered N-terminal encodes two regions of high conservation termed the octapeptide region (OR)

and a region rich in hydrophobic amino acid content spanning 22-90 and 111-134, respectively. The OR encodes four to five octameric repeats possessing a high affinity for divalent transition metals (Cu^{2+} , Ni^{2+} , Zn^{2+} and Mn^{2+}) [68].

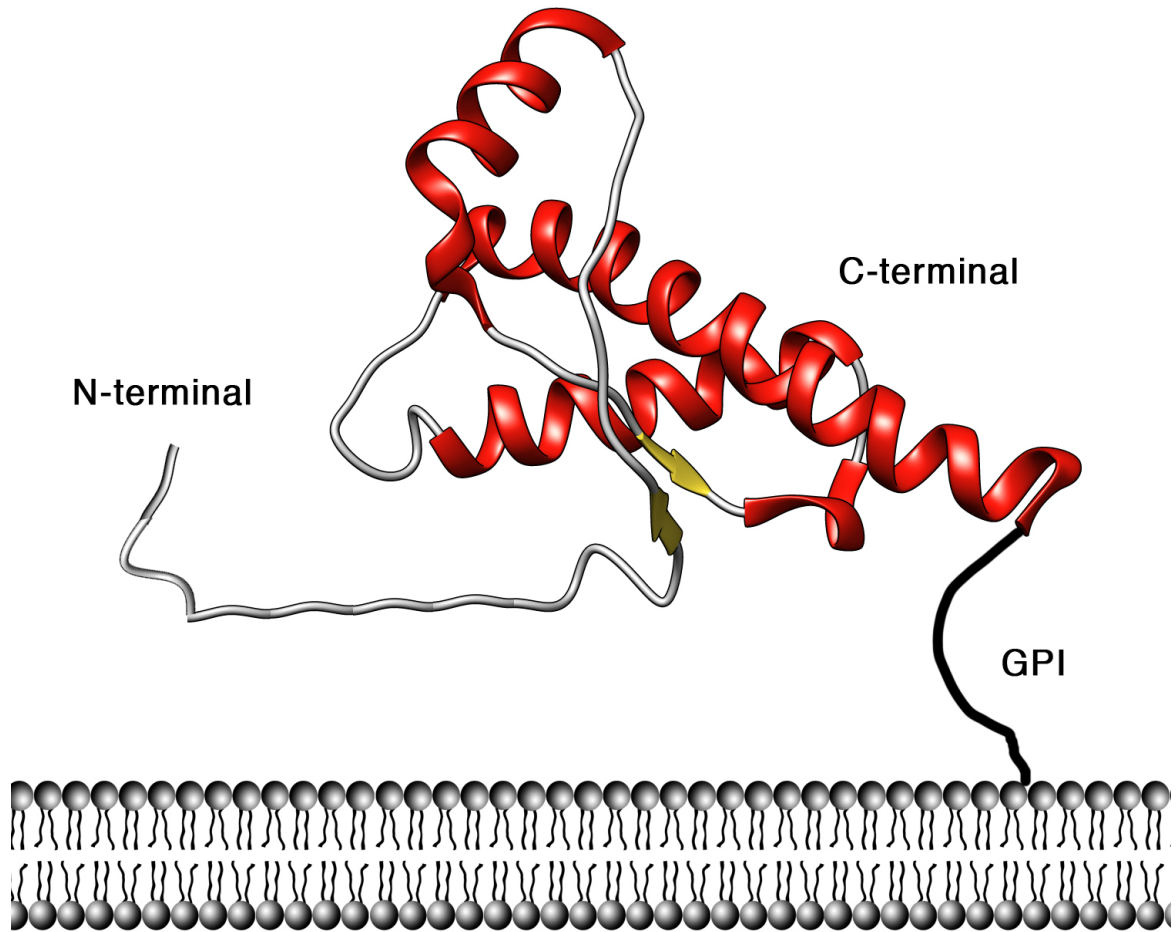


Figure 1.2. Structure of cellular prion protein (PrP^C).

PrP^C is composed of a disordered N-terminal and a C-terminal globular domain rich in α -helical content. The protein is tethered to the extracellular face of the plasma membrane by glycosphosphatidylinositol (GPI) anchor. (PDB: 1AG2) [66].

The globular C-terminal presents a highly α -helical fold composed of three helices (residues 145-151, 173-188 and 200-229) and a short β -sheet formed by residues 128-131 and 161-164 [66, 67]. A single disulfide bond connects α -helices 2 and 3, significantly contributing to PrP^C stability [69]. PrP^C is subject to glycosylation at N181 and N197 positions in human PrP^C (N180 and N196 in mouse) and has been isolated in the unglycosylated, mono- or di-glycosylated forms [70]. Different glycosylation states have been reported to be differentially distributed through the central nervous system and other tissues [71-73]. High-resolution structural studies by solution nuclear magnetic resonance (NMR) spectroscopy and X-ray crystallography have revealed a high degree of inter-species structural homology [67, 74, 75].

The prion protein is ubiquitously expressed in adult tissues and highly enriched within cholesterol-rich lipid rafts of neuronal postsynaptic membranes in the central nervous system (CNS) [76]. As well, high expression has been noted in elements of the immune system, hematopoietic stem cells (HSCs), blood and lymphoid organs [77].

PrP^C is a scaffold protein that modulates cellular signaling at the cellular membrane through protein-protein interactions with various cellular ligands [76]. These include a diverse set of ligands including laminin, heparin sulfate, casein kinase 2 (CK2) and 14-3-3 [78-81]. Protein-protein interactions have been mapped throughout the extent of the protein; however, large numbers of PrP^C binding partners interact through the disordered N-terminal region, presumably due to its increased accessibility on the plasma membrane compared to its C-terminal GPI-anchored globular domain.

PrP^C has been identified as a high affinity receptor for soluble A β O, in an unbiased screen of a cDNA library expressed in COS-7 cells [82]. PrP^C associates with A β O with sub-nanomolar affinity through residues 23-27 and 95-110 of the N-terminal of PrP^C [82-84]. Immuno-staining of neuronal cultures following A β O results in characteristic punctate staining on the neuronal surface [82]. A β O staining can be significantly reduced by pretreatment with anti-PrP^C antibodies or RNA silencing of PrP^C; however these strategies do not eliminate A β O binding suggesting A β O retains the capacity to bind neuronal cells through alternate mechanisms such as other identified binding partners [82, 85].

Association of PrP^C or the disordered N-terminal containing these binding sites inhibited the oligomerization and fibrillization of A β O *in vitro* [86, 87]. Alternatively, PrP^C disassembled mature fibrils into smaller A β O species, potentially stimulating formation of neurotoxic species [88]. Thus, binding of A β O to PrP^C may influence the kinetics of A β oligomerization and the toxicity of the generated A β species; however, the implications of these observation on neurotoxicity are currently unknown.

PrP^C is required for cell death *in vitro*, epileptiform discharges, synapse loss, serotonin axon degeneration and cognitive and memory deficits associated with A β O [82, 89-91]. Association of A β O or AD brain extracts resulted in the inhibition of LTP in CA1 hippocampal slices in a PrP^C dependent manner [82].

PrP^C directly interacts with mGluR5 [92, 93]. Synthetic A β O or A β O isolated from AD disease brain resulted in PrP^C-dependent activation of Fyn kinase [12]. A β O-PrP^C engagement resulted in increased intracellular Ca²⁺ levels, eEF2 phosphorylation,

reduction in global transcription, and dendritic spine loss. PrP^C- A β O complex formation also disrupts NMDA receptor activity resulting in a biphasic transient increase in Ca²⁺ and NMDA receptor surface expression [13].

Initially, binding of A β O to PrP^C resulted in Fyn activation, NR2B subunit phosphorylation, and increased NMDA receptor trafficking to the cell surface. This increase is coupled to increased intracellular Ca²⁺ resulting in excitotoxicity followed by dendritic spine loss. Following 60 minutes of A β O treatment, NMDA receptor surface expression is reduced, desensitizing neuronal cells and resulting in the attenuation of the Ca²⁺ currents.

The cytotoxic stresses induced by PrP^C- A β O complexes have made the interaction an appealing target for therapeutic intervention. Disruption of A β O-PrP^C complexes using monoclonal antibodies directed against the PrP^C-A β O binding site (residues 95-110) or α -helix 1 demonstrated the greatest efficacy, either by directly blocking the binding site or occluding it by steric hindrance [82, 84, 94]. This inhibition translated to inhibition of A β O-induced deficits. Thus, modulation of PrP^C- A β O complex may be of therapeutic value in AD. Interestingly, the PrP^C ligand, stress-inducible phosphoprotein 1 (STIP1) inhibits A β O binding and toxicity implicating the pathway as an endogenous protective mechanism against A β toxicity [95].

1.5 Hsp70 and Hsp90 chaperones

Proper protein folding in the cell is facilitated through a large and diverse class of chaperones termed heat shock proteins (Hsp). Hsp90 is one of the best conserved Hsps and accounts for 1-2% of total protein in the cell [96]. Hsp90 activity is regulated through interactions with a large network of cochaperones to fold a wide range of client proteins that include a number of oncogenic protein kinases and steroid receptors. Initially, client proteins are recruited by Hsp40 and Hsp70 and are transferred to Hsp90 by stress-inducible phosphoprotein 1 (STIP1) [97]. Finally, an additional co-chaperone p23 is recruited and ATP hydrolysis results in structural rearrangements in Hsp90 that promote client maturation and dissociation of the complex [97]. Recent studies suggest Hsp90 has an important role in neurodegeneration. Hsp90 stabilizes toxic aggregates such as A β and phosphorylated tau [98]. Pharmacological inhibition of Hsp90 results in Hsp70 and Hsp40 upregulation, which is thought to channel aberrant folded species for degradation [98].

1.6 Stress-inducible phosphoprotein 1 (STIP1)

Stress-inducible phosphoprotein 1 (STIP1) is a cellular cochaperone that coordinates Hsp70 and Hsp90 activity during client protein folding [99, 100]. STIP1 expression is upregulated during cellular stress in yeast [101]. STIP1 is a modular protein composed of three tetratricopeptide repeat domains (TPR1, TPR2A and TPR2B) and two domains rich in aspartate and proline residues (DP1 and DP2) (Figure 1.3). Tetratricopeptide repeat domains are composed of repeating units of 34 amino acid degenerate sequences that form two anti-parallel α -helices joined by a short flexible linker [102]. Multiple TPR

motifs are arranged in tandem forming an amphipathic groove, which serves as the binding site for protein-protein interactions [103].

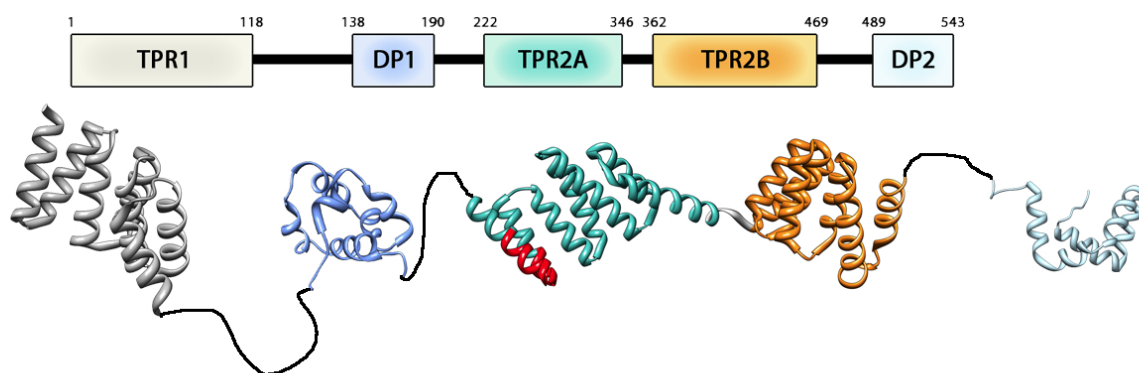


Figure 1.3. Structural schematic of stress-inducible phosphoprotein 1 (STIP1). Individual domain boundaries are highlighted with their corresponding structures depicted below: TPR1 (PDB: 1ELW), DP1 (residues 1138-190 (2LLV), TPR2A-TPR2B (PDB: 3UQ3) and DP2 (PDB: 2LLW) [103, 104].

The TPR domains of STIP1 bind Hsp70 and Hsp90 to facilitate client protein folding. The amphipathic groove of each TPR domain binds the C-terminal 'EEVD' motifs of Hsp70 and Hsp90, anchoring them to the protein [103]. Specificity is achieved through amino acid contacts directly N-terminal of the 'EEVD' motifs of each Hsp. This interaction is predominately mediated through conserved electrostatic interactions forming a two-carboxylate clamp with the Asp residue in each Hsp70 and Hsp90 peptide. While the C-terminal Hsp interactions are critical for TPR and Hsp90 binding, additional contacts are made with the middle domain of Hsp90 [104, 105].

Binding of Hsp90 by STIP1 results in non-competitive inhibition of its ATPase activity through interaction with TPR2A-TPR2B fragment and stabilizes an open conformation in Hsp90; however, the human homologue appears to be an approximately 10-fold less potent inhibitor [106, 107]. Hsp engagement is facilitated through sequential interactions with the individual TPR domains of STIP1 [108]. The function of the DP domains (DP1 and DP2) is less clear. Currently, no protein ligands have been identified for the DP domains of STIP1. Recently, the solution NMR structures of the yeast DP1 and DP2 domains were solved revealing a novel α -helical protein fold encoding six and five α -helices, respectively [104]. DP1 contains an additional α -helix that is believed to stabilize the arrangement of secondary structural elements and occupies a slightly positive groove. This groove is accessible in DP2 and may serve as a potential binding site for as of yet unidentified ligands. The minimal fragment of STIP1 that supports client activation is composed of TPR2A-TPR2B-DP2 C-terminal of STIP1 [104, 109]. As well, the *C. elegans* STIP1 homologue only encodes this fragment which suggest the TPR1-DP1 module may be dispensable for client activation *in vivo* [110].

Interestingly, constructs lacking the DP2 domain did not support glucocorticoid receptor activation in yeast cells [104]. X-ray crystallographic structures of the TPR2A-TPR2B domain revealed the linker between these domains is quite rigid. This results in the TPR domains adopting an S-shaped form with their hydrophobic clefts responsible for binding the C-terminal Hsp residues oriented in opposite directions [104].

Complementary NMR spectroscopy experiments revealed additional inter-domain contacts are formed between the C-terminal helix of TPR2B, the linker connecting TPR2B to the DP2 domain and α -helices 1 and 2 of the DP2 domain. These additional contacts form a rigid C-terminus composed of TPR2A-TPR2B-DP2. These results indicate DP2 contributes to the quaternary structure of STIP1 and rationalizes its importance in STIP1 function.

STIP1 possesses two Hsp70 binding sites located in TPR1 and TPR2B; however, it binds to Hsp70 in a 1:1 stoichiometry [103, 108]. The current model for STIP1 function in Hsp70 and Hsp90 coordination speculates that in the absence of Hsp90, the TPR2B domain represents the high-affinity binding site for Hsp70. Hsp90 binding induces a more 'open' conformation between TPR1-DP1 fragment and the functional C-terminal TPR2A-TPR2B-DP2 domains. Hsp90 binding to TPR2A reduces accessibility of Hsp70 binding to TPR2B, thus the TPR1 domain becomes the predominant binding site for Hsp70 in the ternary complex [108]. Binding of Hsp90 has been observed to affect the dynamics of STIP1, reorienting the TPR1-DP1 module into close proximity to TPR2B, presumably facilitating transfer of Hsp70. Thus, the length of the linker bridging TPR1-DP1 to TPR2A-TPR2B-DP2 impacts STIP1 function in client refolding. Deletion of the linker results in decreased formation of ternary complexes of STIP1-Hsp70-Hsp90 and

decreased protein client activation *in vivo* [108]. Interestingly, this linker is approximately 30 residues shorter in higher order eukaryotes. Thus, differences in dynamics of STIP1-Hsp70-Hsp90 ternary complexes may exist in higher order eukaryotes affecting client protein activation [108].

STIP1 is subject to posttranslational modification, which regulates its cochaperone activity [109]. Five different phosphorylation sites have been identified in human STIP1 homologue corresponding to S16, S189, T198, Y354 and S481. Phosphomimetic mutations resulted in decreased glucocorticoid receptor activation *in vivo* and Hsp70 binding affinities indicating phosphorylation regulates STIP1's co-chaperone function [109]. Interestingly, Y354E phosphomimetic variant located in the loop joining TPR2A-TPR2B, appeared to disrupt the rigid linker joining the two domains and promotes a more dynamic flexibility and leads to a loss of function [109]. Additionally, STIP1 is subject to SUMOylation by PIAS1 whose binding results in its nuclear accumulation [111].

Hsp70 and Hsp90 overexpression is a common phenotype of human cancers and correlates with a poor prognosis [112]. Pharmacological inhibition of the Hsp machinery has become a popular target in cancer treatment [113]. Recent studies have explored inhibition of STIP1 cochaperone function as an alternate strategy in destabilizing Hsp90 oncogenic ligand folding [114, 115]. Studies have demonstrated that STIP1 promotes proliferation and migration in glioblastoma and pancreatic cancer cell lines [116, 117]. Down-regulation of STIP1 by RNAi resulted in decreased pancreatic cell line invasiveness and down-regulation of numerous oncogenic Hsp90 client proteins [116].

Inhibition of Hsp90 interaction with the TPR2A domain of STIP1 using a novel hybrid TPR peptide has demonstrated selective cancer-cell cytotoxicity [118].

Selective inhibition of the Hsp machinery has also garnered interest in neurodegenerative diseases owing to their roles in regulating proper protein folding. Inhibition of Hsp90 results in upregulation of Hsp70 and Hsp40 through transcriptional activation of the transcription factor heat-shock factor 1 (HSF-1). Hsp40 and Hsp70 overexpression are thought to promote protein disaggregation and degradation [119]. Hsp90 is believed to stabilize aberrantly folded proteins, thus inhibition of the chaperone and co-chaperone activity at particular nodes may be of therapeutic value in protein aggregation disorders [120].

1.7 STIP1 as a signaling molecule

In addition to STIP1's well-documented role as an Hsp cochaperone, STIP1 also functions as a neurotrophic and neuroprotective signaling molecule through PrP^C [121-124]. STIP1 is actively secreted by a non-canonical pathway through extracellular vesicles (EVs) [125]. Upon cellular stress, such as irradiation or ischemia, astrocyte STIP1 secretion is enhanced promoting cell survival through PrP^C-dependent pathways [121, 122]. The hydrophobic core of PrP^C (residues 113-128) has been determined to engage in complex formation with the TPR2A (residues 230-245) of STIP1. Complex formation promotes perturbation of PrP α -helix (143-153) of the globular C-terminal of PrP^C and compaction of STIP1 structure in PrP^C-STIP1 complex [126]. These structural remodeling events may recruit additional protein interactions and is consistent with PrP^C function as a scaffold protein-modulating cell signaling events.

PrP^C- STIP1 engagement results in an increase in intracellular Ca²⁺ concentration through the α 7 nicotinic acetylcholine receptor (α 7nAChR) (Figure 1.4) [127]. Signaling induces neuroprotection and neuroproliferative signaling through PKA and ERK1/2 pathways, with the latter requiring internalization of PrP^C [128]. α 7nAChR expression is altered in AD models and the receptor itself has been identified as an A β O receptor [129]. Inhibitors against A β O binding to α 7nAChR show beneficial effects in AD models, suggesting modulation of this pathway may play an important role in AD [130].

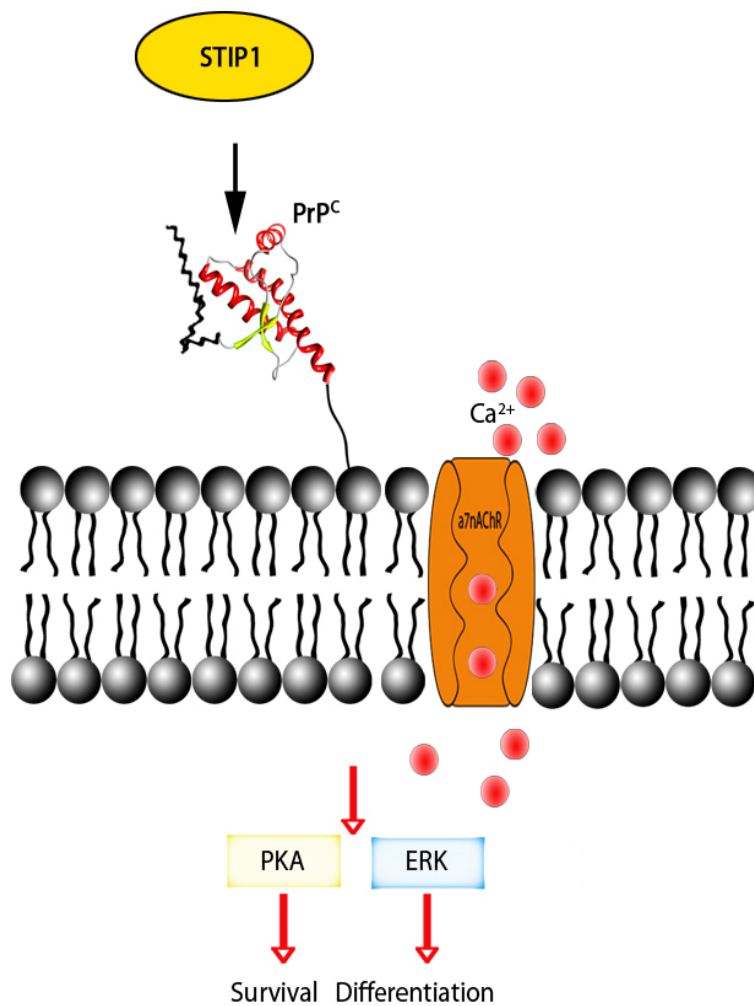


Figure 1.4. STIP1 signaling pathway through PrP^C at the cellular membrane. STIP1 binding to the N-terminal flexible tail of PrP^C results in intracellular Ca²⁺ influx from the outside environment through the α7nAChR. The resulting cascade leads to PKA and ERK activation, which promote cell survival and differentiation, respectively.

In addition, STIP1 signaling through PrP^C enhances neuronal protein synthesis through PI3K-Akt-mTOR activation and phosphorylation of eIF4E-binding proteins (4E-BPs), which release eIF4E initiation factor, promoting translation initiation [131]. Regulation of protein synthesis by extracellular signaling molecules is involved in critical pathways in neuronal development and synaptic plasticity in the nervous system [132]. Stimulation of neuronal protein synthesis is corrupted by scrapie prion (PrP^{Sc}) infection, thus loss-of function of this pathway may contribute to the neurodegeneration seen in prion diseases [131].

Deletion of STIP1 in mouse models is embryonic lethal by E 10.5 and embryos presented malformed neural tube and limb buds due to increased levels of apoptotic cell death [122]. Maternal extraembryonic STIP1 protein, possibly transferred, from placental disruption is sufficient for initial blastocyst (E 3.5) implantation and survival; however, is not present in E10.5 embryos. Embryonic fibroblasts from STIP1 deficient embryos present increased DNA damage marker γ -H2AX [122]. Enhanced cellular stress induces STIP1 translocation and accumulation of STIP1 in the nucleus [133]. Nuclear localization is regulated by phosphorylation at S189 and T198 located in the linker joining TPR1-DP1 to the C-terminal of STIP1 and adjacent to the functional NLS (residues 222-239) [134]. As well, interaction of STIP1 with the E3 SUMO ligase PIAS1 results in STIP1 accumulation after genotoxic stress following irradiation [111]. Thus, STIP1 nuclear accumulation is influenced by cellular stress and by protein posttranslational modifications and ligand interactions.

A growing body of evidence has revealed alternate functions of STIP1 unrelated to its regulation of Hsp70/Hsp90 activity. Importantly, extracellular STIP1 is a potent

neuroprotective signaling molecule through PrP^C [95, 124, 127, 128]. STIP1 can directly inhibit A β O binding to PrP^C *in vitro* by physically occluding the A β O site and neuroprotective signal transmission through α 7nAChR, which translated to rescue of A β O induced toxicity [95]. A thorough molecular understanding of the PrP^C-STIP1 interaction may provide insight into cellular mechanisms involved in the early stages of disease and potential therapeutic strategies in AD.

1.8 S100A1

Disruption of calcium homeostasis is implicated in numerous and diverse human diseases including heart disease and several neurological disorders [135]. Calcium signaling mechanisms are tissue and cell specific, temporarily regulated and undergoing continuous remodeling. Diverse signaling cascades promote mobilization of intracellular or extracellular stores through numerous Ca²⁺ channels, pumps and exchangers [136]. Deregulation of calcium signaling resulting in disruption of membrane conductance has long been associated with AD pathology, preceding deposition of A β plaque deposition and inflammation that define AD pathology [137-139]. Intracellular A β O have been demonstrated to induce Ca²⁺ flux by directly permeabilizing the membrane or through activation receptor signaling complexes and Ca²⁺ channels [39, 49, 140]. Fluctuations in Ca²⁺ influence synaptic plasticity and processes such LTP and long term depression (LTD) and thus A β O can disrupt learning and memory in AD.

Ca²⁺ also functions as an important cofactor in a large set of calcium sensor proteins, modifying protein-protein interactions and influencing downstream events. The S100 – family of proteins is a well-studied family of calcium sensor proteins encompassing

approximately 20 member proteins [141]. S100-family function as modulators in calcium signaling. Expression of these proteins is cell type and tissue specific and their differential expression has been implicated in a diverse range of diseases, including psoriasis, rheumatoid arthritis, cardiomyopathy, multiple sclerosis, Down's Syndrome, Alzheimer's disease and several forms of cancer [142-145]. Thus, many S100 proteins serve as diagnostic biomarkers in disease.

S100 proteins are homo or hetero dimeric proteins of the EF-hand superfamily. Each subunit is composed of two helix-loop-helix EF-hand motifs (residues 19-32 and 62-73 in S100A1), which coordinate four calcium ions [146-148] (Figure 1.5). In the apo-state α -helices III lie nearly perpendicular to α -helices IV, burying a large hydrophobic pocket that serves as the binding site for many S100 ligands [148]. Upon calcium binding, α -helix III of each subunit undergoes a large conformational reorientation of approximately 100° exposing the hydrophobic face of α -helices IV, which along with residues of α -helices III and the interconnecting hinge region, serve as the predominant ligand binding site in Ca^{2+} dependant protein-protein interactions (Figure 1.5) [149].

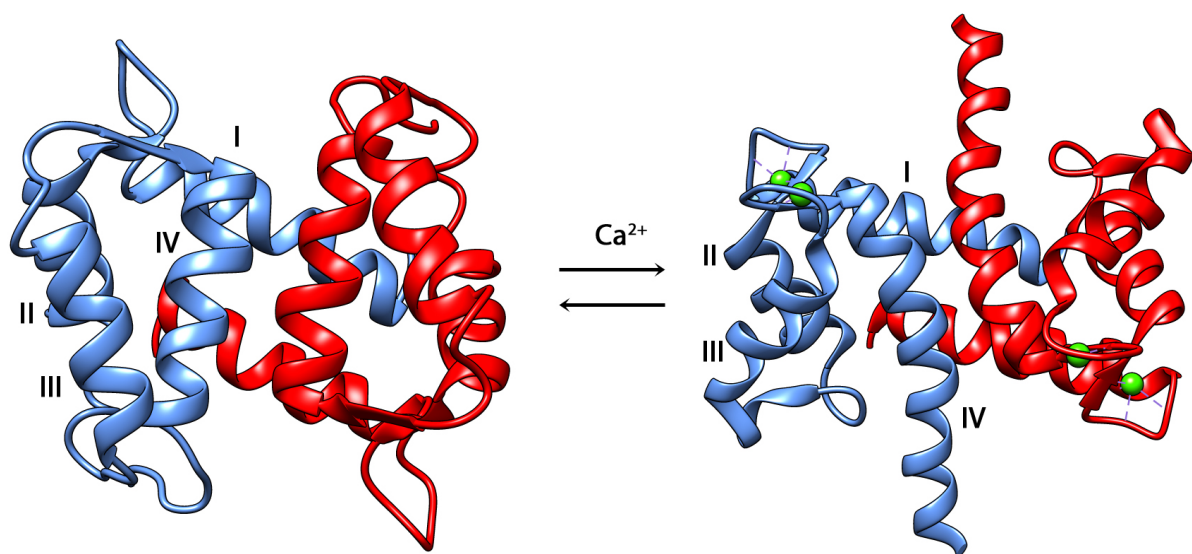


Figure 1.5. Ribbon diagram of apo-S100A1 (left) (PDB: 1K2H) and Ca²⁺-bound S100A1 (right) (PDB: 1ZFS).

Ca²⁺ induces a conformational change, which reorients α -helices III of each protomer exposes a hydrophobic region in α -helices IV. The α -helices of a single protomer are labeled [146].

S100A1 was one of the first family members discovered and originally isolated from bovine brain tissue [150]. The protein is abundantly expressed in heart, skeletal muscle and brain tissues [151]. S100A1 expression has been implicated in multiple and diverse human diseases including specific types of cancer, heart failure and neurological diseases, importantly AD. S100A1 is found in the hippocampus, cerebral cortex and amygdala [152]. The protein is found both in intracellular compartments as well as in the extracellular space where it interacts with several cell surface receptors [151, 153]. S100A1 has been found to regulate APP processing, tau phosphorylation and A β oligomer induced neuronal cell death. Knockout of S100A1 in AD mouse models resulted in decreased hippocampal inflammation, and decreased A β amyloid plaque burden [144, 154]. As well, numerous S100A1 ligands have been implicated in AD such as the receptor for advanced glycation end products (RAGE) and ryanodine receptors [154] [155].

Recent studies have implicated S100A1's role in the regulation of co-chaperone interactions with Hsp70/Hsp90 chaperone machinery [156]. These co-chaperones include protein phosphatase 5 (PP5), FK506-binding protein (FKBP52), cyclophilin 40 (Cyp40) and STIP1 [156] [157]. S100A1 inhibited their association through binding each ligand's respective TPR domains, which are commonly used by co-chaperones to interface with the conserved C-terminal 'EEVD' motifs found in Hsp70 and Hsp90. Therefore, S100A1 may regulate Hsp activity during client protein refolding through regulation of co-chaperone complexes.

1.9 Scope of thesis

STIP1 is a multifaceted protein molecule that functions as a cellular cochaperone, regulating Hsp70 and Hsp90 activity and client maturation. STIP1 binding to S100A1 protein has been suggested to influence its interactions with Hsps. Additionally, extracellular STIP1 acts as a potent neuroprotective and neurotrophic signaling molecule through PrP^C. Therefore, molecular understanding of STIP1 ligand interactions has implications in numerous cellular diseases including cancer and neurodegeneration.

In order to ascertain the structural details of STIP1 ligand complexes, extensive NMR characterization of STIP1 was undertaken. ¹H-¹⁵N HSQC spectra revealed the protein was too large to acquire adequate information on STIP1 complexes, thus the individual TPR (TPR1, TPR2A and TPR2B) and DP (DP1 and DP2) domains were cloned and studied individually (chapter 2). NMR backbone assignments were completed and confirmed to agree with the currently available literature. These NMR assignments provide the foundation for the study of STIP1-ligand complexes. As well, the impact of a wide range of conditions on the stability of the previously identified ligand binding domains of STIP1, the TPR domains, was assessed.

The modular structure of STIP1 and structural similarity of the TPR domains lead us to explore the potential of alternate binding sites of PrP^C than previously reported. We discovered that in addition to the TPR2A domain, the TPR1 and DP1 domains bound PrP. DP1 bound the flexible N-terminal of PrP^C, while the TPR domains bound competitively to PrP (90-231). In addition, the AβO binding site on PrP was refined to residues 90-110. The TPR1 and TPR2A domains could inhibit AβO to PrP^C *in vitro* and

in primary neuronal mouse cultures. Importantly, this inhibition translated to reduced neuronal cell death.

Finally, the molecular details of the recently identified and poorly understood STIP1-S100A1 complex was investigated. Both proteins are secreted and S100A1 is a marker for neuronal stress and injury [125, 142]. S100A1 may regulate STIP1 interactions in the extracellular and intracellular environment. The stoichiometry of binding was determined to be 3 S100A1 dimers per STIP1 molecule. Each TPR domain of STIP1 participated in binding to each S100A1 dimer; however, with significantly different binding affinities determined by isothermal titration calorimetry (ITC). NMR was used to define the binding interfaces for S100A1 and individual TPR domains. The binding interface for each TPR domain on S100A1 was determined to encompass a large hydrophobic groove spanning α -helix III of S100A1 and was shared amongst each TPR domain. These results suggested differences in binding were due to the amino acid composition of each TPR. Due to spectral broadening, the binding site on each TPR could not be identified with great confidence and alternate strategies for obtaining the S100A1 binding site on TPR domains are discussed.

The work presented in this thesis has advanced our understanding of molecular complexes of STIP1 involved in AD. The structural details of interaction between STIP1 and PrP were explored and novel regions were identified to mediate binding and inhibit A β O toxicity in neuronal cultures. As well, the molecular details of the poorly understood STIP1-S100A1 complex were defined. These results provide structural details and provide the foundation for future studies of STIP1 ligand complexes beyond the traditionally studied co-chaperone activity with Hsp proteins.

1.10 References

- 1 Ross, C. A. and Poirier, M. A. (2004) Protein aggregation and neurodegenerative disease. *Nat Med.* **10 Suppl**, S10-17
- 2 Ferri, C. P., Prince, M., Brayne, C., Brodaty, H., Fratiglioni, L., Ganguli, M., Hall, K., Hasegawa, K., Hendrie, H., Huang, Y., Jorm, A., Mathers, C., Menezes, P. R., Rimmer, E. and Sczufca, M. (2005) Global prevalence of dementia: a Delphi consensus study. *Lancet.* **366**, 2112-2117
- 3 Bekris, L. M., Yu, C. E., Bird, T. D. and Tsuang, D. W. (2010) Genetics of Alzheimer disease. *J Geriatr Psychiatry Neurol.* **23**, 213-227
- 4 Ramirez-Bermudez, J. (2012) Alzheimer's disease: critical notes on the history of a medical concept. *Arch Med Res.* **43**, 595-599
- 5 Mucke, L. and Selkoe, D. J. (2012) Neurotoxicity of amyloid beta-protein: synaptic and network dysfunction. *Cold Spring Harb Perspect Med.* **2**, a006338
- 6 Bloom, G. S. (2014) Amyloid-beta and tau: the trigger and bullet in Alzheimer disease pathogenesis. *JAMA Neurol.* **71**, 505-508
- 7 Gotz, J., Chen, F., van Dorpe, J. and Nitsch, R. M. (2001) Formation of neurofibrillary tangles in P3011 tau transgenic mice induced by A β 42 fibrils. *Science.* **293**, 1491-1495
- 8 Lewis, J., Dickson, D. W., Lin, W. L., Chisholm, L., Corral, A., Jones, G., Yen, S. H., Sahara, N., Skipper, L., Yager, D., Eckman, C., Hardy, J., Hutton, M. and McGowan, E. (2001) Enhanced neurofibrillary degeneration in transgenic mice expressing mutant tau and APP. *Science.* **293**, 1487-1491
- 9 Lloret, A., Badia, M. C., Giraldo, E., Ermak, G., Alonso, M. D., Pallardo, F. V., Davies, K. J. and Vina, J. (2011) Amyloid-beta toxicity and tau hyperphosphorylation are linked via RCAN1 in Alzheimer's disease. *J Alzheimers Dis.* **27**, 701-709
- 10 Engmann, O. and Giese, K. P. (2009) Crosstalk between Cdk5 and GSK3 β : Implications for Alzheimer's Disease. *Front Mol Neurosci.* **2**, 2
- 11 Song, M. S., Rauw, G., Baker, G. B. and Kar, S. (2008) Memantine protects rat cortical cultured neurons against beta-amyloid-induced toxicity by attenuating tau phosphorylation. *Eur J Neurosci.* **28**, 1989-2002
- 12 Um, J. W., Kaufman, A. C., Kostylev, M., Heiss, J. K., Stagi, M., Takahashi, H., Kerrisk, M. E., Vortmeyer, A., Wisniewski, T., Koleske, A. J., Gunther, E. C., Nygaard, H. B. and Strittmatter, S. M. (2013) Metabotropic glutamate receptor 5 is a coreceptor for Alzheimer abeta oligomer bound to cellular prion protein. *Neuron.* **79**, 887-902

- 13 Um, J. W., Nygaard, H. B., Heiss, J. K., Kostylev, M. A., Stagi, M., Vortmeyer, A., Wisniewski, T., Gunther, E. C. and Strittmatter, S. M. (2012) Alzheimer amyloid-beta oligomer bound to postsynaptic prion protein activates Fyn to impair neurons. *Nat Neurosci.* **15**, 1227-1235
- 14 Shankar, G. M., Bloodgood, B. L., Townsend, M., Walsh, D. M., Selkoe, D. J. and Sabatini, B. L. (2007) Natural oligomers of the Alzheimer amyloid-beta protein induce reversible synapse loss by modulating an NMDA-type glutamate receptor-dependent signaling pathway. *J Neurosci.* **27**, 2866-2875
- 15 Um, J. W. and Strittmatter, S. M. (2012) Amyloid-beta induced signaling by cellular prion protein and Fyn kinase in Alzheimer disease. *Prion.* **7**, 37-41
- 16 Bayer, T. A., Cappai, R., Masters, C. L., Beyreuther, K. and Multhaup, G. (1999) It all sticks together--the APP-related family of proteins and Alzheimer's disease. *Mol Psychiatry.* **4**, 524-528
- 17 Ehehalt, R., Keller, P., Haass, C., Thiele, C. and Simons, K. (2003) Amyloidogenic processing of the Alzheimer beta-amyloid precursor protein depends on lipid rafts. *J Cell Biol.* **160**, 113-123
- 18 Furukawa, K., Sopher, B. L., Rydel, R. E., Begley, J. G., Pham, D. G., Martin, G. M., Fox, M. and Mattson, M. P. (1996) Increased activity-regulating and neuroprotective efficacy of alpha-secretase-derived secreted amyloid precursor protein conferred by a C-terminal heparin-binding domain. *J Neurochem.* **67**, 1882-1896
- 19 De Strooper, B. (2010) Proteases and proteolysis in Alzheimer disease: a multifactorial view on the disease process. *Physiol Rev.* **90**, 465-494
- 20 Benilova, I., Karran, E. and De Strooper, B. (2012) The toxic Aβ oligomer and Alzheimer's disease: an emperor in need of clothes. *Nat Neurosci.* **15**, 349-357
- 21 Spies, P. E., Slats, D., Sjogren, J. M., Kremer, B. P., Verhey, F. R., Rikkert, M. G. and Verbeek, M. M. (2010) The cerebrospinal fluid amyloid beta_{42/40} ratio in the differentiation of Alzheimer's disease from non-Alzheimer's dementia. *Curr Alzheimer Res.* **7**, 470-476
- 22 O'Brien, R. J. and Wong, P. C. (2011) Amyloid precursor protein processing and Alzheimer's disease. *Annu Rev Neurosci.* **34**, 185-204
- 23 Perrin, R. J., Fagan, A. M. and Holtzman, D. M. (2009) Multimodal techniques for diagnosis and prognosis of Alzheimer's disease. *Nature.* **461**, 916-922
- 24 Crystal, H., Dickson, D., Fuld, P., Masur, D., Scott, R., Mehler, M., Masdeu, J., Kawas, C., Aronson, M. and Wolfson, L. (1988) Clinico-pathologic studies in dementia: nondemented subjects with pathologically confirmed Alzheimer's disease. *Neurology.* **38**, 1682-1687

- 25 Lue, L. F., Brachova, L., Civin, W. H. and Rogers, J. (1996) Inflammation, A beta deposition, and neurofibrillary tangle formation as correlates of Alzheimer's disease neurodegeneration. *J Neuropathol Exp Neurol.* **55**, 1083-1088
- 26 Erten-Lyons, D., Woltjer, R. L., Dodge, H., Nixon, R., Vorobik, R., Calvert, J. F., Leahy, M., Montine, T. and Kaye, J. (2009) Factors associated with resistance to dementia despite high Alzheimer disease pathology. *Neurology.* **72**, 354-360
- 27 Lambert, M. P., Barlow, A. K., Chromy, B. A., Edwards, C., Freed, R., Liosatos, M., Morgan, T. E., Rozovsky, I., Trommer, B., Viola, K. L., Wals, P., Zhang, C., Finch, C. E., Krafft, G. A. and Klein, W. L. (1998) Diffusible, nonfibrillar ligands derived from Abeta1-42 are potent central nervous system neurotoxins. *Proc Natl Acad Sci U S A.* **95**, 6448-6453
- 28 McLean, C. A., Cherny, R. A., Fraser, F. W., Fuller, S. J., Smith, M. J., Beyreuther, K., Bush, A. I. and Masters, C. L. (1999) Soluble pool of Abeta amyloid as a determinant of severity of neurodegeneration in Alzheimer's disease. *Ann Neurol.* **46**, 860-866
- 29 Mc Donald, J. M., Savva, G. M., Brayne, C., Welzel, A. T., Forster, G., Shankar, G. M., Selkoe, D. J., Ince, P. G. and Walsh, D. M. (2010) The presence of sodium dodecyl sulphate-stable Abeta dimers is strongly associated with Alzheimer-type dementia. *Brain.* **133**, 1328-1341
- 30 Noguchi, A., Matsumura, S., Dezawa, M., Tada, M., Yanazawa, M., Ito, A., Akioka, M., Kikuchi, S., Sato, M., Ideno, S., Noda, M., Fukunari, A., Muramatsu, S., Itokazu, Y., Sato, K., Takahashi, H., Teplow, D. B., Nabeshima, Y., Kakita, A., Imahori, K. and Hoshi, M. (2009) Isolation and characterization of patient-derived, toxic, high mass amyloid beta-protein (Abeta) assembly from Alzheimer disease brains. *J Biol Chem.* **284**, 32895-32905
- 31 Stine, W. B., Jr., Dahlgren, K. N., Krafft, G. A. and LaDu, M. J. (2003) In vitro characterization of conditions for amyloid-beta peptide oligomerization and fibrillogenesis. *J Biol Chem.* **278**, 11612-11622
- 32 Walsh, D. M., Tseng, B. P., Rydel, R. E., Podlisny, M. B. and Selkoe, D. J. (2000) The oligomerization of amyloid beta-protein begins intracellularly in cells derived from human brain. *Biochemistry.* **39**, 10831-10839
- 33 Lesne, S., Koh, M. T., Kotilinek, L., Kaye, R., Glabe, C. G., Yang, A., Gallagher, M. and Ashe, K. H. (2006) A specific amyloid-beta protein assembly in the brain impairs memory. *Nature.* **440**, 352-357
- 34 Kuo, Y. M., Emmerling, M. R., Vigo-Pelfrey, C., Kasunic, T. C., Kirkpatrick, J. B., Murdoch, G. H., Ball, M. J. and Roher, A. E. (1996) Water-soluble Abeta (N-40, N-42) oligomers in normal and Alzheimer disease brains. *J Biol Chem.* **271**, 4077-4081

- 35 Snyder, S. W., Lador, U. S., Wade, W. S., Wang, G. T., Barrett, L. W., Matayoshi, E. D., Huffaker, H. J., Krafft, G. A. and Holzman, T. F. (1994) Amyloid-beta aggregation: selective inhibition of aggregation in mixtures of amyloid with different chain lengths. *Biophys J.* **67**, 1216-1228
- 36 Lambert, M. P., Viola, K. L., Chromy, B. A., Chang, L., Morgan, T. E., Yu, J., Venton, D. L., Krafft, G. A., Finch, C. E. and Klein, W. L. (2001) Vaccination with soluble Abeta oligomers generates toxicity-neutralizing antibodies. *J Neurochem.* **79**, 595-605
- 37 Demuro, A., Mina, E., Kaye, R., Milton, S. C., Parker, I. and Glabe, C. G. (2005) Calcium dysregulation and membrane disruption as a ubiquitous neurotoxic mechanism of soluble amyloid oligomers. *J Biol Chem.* **280**, 17294-17300
- 38 Arispe, N., Pollard, H. B. and Rojas, E. (1993) Giant multilevel cation channels formed by Alzheimer disease amyloid beta-protein [A beta P-(1-40)] in bilayer membranes. *Proc Natl Acad Sci U S A.* **90**, 10573-10577
- 39 Arispe, N., Rojas, E. and Pollard, H. B. (1993) Alzheimer disease amyloid beta protein forms calcium channels in bilayer membranes: blockade by tromethamine and aluminum. *Proc Natl Acad Sci U S A.* **90**, 567-571
- 40 Di Scala, C., Chahinian, H., Yahi, N., Garmy, N. and Fantini, J. (2014) Interaction of Alzheimer's beta-amyloid peptides with cholesterol: mechanistic insights into amyloid pore formation. *Biochemistry.* **53**, 4489-4502
- 41 Yatin, S. M., Aksenova, M., Aksenov, M., Markesbery, W. R., Aulick, T. and Butterfield, D. A. (1998) Temporal relations among amyloid beta-peptide-induced free-radical oxidative stress, neuronal toxicity, and neuronal defensive responses. *J Mol Neurosci.* **11**, 183-197
- 42 Kaye, R. and Lasagna-Reeves, C. A. (2013) Molecular mechanisms of amyloid oligomers toxicity. *J Alzheimers Dis.* **33 Suppl 1**, S67-78
- 43 Kam, T. I., Gwon, Y. and Jung, Y. K. (2014) Amyloid beta receptors responsible for neurotoxicity and cellular defects in Alzheimer's disease. *Cell Mol Life Sci.* **71**, 4803-4813
- 44 Meldrum, B. S. (2000) Glutamate as a neurotransmitter in the brain: review of physiology and pathology. *J Nutr.* **130**, 1007S-1015S
- 45 Revett, T. J., Baker, G. B., Jhamandas, J. and Kar, S. (2013) Glutamate system, amyloid ss peptides and tau protein: functional interrelationships and relevance to Alzheimer disease pathology. *J Psychiatry Neurosci.* **38**, 6-23
- 46 Li, S., Hong, S., Shepardson, N. E., Walsh, D. M., Shankar, G. M. and Selkoe, D. (2009) Soluble oligomers of amyloid Beta protein facilitate hippocampal long-term depression by disrupting neuronal glutamate uptake. *Neuron.* **62**, 788-801

- 47 Harkany, T., Penke, B. and Luiten, P. G. (2000) beta-Amyloid excitotoxicity in rat magnocellular nucleus basalis. Effect of cortical deafferentation on cerebral blood flow regulation and implications for Alzheimer's disease. *Ann N Y Acad Sci.* **903**, 374-386
- 48 Renner, M., Lacor, P. N., Velasco, P. T., Xu, J., Contractor, A., Klein, W. L. and Triller, A. (2010) Deleterious effects of amyloid beta oligomers acting as an extracellular scaffold for mGluR5. *Neuron.* **66**, 739-754
- 49 Li, S., Jin, M., Koeglsperger, T., Shepardson, N. E., Shankar, G. M. and Selkoe, D. J. (2011) Soluble Abeta oligomers inhibit long-term potentiation through a mechanism involving excessive activation of extrasynaptic NR2B-containing NMDA receptors. *J Neurosci.* **31**, 6627-6638
- 50 Weissmann, C. (2004) The state of the prion. *Nat Rev Microbiol.* **2**, 861-871
- 51 Post, K., Pitschke, M., Schafer, O., Wille, H., Appel, T. R., Kirsch, D., Mehlhorn, I., Serban, H., Prusiner, S. B. and Riesner, D. (1998) Rapid acquisition of beta-sheet structure in the prion protein prior to multimer formation. *Biol Chem.* **379**, 1307-1317
- 52 Prusiner, S. B. (1991) Molecular biology of prion diseases. *Science.* **252**, 1515-1522
- 53 Prusiner, S. B. and Scott, M. R. (1997) Genetics of prions. *Annu Rev Genet.* **31**, 139-175
- 54 Bueler, H., Fischer, M., Lang, Y., Bluethmann, H., Lipp, H. P., DeArmond, S. J., Prusiner, S. B., Aguet, M. and Weissmann, C. (1992) Normal development and behaviour of mice lacking the neuronal cell-surface PrP protein. *Nature.* **356**, 577-582
- 55 Bueler, H., Aguzzi, A., Sailer, A., Greiner, R. A., Autenried, P., Aguet, M. and Weissmann, C. (1993) Mice devoid of PrP are resistant to scrapie. *Cell.* **73**, 1339-1347
- 56 Maglio, L. E., Martins, V. R., Izquierdo, I. and Ramirez, O. A. (2006) Role of cellular prion protein on LTP expression in aged mice. *Brain Res.* **1097**, 11-18
- 57 Tobler, I., Gaus, S. E., Deboer, T., Achermann, P., Fischer, M., Rulicke, T., Moser, M., Oesch, B., McBride, P. A. and Manson, J. C. (1996) Altered circadian activity rhythms and sleep in mice devoid of prion protein. *Nature.* **380**, 639-642
- 58 Criado, J. R., Sanchez-Alavez, M., Conti, B., Giacchino, J. L., Wills, D. N., Henriksen, S. J., Race, R., Manson, J. C., Chesebro, B. and Oldstone, M. B. (2005) Mice devoid of prion protein have cognitive deficits that are rescued by reconstitution of PrP in neurons. *Neurobiol Dis.* **19**, 255-265
- 59 Roesler, R., Walz, R., Quevedo, J., de-Paris, F., Zanata, S. M., Graner, E., Izquierdo, I., Martins, V. R. and Brentani, R. R. (1999) Normal inhibitory avoidance

learning and anxiety, but increased locomotor activity in mice devoid of PrP(C). *Brain Res Mol Brain Res.* **71**, 349-353

60 Bremer, J., Baumann, F., Tiberi, C., Wessig, C., Fischer, H., Schwarz, P., Steele, A. D., Toyka, K. V., Nave, K. A., Weis, J. and Aguzzi, A. (2010) Axonal prion protein is required for peripheral myelin maintenance. *Nat Neurosci.* **13**, 310-318

61 Stahl, N., Borchelt, D. R., Hsiao, K. and Prusiner, S. B. (1987) Scrapie prion protein contains a phosphatidylinositol glycolipid. *Cell.* **51**, 229-240

62 Hegde, R. S., Mastrianni, J. A., Scott, M. R., DeFea, K. A., Tremblay, P., Torchia, M., DeArmond, S. J., Prusiner, S. B. and Lingappa, V. R. (1998) A transmembrane form of the prion protein in neurodegenerative disease. *Science.* **279**, 827-834

63 Parizek, P., Roeckl, C., Weber, J., Flechsig, E., Aguzzi, A. and Raeber, A. J. (2001) Similar turnover and shedding of the cellular prion protein in primary lymphoid and neuronal cells. *J Biol Chem.* **276**, 44627-44632

64 Lee, K. S., Magalhaes, A. C., Zanata, S. M., Brentani, R. R., Martins, V. R. and Prado, M. A. (2001) Internalization of mammalian fluorescent cellular prion protein and N-terminal deletion mutants in living cells. *J Neurochem.* **79**, 79-87

65 Shyng, S. L., Moulder, K. L., Lesko, A. and Harris, D. A. (1995) The N-terminal domain of a glycolipid-anchored prion protein is essential for its endocytosis via clathrin-coated pits. *J Biol Chem.* **270**, 14793-14800

66 Riek, R., Hornemann, S., Wider, G., Billeter, M., Glockshuber, R. and Wuthrich, K. (1996) NMR structure of the mouse prion protein domain PrP(121-231). *Nature.* **382**, 180-182

67 Riek, R., Hornemann, S., Wider, G., Glockshuber, R. and Wuthrich, K. (1997) NMR characterization of the full-length recombinant murine prion protein, mPrP(23-231). *FEBS Lett.* **413**, 282-288

68 Choi, C. J., Kanthasamy, A., Anantharam, V. and Kanthasamy, A. G. (2006) Interaction of metals with prion protein: possible role of divalent cations in the pathogenesis of prion diseases. *Neurotoxicology.* **27**, 777-787

69 Maiti, N. R. and Surewicz, W. K. (2001) The role of disulfide bridge in the folding and stability of the recombinant human prion protein. *J Biol Chem.* **276**, 2427-2431

70 Endo, T., Groth, D., Prusiner, S. B. and Kobata, A. (1989) Diversity of oligosaccharide structures linked to asparagines of the scrapie prion protein. *Biochemistry.* **28**, 8380-8388

71 Cancellotti, E., Wiseman, F., Tuzi, N. L., Baybutt, H., Monaghan, P., Aitchison, L., Simpson, J. and Manson, J. C. (2005) Altered glycosylated PrP proteins can have

different neuronal trafficking in brain but do not acquire scrapie-like properties. *J Biol Chem.* **280**, 42909-42918

72 Beringue, V., Mallinson, G., Kaisar, M., Tayebi, M., Sattar, Z., Jackson, G., Anstee, D., Collinge, J. and Hawke, S. (2003) Regional heterogeneity of cellular prion protein isoforms in the mouse brain. *Brain.* **126**, 2065-2073

73 Li, R., Liu, D., Zanusso, G., Liu, T., Fayen, J. D., Huang, J. H., Petersen, R. B., Gambetti, P. and Sy, M. S. (2001) The expression and potential function of cellular prion protein in human lymphocytes. *Cell Immunol.* **207**, 49-58

74 Baral, P. K., Swayampakula, M., Aguzzi, A. and James, M. N. (2015) X-ray structural and molecular dynamical studies of the globular domains of cow, deer, elk and Syrian hamster prion proteins. *J Struct Biol.* **192**, 37-47

75 Biljan, I., Giachin, G., Ilc, G., Zhukov, I., Plavec, J. and Legname, G. (2012) Structural basis for the protective effect of the human prion protein carrying the dominant-negative E219K polymorphism. *Biochem J.* **446**, 243-251

76 Linden, R., Martins, V. R., Prado, M. A., Cammarota, M., Izquierdo, I. and Brentani, R. R. (2008) Physiology of the prion protein. *Physiol Rev.* **88**, 673-728

77 Isaacs, J. D., Jackson, G. S. and Altmann, D. M. (2006) The role of the cellular prion protein in the immune system. *Clin Exp Immunol.* **146**, 1-8

78 Coitinho, A. S., Freitas, A. R., Lopes, M. H., Hajj, G. N., Roesler, R., Walz, R., Rossato, J. I., Cammarota, M., Izquierdo, I., Martins, V. R. and Brentani, R. R. (2006) The interaction between prion protein and laminin modulates memory consolidation. *Eur J Neurosci.* **24**, 3255-3264

79 Horonchik, L., Tzaban, S., Ben-Zaken, O., Yedidia, Y., Rouvinski, A., Papy-Garcia, D., Barritault, D., Vlodayky, I. and Taraboulos, A. (2005) Heparan sulfate is a cellular receptor for purified infectious prions. *J Biol Chem.* **280**, 17062-17067

80 Meggio, F., Negro, A., Sarno, S., Ruzzene, M., Bertoli, A., Sorgato, M. C. and Pinna, L. A. (2000) Bovine prion protein as a modulator of protein kinase CK2. *Biochem J.* **352 Pt 1**, 191-196

81 Satoh, J., Onoue, H., Arima, K. and Yamamura, T. (2005) The 14-3-3 protein forms a molecular complex with heat shock protein Hsp60 and cellular prion protein. *J Neuropathol Exp Neurol.* **64**, 858-868

82 Lauren, J., Gimbel, D. A., Nygaard, H. B., Gilbert, J. W. and Strittmatter, S. M. (2009) Cellular prion protein mediates impairment of synaptic plasticity by amyloid-beta oligomers. *Nature.* **457**, 1128-1132

- 83 Chen, S., Yadav, S. P. and Surewicz, W. K. (2010) Interaction between human prion protein and amyloid-beta (A β) oligomers: role OF N-terminal residues. *J Biol Chem.* **285**, 26377-26383
- 84 Freir, D. B., Nicoll, A. J., Klyubin, I., Panico, S., Mc Donald, J. M., Risse, E., Asante, E. A., Farrow, M. A., Sessions, R. B., Saibil, H. R., Clarke, A. R., Rowan, M. J., Walsh, D. M. and Collinge, J. (2011) Interaction between prion protein and toxic amyloid beta assemblies can be therapeutically targeted at multiple sites. *Nat Commun.* **2**, 336
- 85 Rushworth, J. V., Griffiths, H. H., Watt, N. T. and Hooper, N. M. (2013) Prion protein-mediated toxicity of amyloid-beta oligomers requires lipid rafts and the transmembrane LRP1. *J Biol Chem.* **288**, 8935-8951
- 86 Younan, N. D., Sarell, C. J., Davies, P., Brown, D. R. and Viles, J. H. (2013) The cellular prion protein traps Alzheimer's A β in an oligomeric form and disassembles amyloid fibers. *FASEB J.* **27**, 1847-1858
- 87 Nieznanski, K., Choi, J. K., Chen, S., Surewicz, K. and Surewicz, W. K. (2012) Soluble prion protein inhibits amyloid-beta (A β) fibrillization and toxicity. *J Biol Chem.* **287**, 33104-33108
- 88 Younan, N. D., Sarell, C. J., Davies, P., Brown, D. R. and Viles, J. H. The cellular prion protein traps Alzheimer's A β in an oligomeric form and disassembles amyloid fibers. *FASEB J.* **27**, 1847-1858
- 89 Gimbel, D. A., Nygaard, H. B., Coffey, E. E., Gunther, E. C., Lauren, J., Gimbel, Z. A. and Strittmatter, S. M. (2010) Memory impairment in transgenic Alzheimer mice requires cellular prion protein. *J Neurosci.* **30**, 6367-6374
- 90 Bate, C. and Williams, A. (2011) Amyloid-beta-induced synapse damage is mediated via cross-linkage of cellular prion proteins. *J Biol Chem.* **286**, 37955-37963
- 91 Kudo, W., Lee, H. P., Zou, W. Q., Wang, X., Perry, G., Zhu, X., Smith, M. A., Petersen, R. B. and Lee, H. G. (2012) Cellular prion protein is essential for oligomeric amyloid-beta-induced neuronal cell death. *Hum Mol Genet.* **21**, 1138-1144
- 92 Haas, L. T., Kostylev, M. A. and Strittmatter, S. M. (2014) Therapeutic molecules and endogenous ligands regulate the interaction between brain cellular prion protein (PrPC) and metabotropic glutamate receptor 5 (mGluR5). *J Biol Chem.* **289**, 28460-28477
- 93 Beraldo, F. H., Arantes, C. P., Santos, T. G., Machado, C. F., Roffe, M., Hajj, G. N., Lee, K. S., Magalhaes, A. C., Caetano, F. A., Mancini, G. L., Lopes, M. H., Americo, T. A., Magdesian, M. H., Ferguson, S. S., Linden, R., Prado, M. A. and Martins, V. R. (2010) Metabotropic glutamate receptors transduce signals for neurite outgrowth after binding of the prion protein to laminin gamma1 chain. *FASEB J.* **25**, 265-279

- 94 Barry, A. E., Klyubin, I., Mc Donald, J. M., Mably, A. J., Farrell, M. A., Scott, M., Walsh, D. M. and Rowan, M. J. (2011) Alzheimer's disease brain-derived amyloid-beta-mediated inhibition of LTP in vivo is prevented by immunotargeting cellular prion protein. *J Neurosci.* **31**, 7259-7263
- 95 Ostapchenko, V. G., Beraldo, F. H., Mohammad, A. H., Xie, Y. F., Hirata, P. H., Magalhaes, A. C., Lamour, G., Li, H., Maciejewski, A., Belrose, J. C., Teixeira, B. L., Fahnestock, M., Ferreira, S. T., Cashman, N. R., Hajj, G. N., Jackson, M. F., Choy, W. Y., MacDonald, J. F., Martins, V. R., Prado, V. F. and Prado, M. A. (2013) The prion protein ligand, stress-inducible phosphoprotein 1, regulates amyloid-beta oligomer toxicity. *J Neurosci.* **33**, 16552-16564
- 96 Borkovich, K. A., Farrelly, F. W., Finkelstein, D. B., Taulien, J. and Lindquist, S. (1989) hsp82 is an essential protein that is required in higher concentrations for growth of cells at higher temperatures. *Mol Cell Biol.* **9**, 3919-3930
- 97 Taipale, M., Jarosz, D. F. and Lindquist, S. (2010) HSP90 at the hub of protein homeostasis: emerging mechanistic insights. *Nat Rev Mol Cell Biol.* **11**, 515-528
- 98 Luo, W., Rodina, A. and Chiosis, G. (2008) Heat shock protein 90: translation from cancer to Alzheimer's disease treatment? *BMC Neurosci.* **9 Suppl 2**, S7
- 99 Chen, S. and Smith, D. F. (1998) Hop as an adaptor in the heat shock protein 70 (Hsp70) and hsp90 chaperone machinery. *J Biol Chem.* **273**, 35194-35200
- 100 Johnson, B. D., Schumacher, R. J., Ross, E. D. and Toft, D. O. (1998) Hop modulates Hsp70/Hsp90 interactions in protein folding. *J Biol Chem.* **273**, 3679-3686
- 101 Nicolet, C. M. and Craig, E. A. (1989) Isolation and characterization of STI1, a stress-inducible gene from *Saccharomyces cerevisiae*. *Mol Cell Biol.* **9**, 3638-3646
- 102 Allan, R. K. and Ratajczak, T. (2011) Versatile TPR domains accommodate different modes of target protein recognition and function. *Cell Stress Chaperones.* **16**, 353-367
- 103 Scheufler, C., Brinker, A., Bourenkov, G., Pegoraro, S., Moroder, L., Bartunik, H., Hartl, F. U. and Moarefi, I. (2000) Structure of TPR domain-peptide complexes: critical elements in the assembly of the Hsp70-Hsp90 multichaperone machine. *Cell.* **101**, 199-210
- 104 Schmid, A. B., Lagleder, S., Grawert, M. A., Rohl, A., Hagn, F., Wandinger, S. K., Cox, M. B., Demmer, O., Richter, K., Groll, M., Kessler, H. and Buchner, J. (2012) The architecture of functional modules in the Hsp90 co-chaperone Sti1/Hop. *EMBO J.* **31**, 1506-1517
- 105 Lee, C. T., Graf, C., Mayer, F. J., Richter, S. M. and Mayer, M. P. (2012) Dynamics of the regulation of Hsp90 by the co-chaperone Sti1. *EMBO J.* **31**, 1518-1528

- 106 Prodromou, C., Siligardi, G., O'Brien, R., Woolfson, D. N., Regan, L., Panaretou, B., Ladbury, J. E., Piper, P. W. and Pearl, L. H. (1999) Regulation of Hsp90 ATPase activity by tetratricopeptide repeat (TPR)-domain co-chaperones. *EMBO J.* **18**, 754-762
- 107 Richter, K., Soroka, J., Skalniak, L., Leskovar, A., Hessling, M., Reinstein, J. and Buchner, J. (2008) Conserved conformational changes in the ATPase cycle of human Hsp90. *J Biol Chem.* **283**, 17757-17765
- 108 Rohl, A., Wengler, D., Madl, T., Lagleder, S., Tippel, F., Herrmann, M., Hendrix, J., Richter, K., Hack, G., Schmid, A. B., Kessler, H., Lamb, D. C. and Buchner, J. (2015) Hsp90 regulates the dynamics of its cochaperone Sti1 and the transfer of Hsp70 between modules. *Nat Commun.* **6**, 6655
- 109 Rohl, A., Tippel, F., Bender, E., Schmid, A. B., Richter, K., Madl, T. and Buchner, J. (2014) Hop/Sti1 phosphorylation inhibits its co-chaperone function. *EMBO Rep.* **16**, 240-249
- 110 Gaiser, A. M., Brandt, F. and Richter, K. (2009) The non-canonical Hop protein from *Caenorhabditis elegans* exerts essential functions and forms binary complexes with either Hsc70 or Hsp90. *J Mol Biol.* **391**, 621-634
- 111 Soares, I. N., Caetano, F. A., Pinder, J., Rodrigues, B. R., Beraldo, F. H., Ostapchenko, V. G., Durette, C., Pereira, G. S., Lopes, M. H., Queiroz-Hazarbassanov, N., Cunha, I. W., Sanematsu, P. I., Suzuki, S., Bleggi-Torres, L. F., Schild-Poulter, C., Thibault, P., Dellaire, G., Martins, V. R., Prado, V. F. and Prado, M. A. (2013) Regulation of stress-inducible phosphoprotein 1 nuclear retention by protein inhibitor of activated STAT PIAS1. *Mol Cell Proteomics.* **12**, 3253-3270
- 112 Whitesell, L. and Lindquist, S. L. (2005) HSP90 and the chaperoning of cancer. *Nat Rev Cancer.* **5**, 761-772
- 113 Solit, D. B., Ivy, S. P., Kopil, C., Sikorski, R., Morris, M. J., Slovin, S. F., Kelly, W. K., DeLaCruz, A., Curley, T., Heller, G., Larson, S., Schwartz, L., Egorin, M. J., Rosen, N. and Scher, H. I. (2007) Phase I trial of 17-allylamino-17-demethoxygeldanamycin in patients with advanced cancer. *Clin Cancer Res.* **13**, 1775-1782
- 114 Yi, F. and Regan, L. (2008) A novel class of small molecule inhibitors of Hsp90. *ACS Chem Biol.* **3**, 645-654
- 115 Pimienta, G., Herbert, K. M. and Regan, L. (2011) A compound that inhibits the HOP-Hsp90 complex formation and has unique killing effects in breast cancer cell lines. *Mol Pharm.* **8**, 2252-2261
- 116 Walsh, N., Larkin, A., Swan, N., Conlon, K., Dowling, P., McDermott, R. and Clynes, M. (2011) RNAi knockdown of Hop (Hsp70/Hsp90 organising protein) decreases invasion via MMP-2 down regulation. *Cancer Lett.* **306**, 180-189

- 117 Fonseca, A. C., Romao, L., Amaral, R. F., Assad Kahn, S., Lobo, D., Martins, S., Marcondes de Souza, J., Moura-Neto, V. and Lima, F. R. (2012) Microglial stress inducible protein 1 promotes proliferation and migration in human glioblastoma cells. *Neuroscience*. **200**, 130-141
- 118 Horibe, T., Kohno, M., Haramoto, M., Ohara, K. and Kawakami, K. (2011) Designed hybrid TPR peptide targeting Hsp90 as a novel anticancer agent. *J Transl Med*. **9**, 8
- 119 Klettner, A. (2004) The induction of heat shock proteins as a potential strategy to treat neurodegenerative disorders. *Drug News Perspect*. **17**, 299-306
- 120 Waza, M., Adachi, H., Katsuno, M., Minamiyama, M., Tanaka, F., Doyu, M. and Sobue, G. (2006) Modulation of Hsp90 function in neurodegenerative disorders: a molecular-targeted therapy against disease-causing protein. *J Mol Med (Berl)*. **84**, 635-646
- 121 Zanata, S. M., Lopes, M. H., Mercadante, A. F., Hajj, G. N., Chiarini, L. B., Nomizo, R., Freitas, A. R., Cabral, A. L., Lee, K. S., Juliano, M. A., de Oliveira, E., Jachieri, S. G., Burlingame, A., Huang, L., Linden, R., Brentani, R. R. and Martins, V. R. (2002) Stress-inducible protein 1 is a cell surface ligand for cellular prion that triggers neuroprotection. *EMBO J*. **21**, 3307-3316
- 122 Beraldo, F. H., Soares, I. N., Goncalves, D. F., Fan, J., Thomas, A. A., Santos, T. G., Mohammad, A. H., Roffe, M., Calder, M. D., Nikolova, S., Hajj, G. N., Guimaraes, A. L., Massensini, A. R., Welch, I., Betts, D. H., Gros, R., Drangova, M., Watson, A. J., Bartha, R., Prado, V. F., Martins, V. R. and Prado, M. A. (2013) Stress-inducible phosphoprotein 1 has unique cochaperone activity during development and regulates cellular response to ischemia via the prion protein. *FASEB J*. **27**, 3594-3607
- 123 Santos, T. G., Beraldo, F. H., Hajj, G. N., Lopes, M. H., Roffe, M., Lupinacci, F. C., Ostapchenko, V. G., Prado, V. F., Prado, M. A. and Martins, V. R. (2013) Laminin-gamma1 chain and stress inducible protein 1 synergistically mediate PrPC-dependent axonal growth via Ca²⁺ mobilization in dorsal root ganglia neurons. *J Neurochem*. **124**, 210-223
- 124 Lopes, M. H., Hajj, G. N., Muras, A. G., Mancini, G. L., Castro, R. M., Ribeiro, K. C., Brentani, R. R., Linden, R. and Martins, V. R. (2005) Interaction of cellular prion and stress-inducible protein 1 promotes neuritogenesis and neuroprotection by distinct signaling pathways. *J Neurosci*. **25**, 11330-11339
- 125 Hajj, G. N., Arantes, C. P., Dias, M. V., Roffe, M., Costa-Silva, B., Lopes, M. H., Porto-Carreiro, I., Rabachini, T., Lima, F. R., Beraldo, F. H., Prado, M. A., Linden, R. and Martins, V. R. (2013) The unconventional secretion of stress-inducible protein 1 by a heterogeneous population of extracellular vesicles. *Cell Mol Life Sci*. **70**, 3211-3227

- 126 Romano, S. A., Cordeiro, Y., Lima, L. M., Lopes, M. H., Silva, J. L., Foguel, D. and Linden, R. (2009) Reciprocal remodeling upon binding of the prion protein to its signaling partner hop/STI1. *FASEB J.* **23**, 4308-4316
- 127 Beraldo, F. H., Arantes, C. P., Santos, T. G., Queiroz, N. G., Young, K., Rylett, R. J., Markus, R. P., Prado, M. A. and Martins, V. R. (2010) Role of alpha7 nicotinic acetylcholine receptor in calcium signaling induced by prion protein interaction with stress-inducible protein 1. *J Biol Chem.* **285**, 36542-36550
- 128 Caetano, F. A., Lopes, M. H., Hajj, G. N., Machado, C. F., Pinto Arantes, C., Magalhaes, A. C., Vieira Mde, P., Americo, T. A., Massensini, A. R., Priola, S. A., Vorberg, I., Gomez, M. V., Linden, R., Prado, V. F., Martins, V. R. and Prado, M. A. (2008) Endocytosis of prion protein is required for ERK1/2 signaling induced by stress-inducible protein 1. *J Neurosci.* **28**, 6691-6702
- 129 Wang, H. Y., Lee, D. H., D'Andrea, M. R., Peterson, P. A., Shank, R. P. and Reitz, A. B. (2000) beta-Amyloid(1-42) binds to alpha7 nicotinic acetylcholine receptor with high affinity. Implications for Alzheimer's disease pathology. *J Biol Chem.* **275**, 5626-5632
- 130 Nery, A. A., Magdesian, M. H., Trujillo, C. A., Sathler, L. B., Juliano, M. A., Juliano, L., Ulrich, H. and Ferreira, S. T. (2013) Rescue of amyloid-Beta-induced inhibition of nicotinic acetylcholine receptors by a peptide homologous to the nicotine binding domain of the alpha 7 subtype. *PLoS One.* **8**, e67194
- 131 Roffe, M., Beraldo, F. H., Bester, R., Nunziant, M., Bach, C., Mancini, G., Gilch, S., Vorberg, I., Castilho, B. A., Martins, V. R. and Hajj, G. N. (2010) Prion protein interaction with stress-inducible protein 1 enhances neuronal protein synthesis via mTOR. *Proc Natl Acad Sci U S A.* **107**, 13147-13152
- 132 Klann, E. and Sweatt, J. D. (2008) Altered protein synthesis is a trigger for long-term memory formation. *Neurobiol Learn Mem.* **89**, 247-259
- 133 Daniel, S., Bradley, G., Longshaw, V. M., Soti, C., Csermely, P. and Blatch, G. L. (2008) Nuclear translocation of the phosphoprotein Hop (Hsp70/Hsp90 organizing protein) occurs under heat shock, and its proposed nuclear localization signal is involved in Hsp90 binding. *Biochim Biophys Acta.* **1783**, 1003-1014
- 134 Longshaw, V. M., Chapple, J. P., Balda, M. S., Cheetham, M. E. and Blatch, G. L. (2004) Nuclear translocation of the Hsp70/Hsp90 organizing protein mSTI1 is regulated by cell cycle kinases. *J Cell Sci.* **117**, 701-710
- 135 Marambaud, P., Dreses-Werringloer, U. and Vingtdeux, V. (2009) Calcium signaling in neurodegeneration. *Mol Neurodegener.* **4**, 20
- 136 Clapham, D. E. (2007) Calcium signaling. *Cell.* **131**, 1047-1058

- 137 Larson, J., Lynch, G., Games, D. and Seubert, P. (1999) Alterations in synaptic transmission and long-term potentiation in hippocampal slices from young and aged PDAPP mice. *Brain Res.* **840**, 23-35
- 138 Mattson, M. P., Cheng, B., Davis, D., Bryant, K., Lieberburg, I. and Rydel, R. E. (1992) beta-Amyloid peptides destabilize calcium homeostasis and render human cortical neurons vulnerable to excitotoxicity. *J Neurosci.* **12**, 376-389
- 139 Green, K. N. and LaFerla, F. M. (2008) Linking calcium to Abeta and Alzheimer's disease. *Neuron.* **59**, 190-194
- 140 Alberdi, E., Sanchez-Gomez, M. V., Cavaliere, F., Perez-Samartin, A., Zugaza, J. L., Trullas, R., Domercq, M. and Matute, C. (2010) Amyloid beta oligomers induce Ca²⁺ dysregulation and neuronal death through activation of ionotropic glutamate receptors. *Cell Calcium.* **47**, 264-272
- 141 Schafer, B. W. and Heizmann, C. W. (1996) The S100 family of EF-hand calcium-binding proteins: functions and pathology. *Trends Biochem Sci.* **21**, 134-140
- 142 Donato, R., Cannon, B. R., Sorci, G., Riuzzi, F., Hsu, K., Weber, D. J. and Geczy, C. L. (2013) Functions of S100 proteins. *Curr Mol Med.* **13**, 24-57
- 143 de la Monte, S. M. (1999) Molecular abnormalities of the brain in Down syndrome: relevance to Alzheimer's neurodegeneration. *J Neural Transm Suppl.* **57**, 1-19
- 144 Zimmer, D. B., Chaplin, J., Baldwin, A. and Rast, M. (2005) S100-mediated signal transduction in the nervous system and neurological diseases. *Cell Mol Biol (Noisy-le-grand).* **51**, 201-214
- 145 Most, P., Remppis, A., Pleger, S. T., Katus, H. A. and Koch, W. J. (2007) S100A1: a novel inotropic regulator of cardiac performance. Transition from molecular physiology to pathophysiological relevance. *Am J Physiol Regul Integr Comp Physiol.* **293**, R568-577
- 146 Wright, N. T., Varney, K. M., Ellis, K. C., Markowitz, J., Gitti, R. K., Zimmer, D. B. and Weber, D. J. (2005) The three-dimensional solution structure of Ca(2+)-bound S100A1 as determined by NMR spectroscopy. *J Mol Biol.* **353**, 410-426
- 147 Nowakowski, M., Ruszczynska-Bartnik, K., Budzinska, M., Jaremko, L., Jaremko, M., Zdanowski, K., Bierzynski, A. and Ejchart, A. (2013) Impact of calcium binding and thionylation of S100A1 protein on its nuclear magnetic resonance-derived structure and backbone dynamics. *Biochemistry.* **52**, 1149-1159
- 148 Strynadka, N. C. and James, M. N. (1989) Crystal structures of the helix-loop-helix calcium-binding proteins. *Annu Rev Biochem.* **58**, 951-998

- 149 Santamaria-Kisiel, L., Rintala-Dempsey, A. C. and Shaw, G. S. (2006) Calcium-dependent and -independent interactions of the S100 protein family. *Biochem J.* **396**, 201-214
- 150 Moore, B. W. (1965) A soluble protein characteristic of the nervous system. *Biochem Biophys Res Commun.* **19**, 739-744
- 151 Wright, N. T., Cannon, B. R., Zimmer, D. B. and Weber, D. J. (2009) S100A1: Structure, Function, and Therapeutic Potential. *Curr Chem Biol.* **3**, 138-145
- 152 Ackermann, G. E., Marenholz, I., Wolfer, D. P., Chan, W. Y., Schafer, B., Erne, P. and Heizmann, C. W. (2006) S100A1-deficient male mice exhibit increased exploratory activity and reduced anxiety-related responses. *Biochim Biophys Acta.* **1763**, 1307-1319
- 153 Most, P., Boerries, M., Eicher, C., Schweda, C., Ehlermann, P., Pleger, S. T., Loeffler, E., Koch, W. J., Katus, H. A., Schoenenberger, C. A. and Remppis, A. (2003) Extracellular S100A1 protein inhibits apoptosis in ventricular cardiomyocytes via activation of the extracellular signal-regulated protein kinase 1/2 (ERK1/2). *J Biol Chem.* **278**, 48404-48412
- 154 Afanador, L., Roltsch, E. A., Holcomb, L., Campbell, K. S., Keeling, D. A., Zhang, Y. and Zimmer, D. B. (2014) The Ca²⁺ sensor S100A1 modulates neuroinflammation, histopathology and Akt activity in the PSAPP Alzheimer's disease mouse model. *Cell Calcium.* **56**, 68-80
- 155 Huttunen, H. J., Kuja-Panula, J., Sorci, G., Agneletti, A. L., Donato, R. and Rauvala, H. (2000) Coregulation of neurite outgrowth and cell survival by amphotericin and S100 proteins through receptor for advanced glycation end products (RAGE) activation. *J Biol Chem.* **275**, 40096-40105
- 156 Shimamoto, S., Takata, M., Tokuda, M., Oohira, F., Tokumitsu, H. and Kobayashi, R. (2008) Interactions of S100A2 and S100A6 with the tetratricopeptide repeat proteins, Hsp90/Hsp70-organizing protein and kinesin light chain. *J Biol Chem.* **283**, 28246-28258
- 157 Shimamoto, S., Kubota, Y., Tokumitsu, H. and Kobayashi, R. (2010) S100 proteins regulate the interaction of Hsp90 with Cyclophilin 40 and FKBP52 through their tetratricopeptide repeats. *FEBS Lett.* **584**, 1119-1125

2 Structural characterization of STIP1 domains

2.1 Introduction

Proper folding of nascent peptides by molecular chaperones is a fundamental process of life. Heat-shock proteins (Hsp)70 and Hsp90 are evolutionary conserved chaperones which mediate folding of key cellular client proteins involved in proliferation, differentiation and apoptosis [1, 2]. Hsp90 targets include numerous oncogenic proteins implicated in tumor growth and survival including steroid hormone receptors and proto-oncogenic kinases such as Akt [3], Raf-1 [4] and Her2/neu [5]. Hsp90 over-expression correlates with tumor invasiveness and poor prognosis, thus pharmacological inhibition of the chaperone response has become an alluring target for therapeutic intervention in multiple cancer models [6].

Client maturation is facilitated by a number of co-chaperone proteins that regulate Hsp70 and Hsp90 activity. Hop/STIP1 (Hsp-organizing protein/stress-induced-phosphoprotein 1) is a key scaffold protein, which coordinates client transfer from Hsp70 to Hsp90 in the later stages of client maturation [7, 8]. Initially, client proteins complex with Hsp40 and Hsp70 [9, 10]. Hop/STIP1 initiation promotes client transfer from Hsp70 to Hsp90 by simultaneously binding the two chaperones through distinct tetratricopeptide repeat (TPR) domains [11].

Hop/STIP1 is a modular protein composed of three structurally related TPR domains (TPR1, TPR2A and TPR2B) and two aspartate-proline rich regions (DP1 and DP2) [12]. TPR domains are composed of multiple degenerate 34 amino acid repeats forming anti-parallel helix-turn-helix motifs. These serve as protein-protein interaction

modules in multi-protein complexes [13]. Hsp coordination by TPR domains is accomplished through the conserved C-terminal residue ‘EEVD’ motifs of Hsp70 and Hsp90. X-ray crystallographic data of human and yeast TPR domain complexes with Hsp70 and Hsp90 C-terminal peptides indicate specificity is determined by hydrophobic contacts directly N-terminal of the ‘EEVD’ motif [11]; however, additional extensive yet poorly understood contacts are formed between STIP1 and Hsps, stabilizing the interaction [14]. The TPR1 and TPR2B domains facilitate Hsp70 binding, while TPR2A is the primary Hsp90 binding site [15]. During client maturation Hsp70 is initially recruited to the TPR1 domain of STIP1. Upon Hsp90 binding, Hsp70 is transferred to the TPR2B domain to facilitate client transfer from Hsp70 to Hsp90 [15].

The functional roles of the DP domains of STIP1 are more enigmatic. The TPR1 and DP1 domains are dispensable for client protein maturation, with the minimal functional fragment comprising of TPR2A-TPR2B-DP2 [14]. Inter-domain contacts have been identified between the DP2 and TPR2A-TPR2B domains of yeast STIP1, while the DP1 domain is thought to function as a flexible linker facilitating transfer of Hsp70 from the TPR1 to the TPR2B domains [15].

Studies have demonstrated that STIP1 promotes proliferation and migration in glioblastoma and pancreatic cancer cell lines [16, 17]. Down-regulation of STIP1 by RNAi resulted in decreased pancreatic cell line invasiveness and down-regulation of numerous oncogenic Hsp90 client proteins [17]. Inhibition of Hsp90 interaction with the TPR2A domain of STIP1 using a novel hybrid TPR peptide has demonstrated selective cancer-cell cytotoxicity [18]. Thus, inhibition of STIP1 binding to Hsp machinery has been suggested as an alternative approach in novel cancer therapeutics [19, 20].

Secreted STIP1 also functions as a cell-signaling molecule promoting neuriteogenesis and neuroprotection in hippocampal neurons through its interaction with the cellular prion protein (PrP^C) [21-24]. The PrP^C binding site of STIP1 has been localized to the N-terminal of STIP1, with TPR1, DP1 and TPR2A domains of STIP1 contributing to complex formation (See Chapter 3). Recently, neuroprotective signaling induced by PrP^C-STIP1 complex formation rescued primary mouse hippocampal neurons suggesting PrP^C-STIP1 may play a role in the progression of Alzheimer's disease [25].

Nuclear magnetic resonance (NMR) spectroscopy has been proven to be a robust technique in the study of macromolecular complexes. NMR provides detailed structural information on a per residue basis to unambiguously identify regions of macromolecules which interact or undergo conformational changes upon complex formation [26]. The ¹H-¹⁵N HSQC (Heteronuclear Single Quantum Correlation) spectra contain a single peak corresponding to each amino acid in a protein (except proline residues which lack amide protons) and serve as a “finger-print” of a protein [26, 27]. Upon, titration of a binding ligand, residues involved in complex formation or undergoing a conformational change (i.e. change in their chemical environment) demonstrates perturbations in their peak resonances and allows to identify the protein-ligand interfaces at the structural level.

For this approach to be effective, the identity of each peak in the ¹H-¹⁵N HSQC spectra must be correlated to a particular residue in the protein sequence. This requires a series of experiments to assign the individual backbone amides to particular peaks in the spectra. Backbone resonance assignment of the individual domains of STIP1 domains and characterization of the TPR domains will provide the foundation for the study of STIP1 protein-protein interactions, as well as provide the structural basis for the

screening of selective inhibitors of Hsp complex formation that may prove as effective cancer treatments and for future studies involving the STIP1-PrP^C signaling complex and other ligand interactions.

2.2 Materials and Methods

2.2.1 Protein expression and purification

The expression vectors containing mouse full-length STIP1 and the individual domains (TPR1 (residues 1-118), DP1 (residues 119-216), TPR2A (residues 217-352), TPR2B (residues 353-480) and DP2 (residues 481-542)) were transformed in *E. coli* BL21 (DE3) pLysS. For backbone amide resonance assignment of each STIP1 domain (TPR1, DP1, TPR2A, TPR2B and DP2), uniformly ¹⁵N, ¹³C- labeled protein was over-expressed by growing *E. coli* in 1 L M9 media supplemented with 1 g of ¹⁵NH₄Cl and 3 g of ¹³C-glucose at 37°C to an OD₆₀₀ of 0.9, at which point protein over-expression was induced with 1 mM isopropyl β-D-1-thiogalactopyranoside (IPTG). For all other experiments, the protein was grown in M9 minimal media without isotopically labeling the protein. Cultures were grown overnight at 22°C and centrifuged pellets were frozen for storage. N-terminally His-tagged fusion proteins were purified by affinity chromatography using Ni SepharoseTM 6 Fast Flow beads (Amersham Biosciences). The N-terminal His-tag was removed by incubation with His-tagged Tobacco Etch Virus (TEV) protease overnight at 22 °C and proteins were analyzed by SDS-PAGE. TEV protease was removed by an additional Ni²⁺ affinity chromatography step. Proteins were dialyzed into the appropriate buffers for further experimentation as noted.

2.2.2 Circular dichroism (CD) Spectropolarimetry

CD spectra were acquired on a Jasco J-810 spectropolarimeter (Easton, MD). Spectra of TPR1 and TPR2A at approximately 0.1 mg/mL concentrations were collected in 10 mM sodium acetate, pH 5 or 50 mM sodium phosphate pH 7 or 8 buffers supplemented with 1mM DTT at 20°C. Five accumulated scans were used for each spectrum. Thermal denaturation was conducted over a temperature range consisting of 10°C to 95°C. The spectra were deconvoluted using the CDSSTR analysis program from the DichroWeb (<http://dichroweb.cryst.bbk.ac.uk>) online analysis software package using the SMP180 (optimized for 190-240 nm) reference set [28, 29].

2.2.3 Analytical Ultracentrifugation – Sedimentation Equilibrium and Gel Filtration Chromatography

Analytical ultracentrifugation (AUC) experiments were performed at 20 °C in 50 mM sodium phosphate, 50 mM NaCl, 1 mM DTT, pH 7.0 on TPR2A (50 µM) using a Beckman Optima XL-A Analytical Ultracentrifuge equipped with an An60Ti rotor containing six-channel Epon-charcoal centerpieces and 1.2 cm path length. (Biomolecular Interactions and Conformations Facility, University of Western Ontario). Absorbance measurements were collected at 290 nm in 0.002 cm radial steps and averaged over 10 scans. Sedimentation equilibrium measurements were collected at rotor speeds of 16 000, 20 000, 24 000 and 28 000 rpm. Data was fit to the following global single-ideal species model equation using GraphPad Prism

$$C = C_0 \exp\left(\frac{\omega^2}{2RT} M_{\text{obs}}(1 - \bar{v}\rho)(x^2 - x_0^2)\right) + I_0$$

(Equation 1) where C is the concentration of protein at radius x , C_0 is the concentration at initial radius x_0 , ω is the angular velocity, v_{bar} is the partial specific volume of the protein, ρ is the solvent density, R is the ideal gas constant, T is the absolute temperature, I_0 is the baseline offset and M_{obs} is the fit of the molecular weight based on sedimentation data.

Analytical gel filtration of TPR2A was carried out on a Superdex 75 gel filtration column (Amersham Biosciences) in 50 mM sodium phosphate, 50 mM NaCl, 1mM DTT, pH 7 at a flow rate of 0.5 mL/min. The elution profile was compared to the following globular protein standards of known molecular weight: 67 kDa, 43 kDa, 23 kDa, 13.7 kDa.

2.2.4 Backbone amide NMR Resonance Assignments

STIP1 domains (TPR1, DP1, TPR2A, TPR2B, DP2) were dialyzed into 50 mM sodium phosphate buffer, 50 mM NaCl, 1mM DTT at pH 7 and subsequently concentrated to $\sim 500 \mu\text{M}$. NMR samples contained 10 % D_2O and 100 μM 2,2-dimethyl-2-sila-pentane-5-sulfonic acid (DSS) for ^1H and ^{13}C chemical shift referencing. NMR experiments for backbone resonance assignments of each domain were conducted at 25°C on a Varian INOVA 600 MHz spectrometer equipped with either a cryogenic probe or a regular triple resonance probe (UWO Biomolecular NMR Facility). Sequential assignments were obtained for each domain using the following Biopack experiments: TPR1 (HNCACB, CBCA(CO)NH and C(CO)NH), DP1(HNCACB, CBCA(CO)NH and C(CO)NH), TPR2A (HNCACB and CBCA(CO)NH), TPR2B (HNCACB and CBCA(CO)NH) and DP2 (HNCACB, CBCA(CO)NH). All spectra were processed using

NMRPipe and analyzed using CARA [30]. NMR spectral images were presented using NMRViewJ or SPARKY [31-33].

Chemical shift assignments have been deposited in the BioMagResBank (<http://www.bmrb.wisc.edu>), under accession numbers 18691 and 18689 for the TPR1 and TPR2A domains, respectively.

2.2.5 HSP90 chemical shift mapping

Binding of the TPR2A domain to the peptide encoding the C-terminal Hsp90 residues (Ac-MEEVD-NH₂) (GenScript Inc. USA) was confirmed by ¹H-¹⁵N HSQC spectra collected in the presence and absence of equimolar concentrations of Hsp90 peptide (~250 μM). Experiments were collected on a Varian INOVA 600 MHz spectrometer equipped with a cryogenic probe (UWO Biomolecular NMR Facility).

The magnitude of chemical shift perturbations for traceable residues was calculated from the combined chemical shift changes in ¹H and ¹⁵N dimensions ($\Delta\omega = |0.2 * \Delta^{15}\text{N}| + |\Delta^1\text{H}^{\text{N}}|$) in ppm. The resultant chemical shift changes were mapped on to the crystal structure of TPR2A (PDB: 1ELR) and presented using UCSF Chimera Molecular Modeling System [11, 34].

2.3 Results

2.3.1 Structural analysis of STIP1

The relative large molecular weight of STIP1 (63 kDa) and multi-domain assembly raised the question if detailed structural studies by NMR were feasible. Full-length STIP1 was successfully purified from the soluble fractions in *E. coli* BL21

(pLysS) (Figure 2.1B) TEV incubation led to successful removal of the poly-histidine tag and purification of soluble STIP1 of high purity (>95%). ^1H - ^{15}N NMR HSQC spectra of full-length STIP1 contained a small subset of the backbone amide resonances (approximately 150 peaks) expected for a protein of this size (543 residues) (Figure 2.1B) STIP1 appeared to be of the correct molecular weight when analyzed by SDS-PAGE indicating the lack of amide resonances is not the result of protein degradation (Figure 2.1C). The majority of the resonances which are resolved cluster in a narrow region in the HSQC spectrum, spanning ~ 1 ppm. The narrow spectral width of these resonances signifies they likely represent flexible loop-regions or inter-domain linkers of STIP1. The absence of signals from the folded functional domains of STIP1 is likely due to its large molecular size and elongated structure resulting in enhanced relaxation and peak broadening.

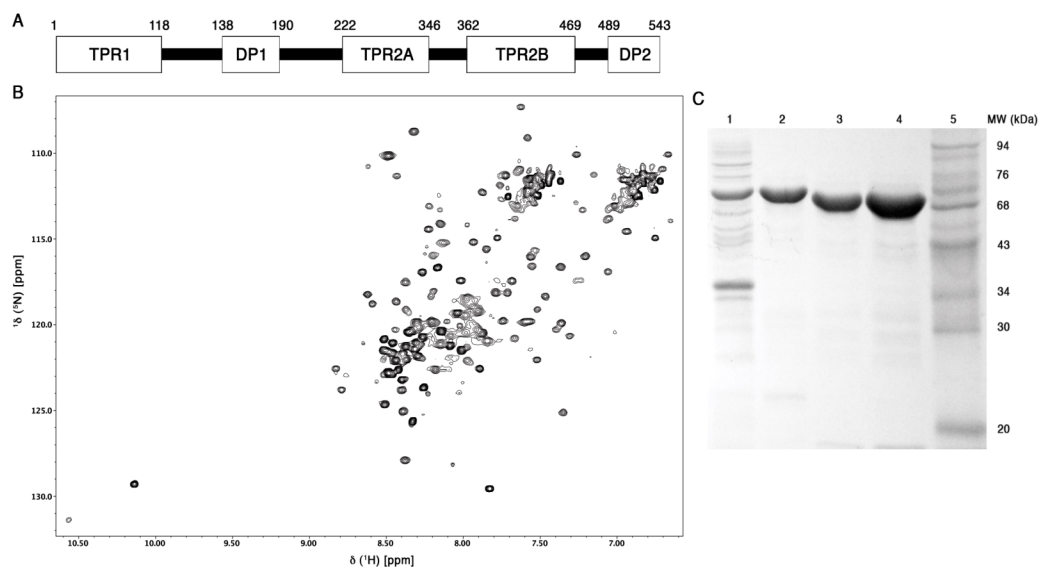


Figure 2.1. ^1H - ^{15}N HSQC of full-length STIP1 indicates NMR spectroscopy of full-length protein is unfeasible due to lack of backbone amide resonances.

(A) ^1H - ^{15}N HSQC spectra of full-length STIP1. (B) SDS-PAGE of purified STIP1. (lane 1) Soluble bacterial lysate of *E. coli* over-expressing STIP1. (lane 2) Ni^{2+} chromatography purified 6xHis-tagged STIP1 (5 μg). (lane 3) STIP1 following incubation with TEV for 6xHis-tag cleavage and removal (5 μg) or (lane 4) (10 μg). (lane 5) Molecular weight markers.

2.3.2 Assignment of structural domains of STIP1

The individual folded functional domains of STIP1 (TPR1, DP1, TPR2A, TPR2B and DP2) were isolated to facilitate study of STIP1 ligand interactions at the molecular level. The molecular weights of individual STIP1 domains range from ~7-17 kDa (Figure 2.1A) making them amenable for study by NMR compared to full-length STIP1.

To the best of our knowledge, no amide backbone assignments are available for the mammalian STIP1 domains, thus NMR experiments were conducted to assign the $^1\text{H}^{\text{N}}$, ^{15}N , $^{13}\text{C}\alpha$ and $^{13}\text{C}\beta$ were obtained for the TPR domains (TPR1, TPR2A and TPR2B) of STIP1. For the TPR1 domain, 97% of the $^1\text{H}^{\text{N}}$ and ^{15}N resonances of non-proline residues, 94% $^{13}\text{C}\alpha$ and 87% $^{13}\text{C}\beta$ of all residues were assigned (Figure 2.2A and B). For the TPR2A domain, 99% of $^1\text{H}^{\text{N}}$ and ^{15}N resonances of non-proline residues, 95% $^{13}\text{C}\alpha$ and 96% $^{13}\text{C}\beta$ of all residues were assigned (Figure 2.3A and B). Secondary structure propensity scores calculated using the assigned $^{13}\text{C}\alpha$ and $^{13}\text{C}\beta$ chemical shifts predict TPR1 and TPR2A to be composed of seven α -helical regions each separated by an interconnecting disordered region with low α -helical propensity (Figure 2.2C and 2.3C) [35]. No β -strand character is seen for the assigned residues. The predicted α -helical propensity and their arrangement correlates with the x-ray crystal structures solved for the human TPR1 and TPR2A domains and their cognate C-terminal Hsp ligands, legitimizing the accuracy of the assignment [11].

For the TPR2B domain, 94% of the $^1\text{H}^{\text{N}}$ and ^{15}N resonances of non-proline residues, 93% $^{13}\text{C}\alpha$ and 95% $^{13}\text{C}\beta$ were assigned (Figure 2.4A and B). Currently, no

high-resolution structural information is available for mammalian TPR2B. However; SSP score predicts 7- α helical structure, which agrees with the TPR1 and TPR2A domains of STIP1 and structurally aligns with the available yeast TPR2B structures (PDB: 3UPV) solved by NMR (Figure 2.4C) [14].

The molecular functions of the DP domains of STIP1 remain enigmatic and no ligand interactions have been identified to date. However; DP1 and the interconnecting linker with TPR2A influences client activation *in vivo* and the DP2 domain has been described as essential in yeast client activation. The solution NMR structure for the yeast DP1 and DP2 domains were recently solved and revealed a novel α -helical fold, with the α -helices of DP2 arranged to form a groove, which may serve as a binding pocket for as of yet unidentified ligands [14]. Thus, we conducted NMR experiments to assign the DP domains of mammalian STIP1. For DP2, 98% of $^1\text{H}^{\text{N}}$ and ^{15}N resonances of non-proline residues were assigned, 98% $^{13}\text{C}\alpha$ and 98% $^{13}\text{C}\beta$ (Figure 2.5A and B). SSP score prediction indicated an all α -helical fold with an disordered C-terminal in agreement with the solved yeast solution structure (Figure 2.5C) [14]. Five regions of α -helical propensity were identified, which align with the solved yeast structure (PDB: 2LLW), suggesting the fold is conserved between yeast and mammalian STIP1 [14].

Unfortunately, due to a large amount of signal degeneracy and poor signal strength of the $^{13}\text{C}\alpha$ and $^{13}\text{C}\beta$ from the HNCACB and CBCA(CO)NH experiments, only 39% of the DP1 domain could be assigned with low confidence (Figure 2.6A). Further experimentation is required to assign the remainder of the DP1 ^1H - ^{15}N HSQC.

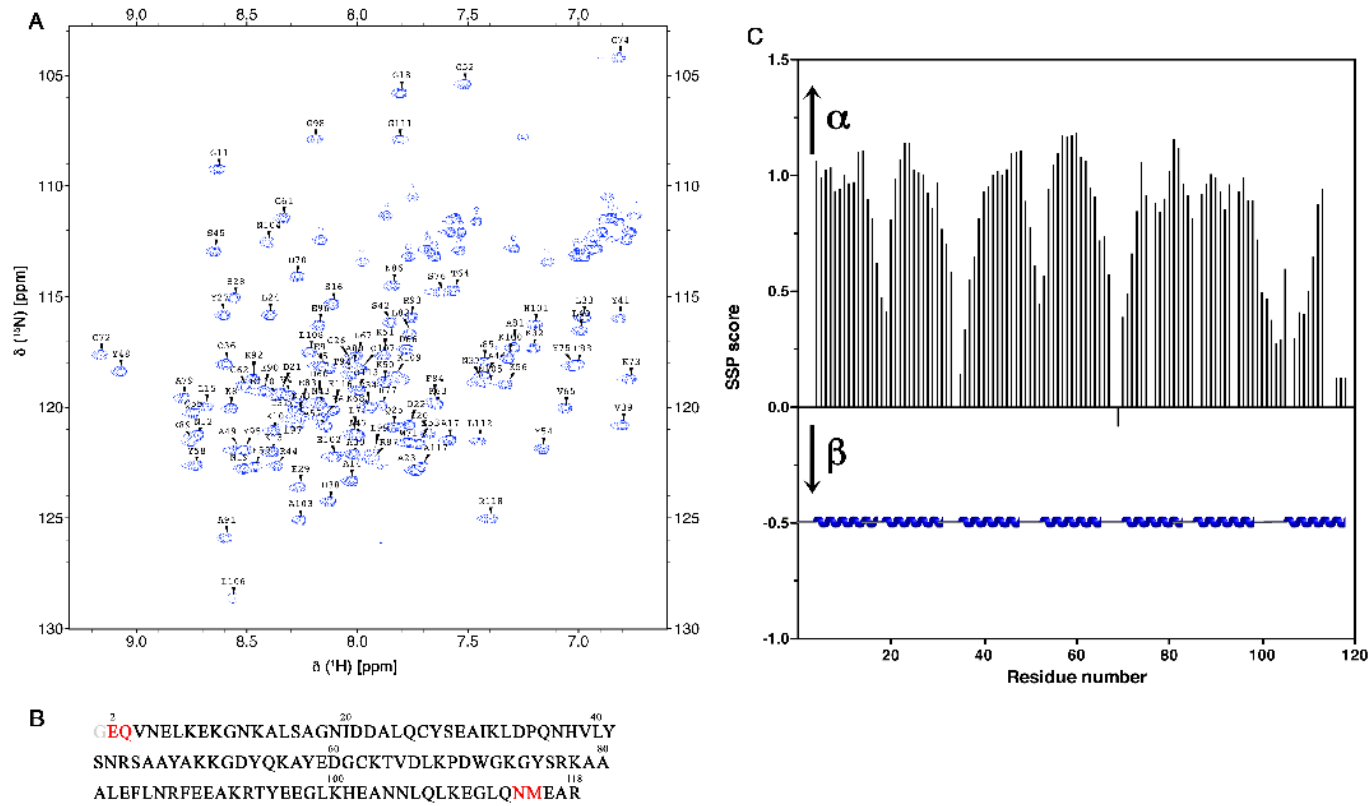


Figure 2.2. (A) ^1H - ^{15}N HSQC spectrum and backbone assignment of $^{15}\text{N}/^{13}\text{C}$ labeled TPR1 domain of STIP1.

(B) Amino acid sequence of TPR1 domain with unassigned residues *colored red*. The N-terminal glycine is a non-native residue from the TEV protease recognition site. (C) Secondary structure propensity (SSP) scores calculated for TPR1 based on $^{13}\text{C}\alpha/\beta$ chemical shifts [35].

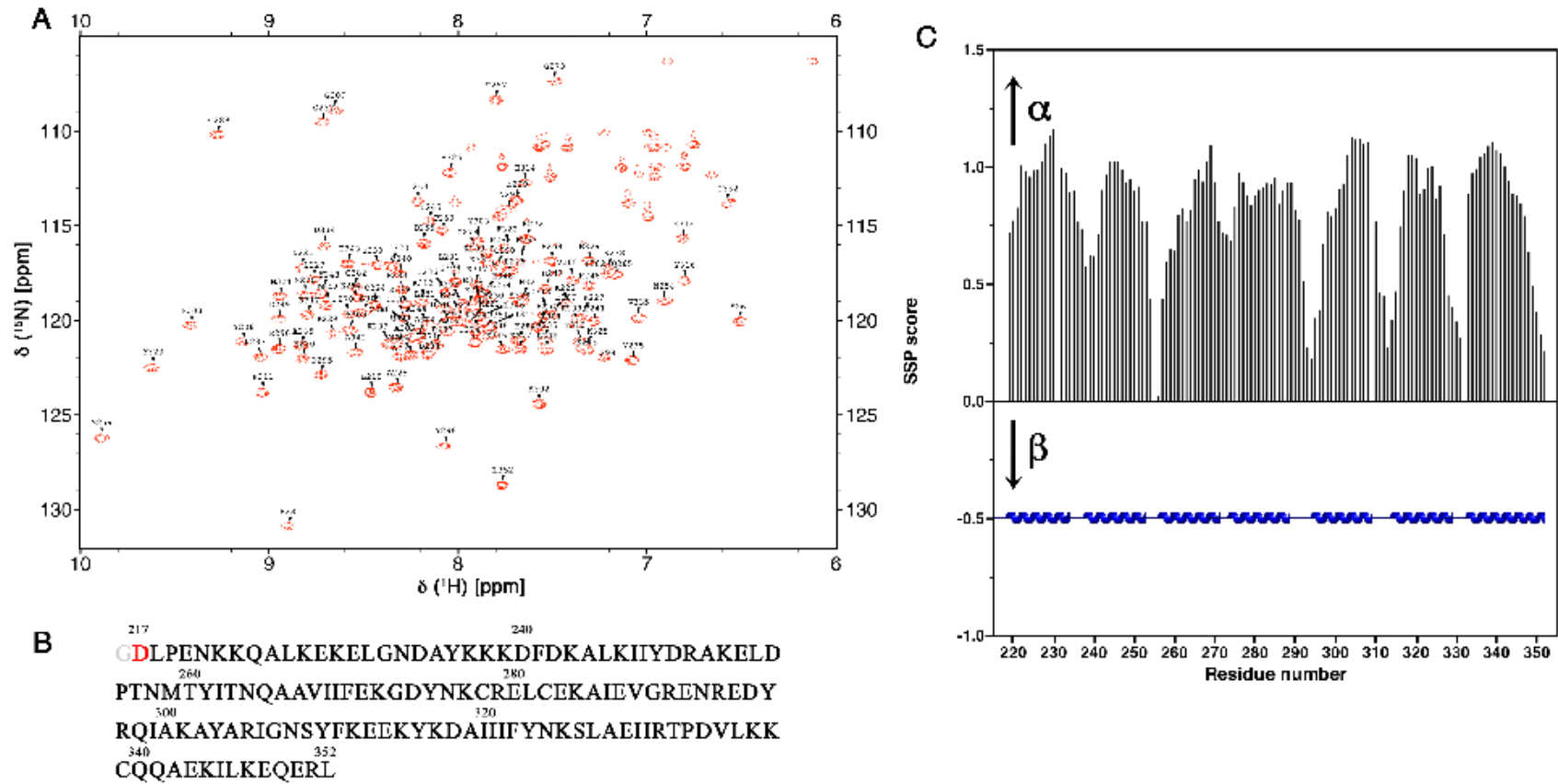


Figure 2.3. (A) ^1H - ^{15}N HSQC spectrum and backbone assignment of $^{15}\text{N}/^{13}\text{C}$ labeled TPR2A domain of STIP1. (B) Amino acid sequence of TPR2A domain with unassigned residues *colored red*. The N-terminal glycine is a non-native residue from the TEV protease recognition site. (C) Secondary structure propensity (SSP) scores calculated for TPR2A based on $^{13}\text{C}\alpha/\beta$ chemical shifts [35].

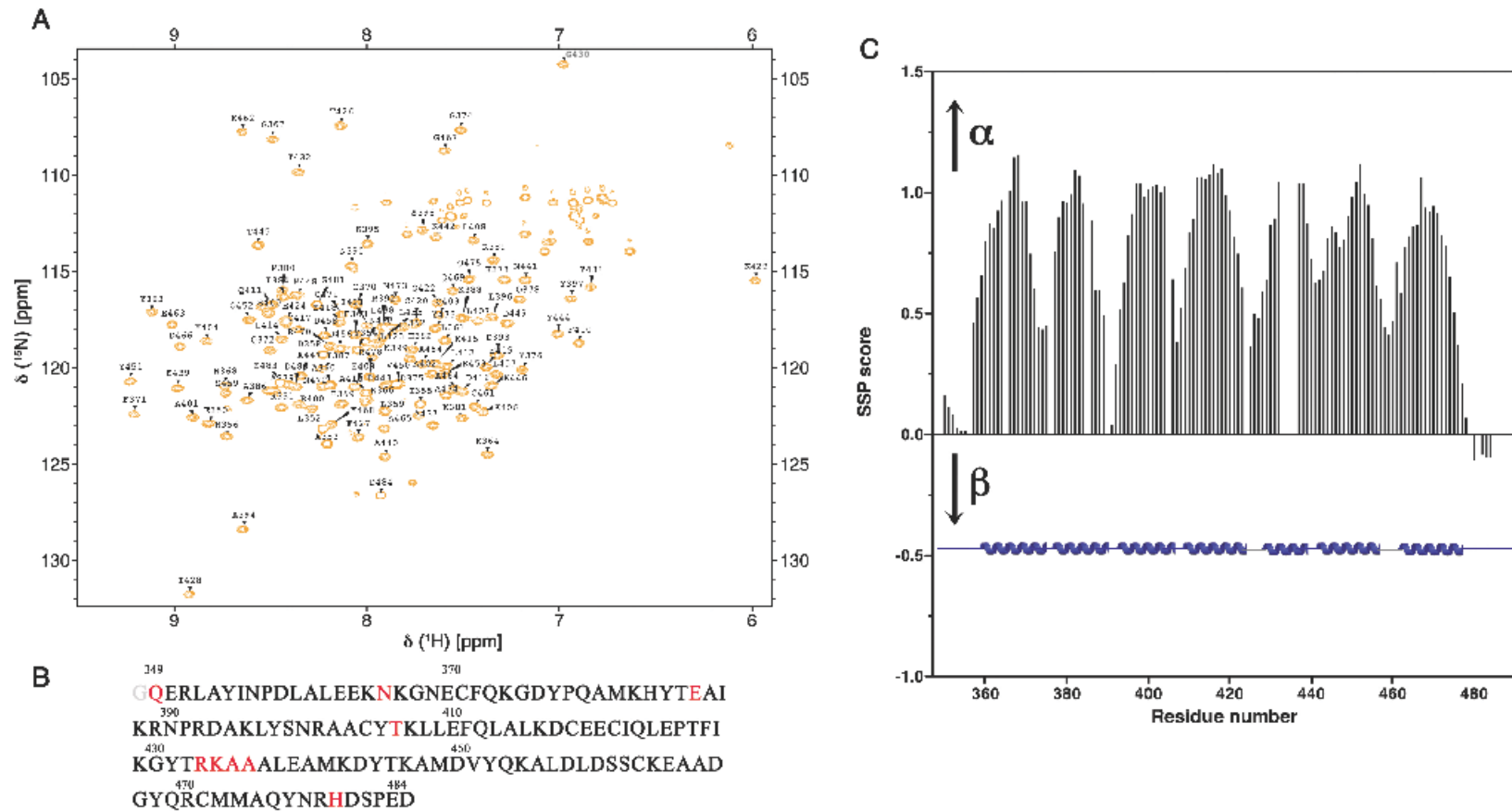


Figure 2.4. (A) ^1H - ^{15}N HSQC spectrum and backbone assignment of $^{15}\text{N}/^{13}\text{C}$ labeled TPR2B domain of STIP1.

(B) Amino acid sequence of TPR2B domain with unassigned residues *colored red*. The N-terminal glycine is a non-native residue from the TEV protease recognition site. (C) Secondary structure propensity (SSP) scores calculated for TPR2B based on $^{13}\text{C}\alpha/\beta$ chemical shifts [35].

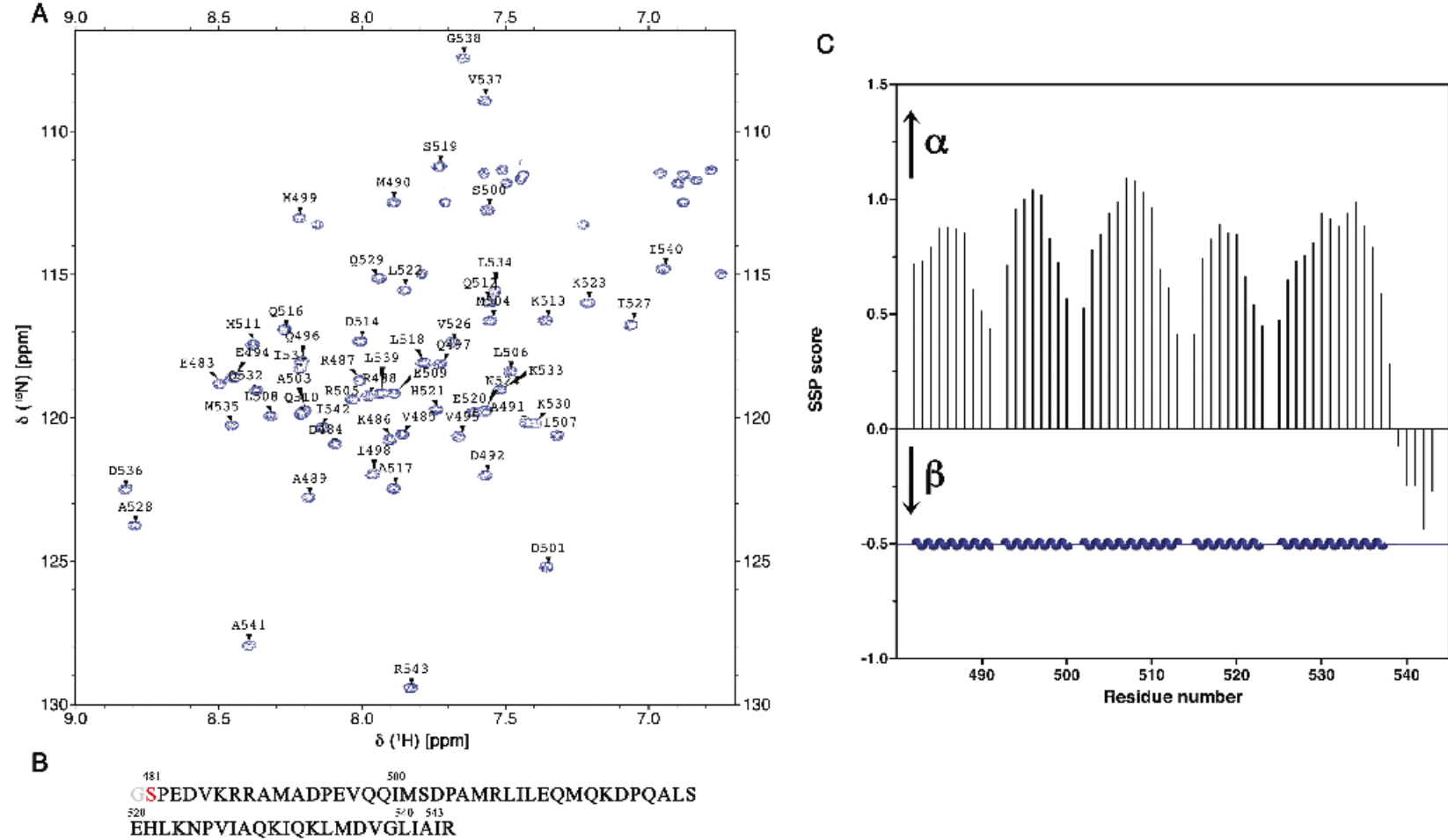


Figure 2.5. (A) ^1H - ^{15}N HSQC spectrum and backbone assignment of $^{15}\text{N}/^{13}\text{C}$ labeled DP2 domain of STIP1.

(B) Amino acid sequence of DP2 domain with unassigned residues colored red. The N-terminal glycine is a non-native residue from the TEV protease recognition site. (C) Secondary structure propensity (SSP) scores calculated for DP2 based on $^{13}\text{C}\alpha/\beta$ chemical shifts [35].

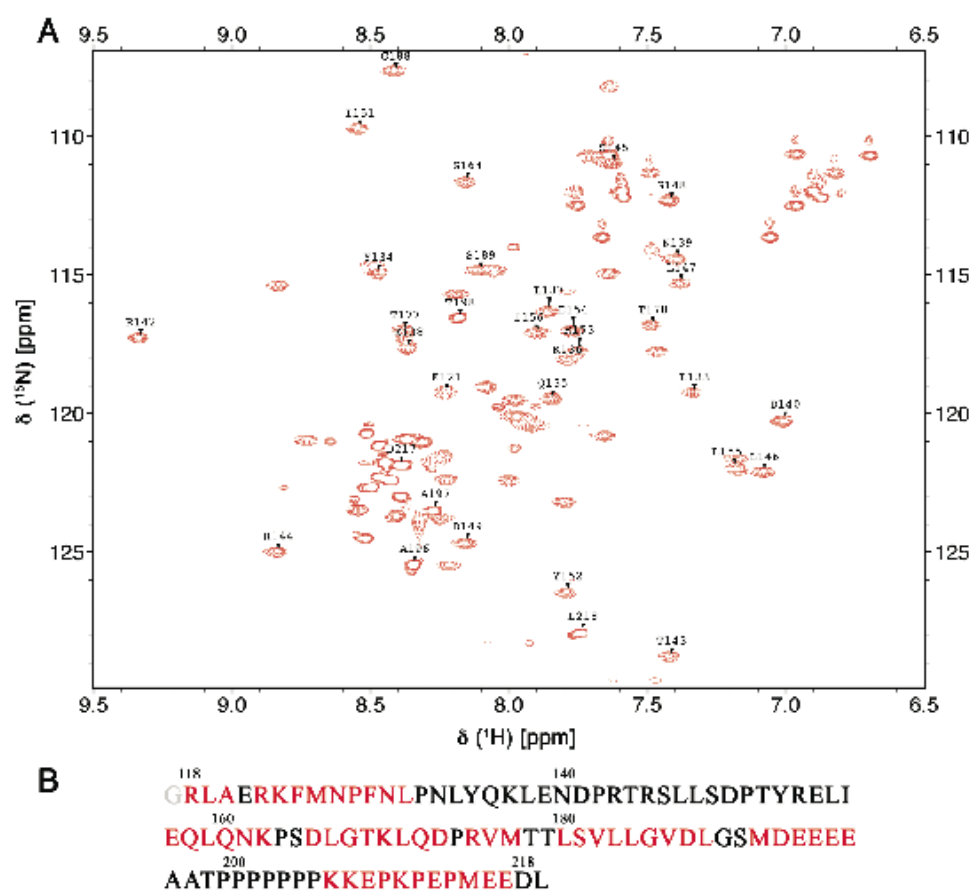


Figure 2.6. (A) ^1H - ^{15}N HSQC spectrum and backbone assignment of $^{15}\text{N}/^{13}\text{C}$ labeled DP1 domain of STIP1.

(B) Amino acid sequence of DP1 domain with unassigned residues colored red. The N-terminal glycine is a non-native residue from the TEV protease recognition site.

2.3.3 Monomeric state of STIP1 and TPR2A

Monomeric and dimeric models of STIP1 have been proposed for the biological unit in solution [15, 36-38]. The TPR2A domain of STIP1 has been suggested as the minimal fragment of STIP1 required for dimerization [36, 38-40]. The isolated TPR2A domain has been reported to migrate as a dimer. Thus, we sought to determine the structural unit of STIP1 and TPR2A to distinguish between monomeric and dimeric models of TPR2A. Gel filtration of the TPR2A domain migrated as a monomer in solution when compared to retention volumes of globular proteins of known molecular weight (Figure 2.7A).

Analytical ultracentrifugation experiments were conducted to confirm the monomeric state of STIP1 and TPR2A in solution. STIP1 presented a M_{obs} value of 55.3 ± 0.9 kDa, reasonably close to the predicted molecular weight of 62.6 kDa and consistent with current monomeric models (see chapter 4). The TPR2A domain sedimented with a M_{obs} of 17.2 ± 0.2 kDa, which is in close agreement to the inferred molecular weight of monomeric TPR2A of 16.2 kDa based on the amino acid sequence (Figure 2.7B). These results indicate TPR2A is indeed a monomer under these conditions.

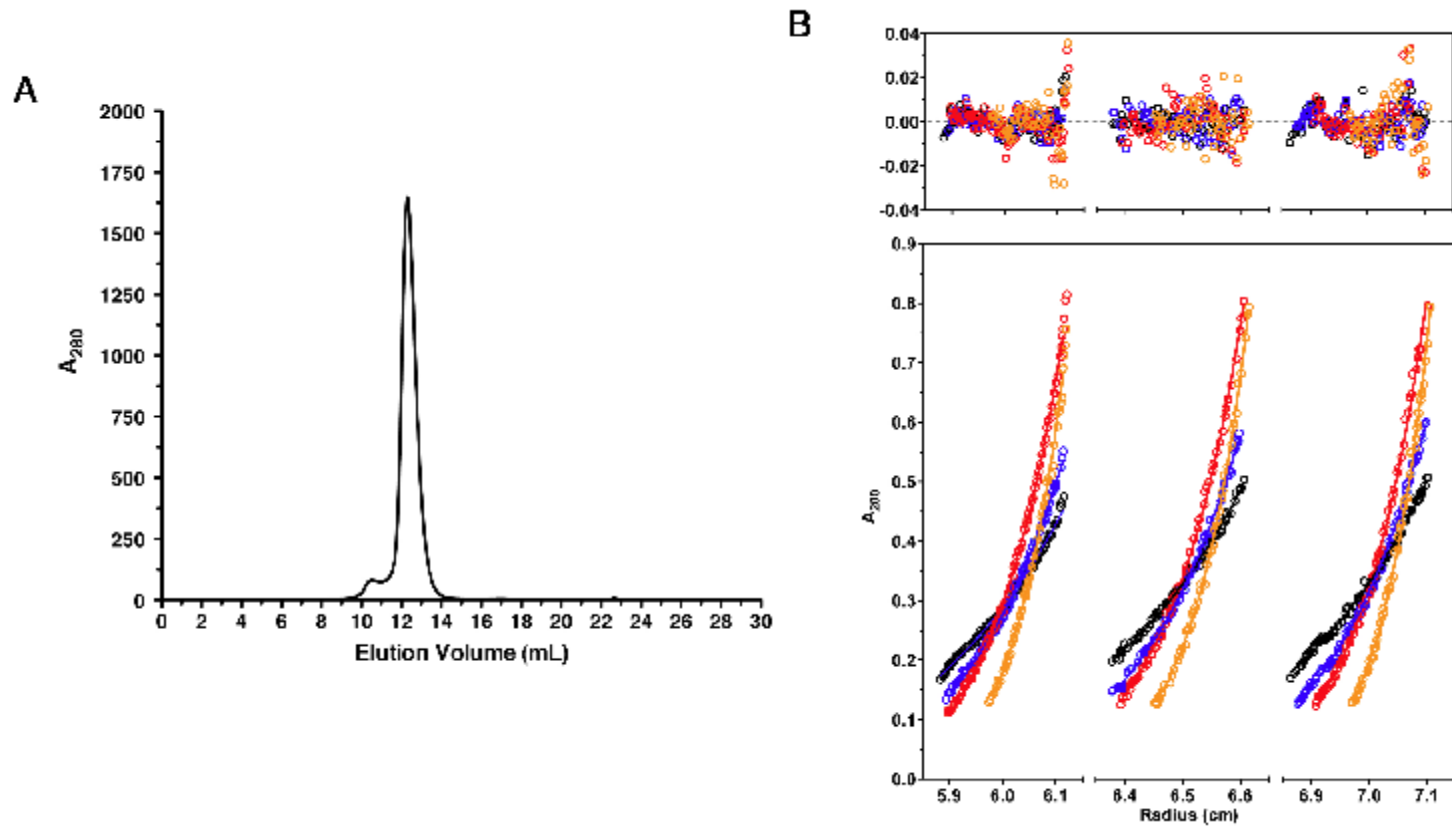


Figure 2.7. TPR2A behaves as a monomer in solution.

(A) Size-exclusion chromatography elution profile of TPR2A monitored by protein absorbance at 280 nm. TPR2A eluted as a single species consistent to a monomer when compared to elution volumes of globular proteins of known molecular weight. (B) Sedimentation equilibrium of AUC TPR2A obtained at rotor speeds 16 000, 20 000, 24 000 and 28 000 rpm (*black, blue, red and orange, respectively*).

2.3.4 Stability of TPR1 and TPR2A

Physiological ligands of STIP1 stability have been reported to vary under different pH conditions. The majority of studies of the cellular prion protein (PrP) are conducted under low pH conditions, thus we aimed to assess the stability of the TPR1 and TPR2A domains under various conditions to optimize future binding studies (See Chapter 3).

The stability of TPR1 and TPR2A domains was investigated by circular dichroism at various pH. Deconvolution of the TPR1 and TPR2A predicted 72.6 and 73.8% α -helical structure at neutral pH, respectively, which is in close agreement with the x-ray crystallographic structures previously solved (Figure 2.8 and 2.9A). A decrease in α -helical character and increase in the predicted disordered regions of the protein was observed at low pH (~5). As well, thermal denaturation of both TPR1 and TPR2A indicated a decrease in stability at low pH compared to neutral conditions indicated by a decrease in the melting temperatures of approximately 10°C for both domains (Figure 2.8 and 2.9B). These results indicate binding studies at neutral pH conditions would be optimal with TPR1 and TPR2A, which is at odds with most PrP studies being conducted at pH 5 [41, 42]. However, low salt conditions at neutral pH have been reported for PrP and will be used to assess TPR1 and TPR2A binding to PrP [43].

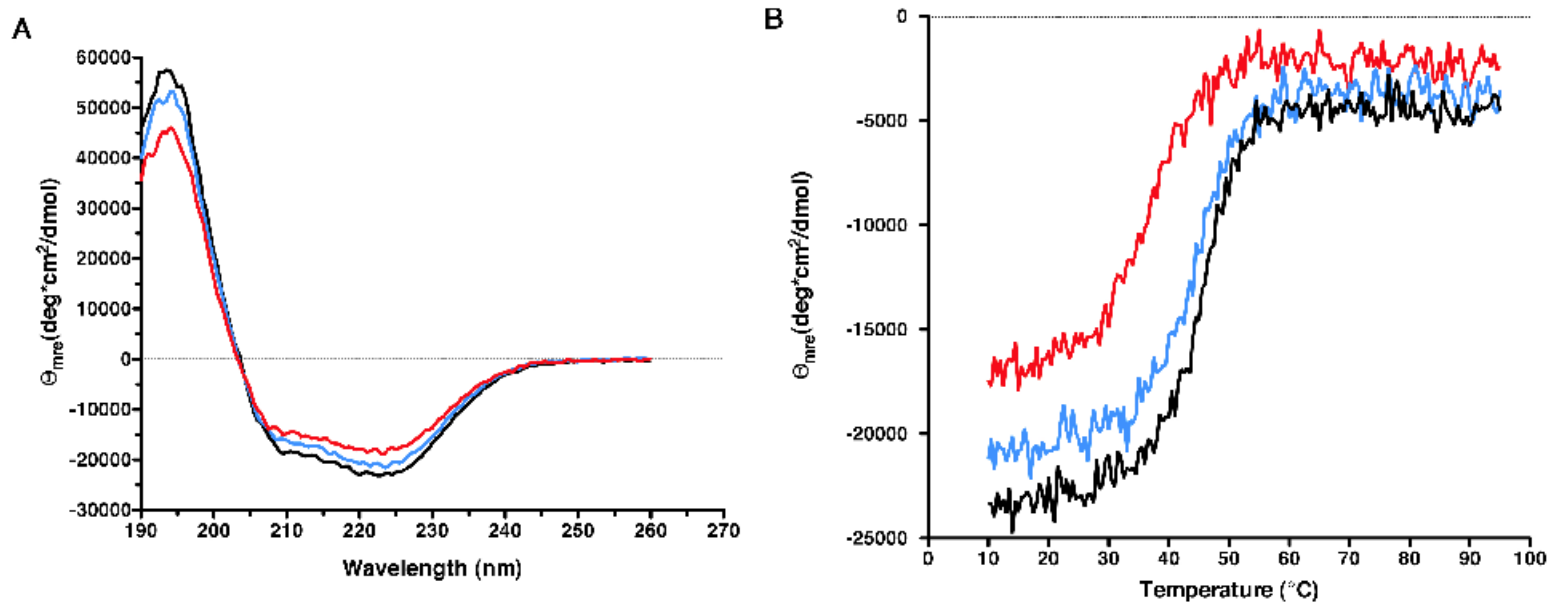


Figure 2.8. TPR1 domain is predominately α -helical and demonstrates increased stability at neutral pH.

(A) CD spectra of TPR1 collected at pH 5 (*red*), pH 6 (*blue*) and pH 7 (*black*). (B) Thermal melts of TPR1 monitored by CD at 220 nm collected at pH 5 (*red*), pH 6 (*blue*) and pH 7 (*black*).

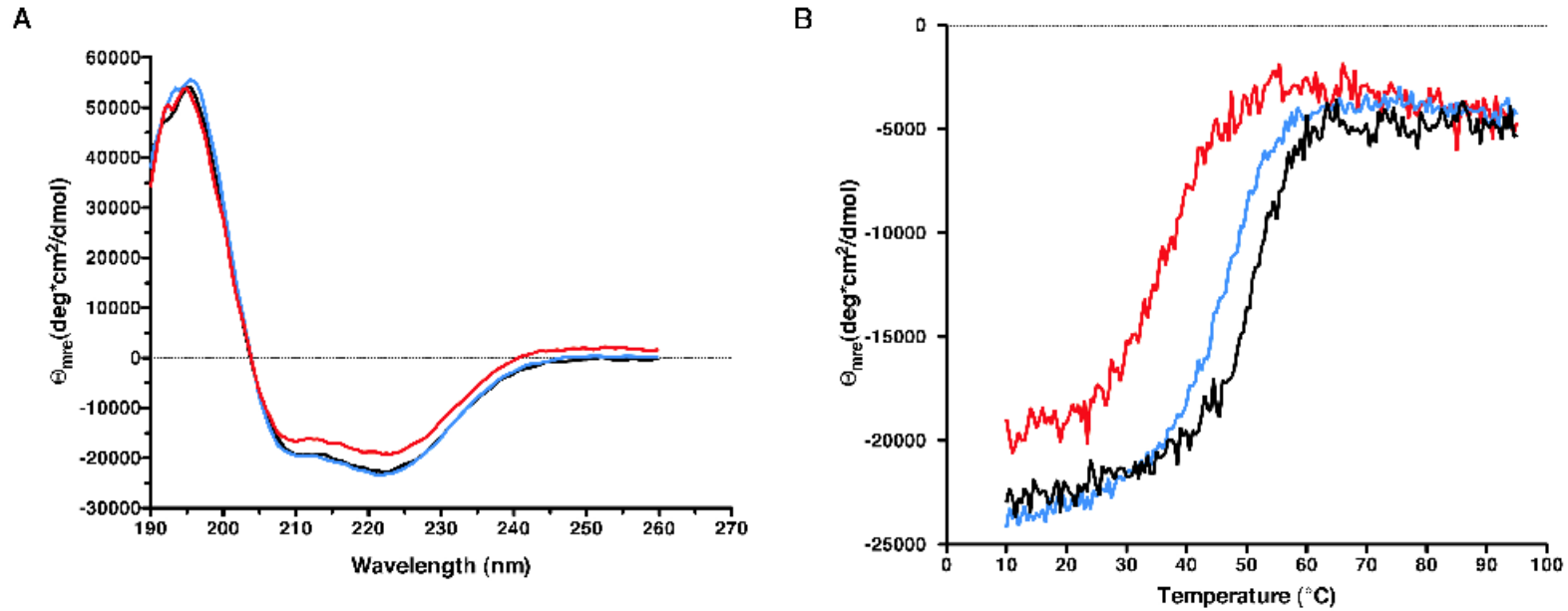


Figure 2.9. TPR2A domain is predominately α -helical and demonstrates increased stability at neutral pH.

(A) CD spectra of TPR2A collected at pH 5 (red), pH 6 (blue) and pH 7 (black). (B) Thermal melts of TPR2A monitored by CD at 220 nm collected at pH 5 (red), pH 6 (blue) and pH 7 (black).

2.3.5 Hsp90 binding to TPR2A

^1H - ^{15}N HSQC of the TPR2A domain collected in the absence and presence of equimolar concentrations of Hsp90 C-terminal peptide produced large chemical shift changes indicative of binding (Figure 2.10A). The magnitude of chemical shift perturbations for traceable residues was calculated from the combined chemical shift changes in ^1H and ^{15}N dimensions ($\Delta\omega = |0.2 * \Delta^{15}\text{N}| + |\Delta^{1\text{H}}\text{N}|$) in ppm. Residues demonstrating the largest combined chemical shift changes (> 0.1 ppm) clustered to the binding interface of the TPR2A-Hsp90 C-terminal peptide complex (Figure 2.10B). Residues mapping to the carboxylate clamp (K229, N233, N264, K301 and R305) which are involved in electrostatic interactions with the 'EEVD' motif based on the solved crystal structure, demonstrated large chemical shift change further confirming the assignment [11].

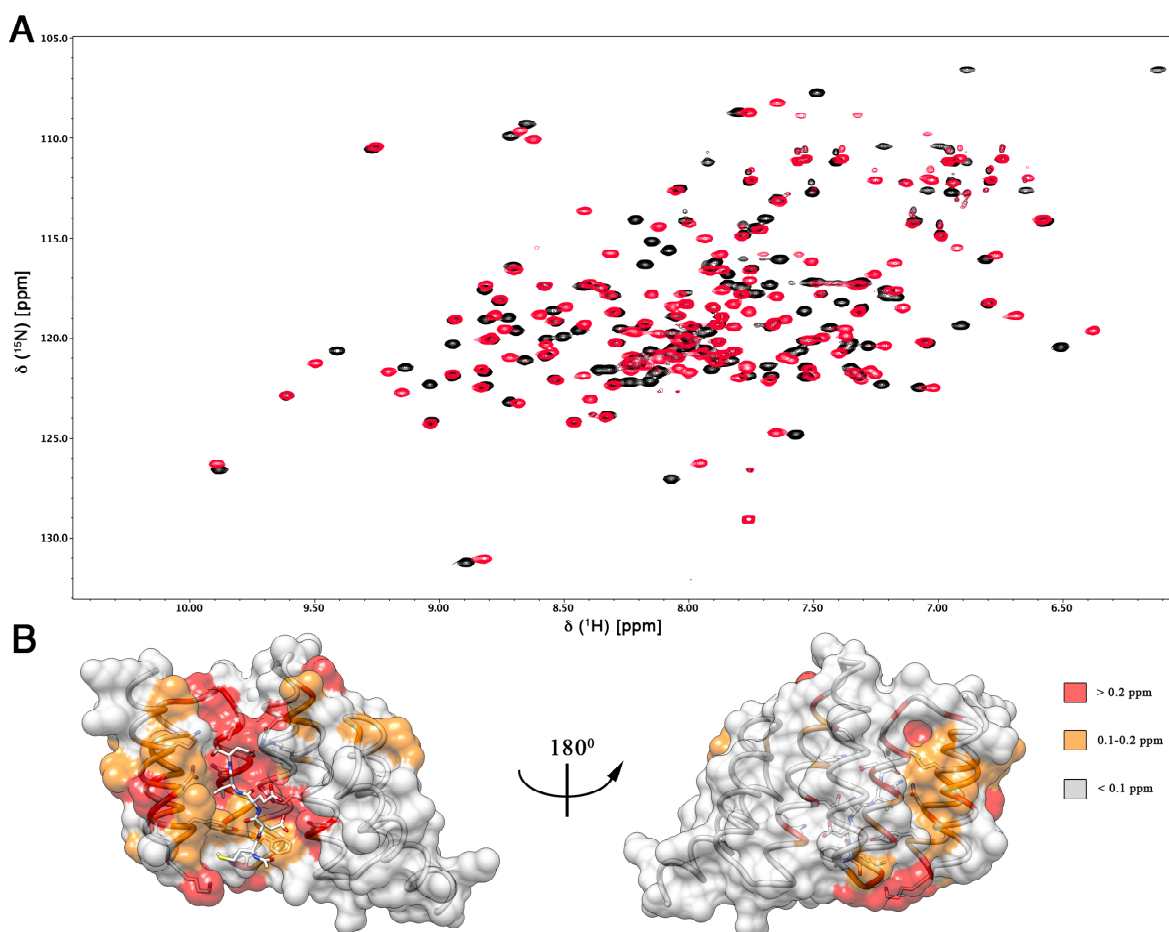


Figure 2.10. Chemical shift mapping of Hsp90 C-terminal peptide binding to TPR2A agrees with the solved crystal structure for the complex.

(A) Overlay of ^1H - ^{15}N HSQC spectra of TPR2A in the absence (*black*) and presence (*red*) of equimolar concentrations of Hsp90 C-terminal peptide. (B) Crystal structure of TPR2A in complex with Hsp90 peptide (PDB: 1ELR) with traceable chemical shift changes upon addition of Hsp90 peptide colored based on the magnitude of the combined chemical shift changes in ^1H and ^{15}N dimensions [11].

2.4 Discussion

STIP1 is composed of three TPR (TPR1, TPR2A and TPR2B) and two aspartate-proline rich (DP1 and DP2) domains that function in a coordinated manner during Hsp70 and Hsp90 client protein refolding [12]. Initial peptide recognition by Hsp70 is facilitated by the TPR1 domain, which is then transferred to TPR2B in the presence of Hsp90 by a flexible linker adjacent to the DP1 domain [15], presumably to mediate transfer of the client-bound Hsp70 to the HSP90 binding site in TPR2A. The minimal functional unit for glucocorticoid receptor activation *in vivo* spans the C-terminal TPR2A-TPR2B-DP2 fragment [14, 44]. Hsp90 clients include a number of proto-oncogenic tyrosine kinases and receptors including cyclin-dependent kinase-4, B-Raf, EGFR, HER2 and Bcr-Abl [45-49]. Traditional approaches in Hsp90 targeting involve small molecular inhibitors such as geldanamycin (GA) and the 17-AAG derivatives, which bind the ATP-binding pocket of Hsp90. However; this class of therapeutics has demonstrated high levels of toxicity in patients including anorexia, nausea, hepatotoxicity [50].

An alternative approach has been explored in small molecule inhibitors that disrupt Hsp90 interaction with TPR2A. These molecules share a 7-azaeridine ring core and inhibited Her2-positive human breast cancer cell lines [20]. The greater than 90% assignments of the TPR domains of mammalian STIP1 can be used to screen and optimize potential inhibitors of Hsp70 and Hsp90 binding and serve as potential cancer therapeutics. Previous structural NMR studies have focused on the yeast STIP1 homologue that shares only approximately 40% sequence identity. Thus, the mouse STIP1 assignments may be of great benefit in this approach as it is nearly identical to human STIP1.

The DP1 and DP2 domain solution structures have recently been solved by NMR, which revealed a novel α -helical fold [14]. The yeast and mouse STIP1's share approximately 40% sequence identity; however, SSP score analysis of the $^{13}\text{C}\alpha$ and $^{13}\text{C}\beta$ chemical shift deviations revealed a predicted α -helical arrangement of five α -helices separated by short interconnecting linkers and is in agreement with the yeast structure [14, 35]. The DP2 assignment may be used in the study of protein-protein interactions between DP2 and potential ligands. As well, disruption of the recently identified interactions with TPR2B of STIP1 may be of great interest, as the minimal functional fragment of STIP1 spans the TPR2A-TPR2B-DP2 domains and DP2 contacts with these TPRs may serve as another possible strategy to inhibit STIP1 function in oncogenic client folding [15].

Previous studies have disputed the monomeric state of STIP1 proposing alternate dimeric models as the biological unit [36-38]. Gel filtration chromatography and sedimentation equilibrium experiments presented here confirmed the monomeric state of STIP1 and TPR2A. Current models strongly suggest a monomeric model for STIP1 Hsp coordination with individual TPR domains facilitating concurrent interactions of Hsp70 and Hsp90 [14, 15, 40]. Previous discrepancies may have arisen due to the elongated structure of STIP1 domain arrangement, deviating from predicted globular proteins [14, 51].

To optimize conditions for STIP1 domains identified to bind PrP^C (TPR1 and TPR2A) (See chapter 4), their stability was assessed at various pH. Most PrP^C studies are conducted at low pH (~5); however, TPR stability appeared diminished at low pH based on circular dichroism. Thus, future studies with PrP^C may benefit from neutral conditions.

Indeed, PrP^C interactions and structural studies have been reported at neutral pH in low salt conditions.

The assigned backbone assignments of the TPR (TPR1, TPR2A and TPR2B) and DP (DP1 and DP2) assignments provide the foundation for future NMR studies involved in STIP1 ligands such as inhibitors of the Hsp90 pathway and the cellular prion protein (PrP^C). Stability screening of the PrP^C interacting domains (TPR1 and TPR2A) will facilitate the optimization of such studies.

2.5 References

- 1 Taipale, M., Jarosz, D. F. and Lindquist, S. (2010) HSP90 at the hub of protein homeostasis: emerging mechanistic insights. *Nat Rev Mol Cell Biol.* **11**, 515-528
- 2 Young, J. C., Agashe, V. R., Siegers, K. and Hartl, F. U. (2004) Pathways of chaperone-mediated protein folding in the cytosol. *Nat Rev Mol Cell Biol.* **5**, 781-791
- 3 Sato, S., Fujita, N. and Tsuruo, T. (2000) Modulation of Akt kinase activity by binding to Hsp90. *Proc Natl Acad Sci U S A.* **97**, 10832-10837
- 4 Stancato, L. F., Chow, Y. H., Hutchison, K. A., Perdew, G. H., Jove, R. and Pratt, W. B. (1993) Raf exists in a native heterocomplex with hsp90 and p50 that can be reconstituted in a cell-free system. *J Biol Chem.* **268**, 21711-21716
- 5 Xu, W., Mimnaugh, E., Rosser, M. F., Nicchitta, C., Marcu, M., Yarden, Y. and Neckers, L. (2001) Sensitivity of mature ErbB2 to geldanamycin is conferred by its kinase domain and is mediated by the chaperone protein Hsp90. *J Biol Chem.* **276**, 3702-3708
- 6 Trepel, J., Mollapour, M., Giaccone, G. and Neckers, L. Targeting the dynamic HSP90 complex in cancer. *Nat Rev Cancer.* **10**, 537-549
- 7 Smith, D. F., Sullivan, W. P., Marion, T. N., Zaitsev, K., Madden, B., McCormick, D. J. and Toft, D. O. (1993) Identification of a 60-kilodalton stress-related protein, p60, which interacts with hsp90 and hsp70. *Mol Cell Biol.* **13**, 869-876
- 8 Chen, S. and Smith, D. F. (1998) Hop as an adaptor in the heat shock protein 70 (Hsp70) and hsp90 chaperone machinery. *J Biol Chem.* **273**, 35194-35200
- 9 Hernandez, M. P., Chadli, A. and Toft, D. O. (2002) HSP40 binding is the first step in the HSP90 chaperoning pathway for the progesterone receptor. *J Biol Chem.* **277**, 11873-11881
- 10 Pratt, W. B. and Toft, D. O. (2003) Regulation of signaling protein function and trafficking by the hsp90/hsp70-based chaperone machinery. *Exp Biol Med (Maywood).* **228**, 111-133
- 11 Scheufler, C., Brinker, A., Bourenkov, G., Pegoraro, S., Moroder, L., Bartunik, H., Hartl, F. U. and Moarefi, I. (2000) Structure of TPR domain-peptide complexes: critical elements in the assembly of the Hsp70-Hsp90 multichaperone machine. *Cell.* **101**, 199-210
- 12 Odunuga, O. O., Longshaw, V. M. and Blatch, G. L. (2004) Hop: more than an Hsp70/Hsp90 adaptor protein. *Bioessays.* **26**, 1058-1068
- 13 Cortajarena, A. L. and Regan, L. (2006) Ligand binding by TPR domains. *Protein Sci.* **15**, 1193-1198

- 14 Schmid, A. B., Lagleder, S., Grawert, M. A., Rohl, A., Hagn, F., Wandinger, S. K., Cox, M. B., Demmer, O., Richter, K., Groll, M., Kessler, H. and Buchner, J. (2012) The architecture of functional modules in the Hsp90 co-chaperone Sti1/Hop. *EMBO J.* **31**, 1506-1517
- 15 Rohl, A., Wengler, D., Madl, T., Lagleder, S., Toppel, F., Herrmann, M., Hendrix, J., Richter, K., Hack, G., Schmid, A. B., Kessler, H., Lamb, D. C. and Buchner, J. (2015) Hsp90 regulates the dynamics of its cochaperone Sti1 and the transfer of Hsp70 between modules. *Nat Commun.* **6**, 6655
- 16 Fonseca, A. C., Romao, L., Amaral, R. F., Assad Kahn, S., Lobo, D., Martins, S., Marcondes de Souza, J., Moura-Neto, V. and Lima, F. R. (2012) Microglial stress inducible protein 1 promotes proliferation and migration in human glioblastoma cells. *Neuroscience.* **200**, 130-141
- 17 Walsh, N., Larkin, A., Swan, N., Conlon, K., Dowling, P., McDermott, R. and Clynes, M. (2011) RNAi knockdown of Hop (Hsp70/Hsp90 organising protein) decreases invasion via MMP-2 down regulation. *Cancer Lett.* **306**, 180-189
- 18 Horibe, T., Kohno, M., Haramoto, M., Ohara, K. and Kawakami, K. (2011) Designed hybrid TPR peptide targeting Hsp90 as a novel anticancer agent. *J Transl Med.* **9**, 8
- 19 Yi, F. and Regan, L. (2008) A novel class of small molecule inhibitors of Hsp90. *ACS Chem Biol.* **3**, 645-654
- 20 Pimienta, G., Herbert, K. M. and Regan, L. (2011) A compound that inhibits the HOP-Hsp90 complex formation and has unique killing effects in breast cancer cell lines. *Mol Pharm.* **8**, 2252-2261
- 21 Zanata, S. M., Lopes, M. H., Mercadante, A. F., Hajj, G. N., Chiarini, L. B., Nomizo, R., Freitas, A. R., Cabral, A. L., Lee, K. S., Juliano, M. A., de Oliveira, E., Jachieri, S. G., Burlingame, A., Huang, L., Linden, R., Brentani, R. R. and Martins, V. R. (2002) Stress-inducible protein 1 is a cell surface ligand for cellular prion that triggers neuroprotection. *EMBO J.* **21**, 3307-3316
- 22 Lopes, M. H., Hajj, G. N., Muras, A. G., Mancini, G. L., Castro, R. M., Ribeiro, K. C., Brentani, R. R., Linden, R. and Martins, V. R. (2005) Interaction of cellular prion and stress-inducible protein 1 promotes neuritogenesis and neuroprotection by distinct signaling pathways. *J Neurosci.* **25**, 11330-11339
- 23 Caetano, F. A., Lopes, M. H., Hajj, G. N., Machado, C. F., Pinto Arantes, C., Magalhaes, A. C., Vieira Mde, P., Americo, T. A., Massensini, A. R., Priola, S. A., Vorberg, I., Gomez, M. V., Linden, R., Prado, V. F., Martins, V. R. and Prado, M. A. (2008) Endocytosis of prion protein is required for ERK1/2 signaling induced by stress-inducible protein 1. *J Neurosci.* **28**, 6691-6702

- 24 Beraldo, F. H., Soares, I. N., Goncalves, D. F., Fan, J., Thomas, A. A., Santos, T. G., Mohammad, A. H., Roffe, M., Calder, M. D., Nikolova, S., Hajj, G. N., Guimaraes, A. L., Massensini, A. R., Welch, I., Betts, D. H., Gros, R., Drangova, M., Watson, A. J., Bartha, R., Prado, V. F., Martins, V. R. and Prado, M. A. (2013) Stress-inducible phosphoprotein 1 has unique cochaperone activity during development and regulates cellular response to ischemia via the prion protein. *FASEB J.* **27**, 3594-3607
- 25 Ostapchenko, V. G., Beraldo, F. H., Mohammad, A. H., Xie, Y. F., Hirata, P. H., Magalhaes, A. C., Lamour, G., Li, H., Maciejewski, A., Belrose, J. C., Teixeira, B. L., Fahnestock, M., Ferreira, S. T., Cashman, N. R., Hajj, G. N., Jackson, M. F., Choy, W. Y., MacDonald, J. F., Martins, V. R., Prado, V. F. and Prado, M. A. (2013) The prion protein ligand, stress-inducible phosphoprotein 1, regulates amyloid-beta oligomer toxicity. *J Neurosci.* **33**, 16552-16564
- 26 Pellecchia, M. (2005) Solution nuclear magnetic resonance spectroscopy techniques for probing intermolecular interactions. *Chem Biol.* **12**, 961-971
- 27 Rajagopal, P., Waygood, E. B., Reizer, J., Saier, M. H., Jr. and Klevit, R. E. (1997) Demonstration of protein-protein interaction specificity by NMR chemical shift mapping. *Protein Sci.* **6**, 2624-2627
- 28 Whitmore, L. and Wallace, B. A. (2008) Protein secondary structure analyses from circular dichroism spectroscopy: methods and reference databases. *Biopolymers.* **89**, 392-400
- 29 Sreerama, N. and Woody, R. W. (2000) Estimation of protein secondary structure from circular dichroism spectra: comparison of CONTIN, SELCON, and CDSSTR methods with an expanded reference set. *Anal Biochem.* **287**, 252-260
- 30 Delaglio, F., Grzesiek, S., Vuister, G. W., Zhu, G., Pfeifer, J. and Bax, A. (1995) NMRPipe: a multidimensional spectral processing system based on UNIX pipes. *J Biomol NMR.* **6**, 277-293
- 31 Johnson, B. A. and Blevins, R. A. (1994) NMR View: A computer program for the visualization and analysis of NMR data. *J Biomol NMR.* **4**, 603-614
- 32 Goddard, T. D. and Kneller, D. G. SAPRKY 3. ed.)^eds.)
- 33 Keller, R. (2005) Optimizing the Process of Nuclear Magnetic Spectrum Analysis and Computer Aided Resonance Assignment. ed.)^eds.), Swiss Federal Institute of Technology: Zurich
- 34 Pettersen, E. F., Goddard, T. D., Huang, C. C., Couch, G. S., Greenblatt, D. M., Meng, E. C. and Ferrin, T. E. (2004) UCSF Chimera--a visualization system for exploratory research and analysis. *J Comput Chem.* **25**, 1605-1612

- 35 Marsh, J. A., Singh, V. K., Jia, Z. and Forman-Kay, J. D. (2006) Sensitivity of secondary structure propensities to sequence differences between alpha- and gamma-synuclein: implications for fibrillation. *Protein Sci.* **15**, 2795-2804
- 36 Prodromou, C., Siligardi, G., O'Brien, R., Woolfson, D. N., Regan, L., Panaretou, B., Ladbury, J. E., Piper, P. W. and Pearl, L. H. (1999) Regulation of Hsp90 ATPase activity by tetratricopeptide repeat (TPR)-domain co-chaperones. *EMBO J.* **18**, 754-762
- 37 Carrigan, P. E., Nelson, G. M., Roberts, P. J., Stoffer, J., Riggs, D. L. and Smith, D. F. (2004) Multiple domains of the co-chaperone Hop are important for Hsp70 binding. *J Biol Chem.* **279**, 16185-16193
- 38 Flom, G., Behal, R. H., Rosen, L., Cole, D. G. and Johnson, J. L. (2007) Definition of the minimal fragments of Sti1 required for dimerization, interaction with Hsp70 and Hsp90 and in vivo functions. *Biochem J.* **404**, 159-167
- 39 Siligardi, G., Hu, B., Panaretou, B., Piper, P. W., Pearl, L. H. and Prodromou, C. (2004) Co-chaperone regulation of conformational switching in the Hsp90 ATPase cycle. *J Biol Chem.* **279**, 51989-51998
- 40 Rohl, A., Toppel, F., Bender, E., Schmid, A. B., Richter, K., Madl, T. and Buchner, J. (2014) Hop/Sti1 phosphorylation inhibits its co-chaperone function. *EMBO Rep.* **16**, 240-249
- 41 Hornemann, S., Schorn, C. and Wuthrich, K. (2004) NMR structure of the bovine prion protein isolated from healthy calf brains. *EMBO Rep.* **5**, 1159-1164
- 42 Riek, R., Hornemann, S., Wider, G., Glockshuber, R. and Wuthrich, K. (1997) NMR characterization of the full-length recombinant murine prion protein, mPrP(23-231). *FEBS Lett.* **413**, 282-288
- 43 Hornemann, S., von Schroetter, C., Damberger, F. F. and Wuthrich, K. (2009) Prion protein-detergent micelle interactions studied by NMR in solution. *J Biol Chem.* **284**, 22713-22721
- 44 Chang, H. C., Nathan, D. F. and Lindquist, S. (1997) In vivo analysis of the Hsp90 cochaperone Sti1 (p60). *Mol Cell Biol.* **17**, 318-325
- 45 Mimnaugh, E. G., Chavany, C. and Neckers, L. (1996) Polyubiquitination and proteasomal degradation of the p185c-erbB-2 receptor protein-tyrosine kinase induced by geldanamycin. *J Biol Chem.* **271**, 22796-22801
- 46 Shiotsu, Y., Neckers, L. M., Wortman, I., An, W. G., Schulte, T. W., Soga, S., Murakata, C., Tamaoki, T. and Akinaga, S. (2000) Novel oxime derivatives of radicicol induce erythroid differentiation associated with preferential G(1) phase accumulation against chronic myelogenous leukemia cells through destabilization of Bcr-Abl with Hsp90 complex. *Blood.* **96**, 2284-2291

- 47 Taipale, M., Krykbaeva, I., Koeva, M., Kayatekin, C., Westover, K. D., Karras, G. I. and Lindquist, S. (2012) Quantitative analysis of HSP90-client interactions reveals principles of substrate recognition. *Cell*. **150**, 987-1001
- 48 da Rocha Dias, S., Friedlos, F., Light, Y., Springer, C., Workman, P. and Marais, R. (2005) Activated B-RAF is an Hsp90 client protein that is targeted by the anticancer drug 17-allylamino-17-demethoxygeldanamycin. *Cancer Res*. **65**, 10686-10691
- 49 Ahsan, A., Ramanand, S. G., Whitehead, C., Hiniker, S. M., Rehemtulla, A., Pratt, W. B., Jolly, S., Gouveia, C., Truong, K., Van Waes, C., Ray, D., Lawrence, T. S. and Nyati, M. K. (2012) Wild-type EGFR is stabilized by direct interaction with HSP90 in cancer cells and tumors. *Neoplasia*. **14**, 670-677
- 50 Janin, Y. L. (2010) ATPase inhibitors of heat-shock protein 90, second season. *Drug Discov Today*. **15**, 342-353
- 51 Romano, S. A., Cordeiro, Y., Lima, L. M., Lopes, M. H., Silva, J. L., Foguel, D. and Linden, R. (2009) Reciprocal remodeling upon binding of the prion protein to its signaling partner hop/STI1. *FASEB J*. **23**, 4308-4316

3 Domains of STIP1 responsible for regulating the PrP^C-dependent amyloid- β oligomer toxicity

3.1 Introduction

Neurotoxic assemblies composed of soluble oligomers of the amyloid-beta peptide (A β O), derived from the sequential proteolytic cleavage of the amyloid precursor protein (APP), are thought to be critical for neurotoxicity in Alzheimer's disease (AD) [1, 2]. A β O_s interact with numerous neuronal receptors or channel proteins resulting in impairment of synaptic plasticity, oxidative stress, disruption of Ca²⁺ homeostasis, inhibition of long-term potentiation (LTP) and neuronal cell death [3-6].

The cellular prion protein (PrP^C) is a high affinity A β O receptor that has garnered interest in relation to A β O-induced synaptic dysfunction [6-8]. PrP^C is a highly expressed cell surface glycoprotein which functions as a membrane scaffold for numerous ligands resulting in modulation of cellular signaling events [9]. PrP^C-A β O complex formation is coupled to activation of Fyn kinase through mGluR5 resulting in deregulation of NMDA receptors and calcium signaling [10-12]. Residues 23-27 and 95-110 of the disordered N-terminal region of PrP^C have been proposed to mediate A β O binding [6, 13, 14]. Moreover, impairment of binding to residues 95-110 seems to alleviate A β O neurotoxicity [6, 7]. While PrP^C is not essential for all A β O-induced deficits, inhibition of hippocampal LTP, impaired synaptic plasticity, loss of dendritic spines and neuronal cell death seem to be PrP^C-dependent [6, 8, 15]. Disruption of A β O binding by antibodies directed against PrP^C mitigate A β O induced neurotoxicity, suggesting that modulation of A β O-PrP^C interactions may be of therapeutic value in AD [7, 16-18]. Notably, a ligand of

PrP^C, stress-inducible phosphoprotein 1 (STIP1), can inhibit A β O toxicity in neurons in a PrP^C-dependent manner [19]. Moreover, decreased levels of STIP1 in mammalian neurons or knockdown of STIP1 in *C. elegans* increases the toxicity of amyloid peptides [19, 20].

STIP1 is a cellular cochaperone that coordinates Hsp70 and Hsp90 interactions during folding of various cell cycle regulators and signal transduction proteins [21]. Interestingly, Hsp70, Hsp90 and STIP1 all can be secreted to the extracellular space through non-canonical pathways by extracellular vesicles, where they can increase cellular resilience by acting as extracellular chaperones or by signaling via membrane receptors [22-25]. In particular, STIP1 is secreted by astrocytes into the extracellular space, where it functions as a signaling molecule through PrP^C [22, 26]. Complex formation with PrP^C induces neuroprotective and neuroproliferative signaling via PKA and ERK pathways, respectively [27, 28], which is initiated by Ca²⁺ influx through the α 7 nicotinic acetylcholine receptor (α 7nAChR) in hippocampal neurons [29].

STIP1 is a modular protein composed of three structurally related tetratricopeptide repeat domains (TPR1, TPR2A and TPR2B), as well as two aspartate-proline-rich regions (DP1 and DP2). Hsp engagement is facilitated through sequential interactions with the TPR domains. Binding of Hsp70 and Hsp90 to the TPR1/TPR2B and TPR2A domains of the cochaperone STIP1, respectively, allows the transfer of clients from Hsp70 to Hsp90 [21, 30-33]. However, recent work suggests that interaction between STIP1 and Hsp90 is comprised of more extensive interactions with the N-terminal domain and middle domain of Hsp90 [34, 35]. Previous work indicated that amino acids 113-128 within PrP^C are critical for STIP1 interaction [19, 26, 36]. Giving

that STIP1 could potentially interact with PrP^C, Hsp90 and Hsp70 in the extracellular space, and this may modulate A β O toxicity, it is of importance to understand these protein interactions at the molecular level.

Here we provide structural insights into the roles of individual domains of STIP1 in interacting with PrP as well as in inhibiting the A β O-PrP binding. In addition, the potential of complex formation between STIP1, PrP, and Hsp90 is explored. Our results reveal multiple domain interactions between STIP1 and PrP are involved in complex formation and that the Hsp-interacting domains, TPR1 and TPR2A, directly inhibit A β O binding to PrP and neuronal toxicity. In addition, we show that Hsp90 is able to influence the interaction of STIP1 with PrP, inhibiting the neuroprotective role of STIP1 against A β O insult.

3.2 Materials and methods

3.2.1 Protein expression and purification

pDEST17 expression vectors (Invitrogen) encoding various mouse STIP1 domains (i.e. full-length STIP1, TPR1 (residues 1 -118), DP1 (residues 119-216), TPR2A (residues 217-352), TPR2B (residues 353-480) and DP2 (residues 481-542)) with an additional N-terminal tobacco etch virus (TEV) cleavable 6xHis tag were transformed into *Escherichia coli* (*E. coli*) BL21 (DE3) pLysS strain. *E. coli* were grown in standard M9 minimal media at 37 °C to an OD₆₀₀ of 0.9, at which point over-expression was induced with 1 mM isopropyl β -D-1-thiogalactopyranoside (IPTG). Temperature was reduced to 22 °C and cultures were grown overnight.

Proteins were initially purified by Ni²⁺-affinity chromatography using Ni Sepharose 6 Fast Flow beads (GE Healthcare). 6xHis tag was cleaved by incubation with 6xHis tagged TEV overnight at room temperature. Following cleavage, TEV and 6xHis tag were removed by an additional Ni²⁺-affinity chromatography purification [37]. For nuclear magnetic resonance (NMR) spectroscopy, cells were grown in standard M9 minimal medium supplemented with 1 g/L ¹⁵N-labeled ammonium chloride. Proteins were flash-frozen in liquid nitrogen and stored at -80 °C for no longer than a month. All NMR studies were conducted with freshly prepared protein.

N-terminal 6xHis tagged recombinant mouse PrP (23-231), (90-231) and (23-95) in pRSETA was graciously provided by Dr. Kurt Wüthrich (ETH Zurich, Zurich, Switzerland). Plasmids were transformed into *E. coli* BL21 (DE3) and cultures were grown in lysogeny broth (LB) to an OD₆₀₀ of 0.9. Expression was induced by the addition of 1 mM IPTG and cultures were grown overnight at 22 °C. Inclusion bodies were solubilized in 8 M urea containing 25 mM Tris, 500 mM NaCl, pH 7.5 and the resultant denatured protein was purified using Ni²⁺-affinity chromatography. Solubilized protein was refolded by dialysis against 10 mM sodium acetate, pH 5. Purified protein was exchanged into 10 mM HEPES, pH 7, and the N-terminal 6xHis tag was cleaved by overnight incubation with thrombin (Haematologic Technologies Inc.). Thrombin was then removed by incubation with Benzamidine Sepharose 4 Fast Flow (GE Healthcare).

pET28 vectors encoding Hsp90β containing an N-terminal 6xHis tag separated by a thrombin cleavage site (kindly provided by Dr. Johannes Buchner, Center for integrated protein science (CIPSM) at the Department Chemie, Technische Universität München,

Germany) were purified as described in [35]. Plasmid was transformed in *E. coli* BL21 (DE3) and cultures were grown in LB to an OD₆₀₀ of 0.9 and induced with 1 mM IPTG. Temperature was dropped to 30 °C and cultures were grown overnight. Bacterial pellets were resuspended in 40 mM potassium phosphate, 400 mM KCl, 5 mM ATP, 1 mM MgCl₂, 6 mM imidazole, pH 8, and lysed by French press at 10,000 psi. The resultant protein was purified using Ni²⁺ chromatography. Eluted fractions containing Hsp90β were combined and cleaved overnight by incubation with thrombin at 4 °C. Hsp90β was further purified by gel filtration chromatography with a Superdex S200 column equilibrated in 40 mM HEPES, 150 mM KCl, 5 mM MgCl₂, pH 7.5.

AβOs were prepared from Aβ₁₋₄₂ (rPeptide) as described previously [19]. Briefly, Aβ₁₋₄₂ was dissolved in 1,1,1,3,3,3-hexafluoro-2-propanol (HFIP) and SpeedVac centrifuged generating peptide films. Aβ₁₋₄₂ films were first re-suspended in DMSO to a concentration of 1 mM and diluted in PBS to a final working concentration of 100 μM or 150 μM for NMR experiments. Peptides were incubated for 24 hours at 4 °C and stored at -80 °C or used immediately.

3.2.2 NMR spectroscopy

Experiments were performed on a Varian Inova 600 MHz NMR spectrometer equipped with xyz-gradient triple resonance probe at 25 °C in 5 mM sodium phosphate, pH 7. Data were processed with NMRPipe and analyzed using NMRView [38, 39]. Chemical shift changes were mapped onto PrP (90-231) structure based on a previously completed amide assignment (BMRB 16071 deposited in the BioMagResBank (<http://www.bmrwisc.edu>))[40]. Binding of preformed AβOs to PrP (90-231) and (23-

95) was observed by ^1H - ^{15}N HSQC spectra collected in the presence and absence of equimolar concentration ($\sim 85 \mu\text{M}$) of A β O.

Backbone amide resonance assignments for TPR1 and TPR2A were obtained from the BioMagResBank under accession numbers 18691 and 18689, respectively [37]. ^1H - ^{15}N HSQC spectra of ^{15}N -labelled TPR1 (50 μM) and TPR2A (50 μM) were collected in the absence and presence of PrP(23-231) (50 μM). The magnitude of chemical shift perturbations for traceable residues was calculated from the combined chemical shift changes in the ^1H and ^{15}N dimensions ($\Delta\omega$ (ppm) = $|0.2 * \Delta^{15}\text{N}| + |\Delta^1\text{H}^{\text{N}}|$) and mapped onto the crystal structures of TPR1 (PDB: 1ELW) and TPR2A (PDB:1ELR) [30].

3.2.3 Protein-protein binding assay

10 μg of full-length PrP or N-terminal PrP (23-95) were immobilized onto Falcon 96-well polystyrene plates by incubation overnight at 4 $^\circ\text{C}$. Non-specific sites were blocked by incubation at room temperature for 1 hour with PBS-T (0.05%) containing 1% BSA. Plates were extensively washed with PBS-T and incubated with increasing concentrations of STIP1, different STIP1 domains, or Hsp90 for 1 hour. Following washing, bound proteins were detected using polyclonal antibodies directed towards STIP1 (1:10,000) in PBS-T. After subsequent washing, wells were probed with horseradish peroxidase (HRP)-conjugated anti-rabbit IgG (1:5000) (Bio-Rad) for 1 hour. The signal was visualized using o-phenylenediamine (OPD) and absorbance was measured at 495 nm by microplate reader.

For assessing PrP influence on Hsp90 binding to STIP1, polystyrene plates were covered with 10 μg of STIP1 and blocked as described above. After thorough washing,

plates were incubated with various concentrations of PrP for 1 hour at room temperature, followed by incubation with 2 μ M Hsp90 for 1 hour. After subsequent washing, wells were probed with rabbit anti-Hsp90 (1:1000, Cell Signaling) in PBS-T and bound Hsp90 was detected as outlined above.

TPR1 was labeled with Fluorescein-5-Maleimide (Invitrogen) as per manufacturer's instructions to investigate competition of binding between TPR domains to PrP. PrP was adsorbed on to black polystyrene plates as described above. Plates were incubated with 1 μ M fluorescein labeled TPR1 in the presence of various concentrations of TPR2A. Following washing, fluorescence was measured at excitation and emission wavelengths of 485/535 nm, respectively.

3.2.4 Surface plasmon resonance (SPR)

All SPR experiments were performed using a Biacore X system equipped with a CM 5 sensor chip (GE Healthcare). The chip was uniformly coated with PrP (23-231) using a standard amine-coupling method to an SPR signal of \sim 7000 resonance units (RU). Ligands were injected in 10 mM HEPES, 150 mM NaCl, pH 7, over an association period of 7 minutes at a flow rate of 5 μ L/min. Off-kinetics were measured for an additional 2 minutes following the end of sample injections. The CM5 chip surface was regenerated using a 10 mM hydrochloric acid pulse for 1 minute at a flow rate of 100 μ L/min between ligand injections.

3.2.5 Primary neuronal culture

Primary cultures of hippocampal neurons were obtained from E17.5 brains of wild-type (Prnp^{+/+}) mice from a C57BL6 background and prepared as previously

described [19]. Hippocampi were aseptically dissected in HBSS (Invitrogen) and cells were dissociated in 0.25% trypsin at 37 °C for 20 minutes. Proteolysis was inactivated by re-suspension and dissociation of cells in Minimum Essential Media (MEM) (Invitrogen) supplemented with 10% Fetal Bovine Serum, penicillin (100 IU), streptomycin (100 µg/mL) and glucose (0.5%). Cultures were maintained on poly-lysine-coated coverslips or plates in Neurobasal Media (Invitrogen) supplemented with 2% B-27 (Invitrogen), penicillin (100 IU), streptomycin (100 µg/mL) and L-glutamine (500 µM). Half of the culture media was replaced every 3-4 days for the duration of the culture.

3.2.6 Cell death and viability assay

Hippocampal cultures (10^5 cells/dish) were maintained for 11 days *in vitro* (DIV) then incubated with 1 µM A β O alone or in the presence of STIP1 (1 µM), TPR1 (2 µM), TPR2A (2 µM) or DP1 (2 µM) for 48 hours. Cell death was assayed using LIVE/DEAD Viability/Cytotoxicity Kit for mammalian cells (Invitrogen) as described by the manufacturer. NIH ImageJ Cell Counter plug-in was used to calculate percentage of dead cells (number of dead cells / (number of dead cells + number of viable cells)). For Hsp90 and A β O co-incubation experiments, cell cultures were incubated in the presence or absence of Hsp90 (2 µM) and A β O (1 µM) with various concentrations of STIP1 (0-600 nM) and incubated for 48 hours. Cell death was assayed as described above.

3.2.7 A β O binding to primary hippocampal neurons

13 DIV cultured neurons (6×10^4 cells/dish) were treated for 15 minutes with 200 nM A β O alone or in the presence of 500 nM STIP1 or 1 µM TPR1, TPR2A and DP1 at 37 °C. Following incubation, cells were washed with KRH buffer (125 mM NaCl, 5mM

KCl, 1.8 mM CaCl₂, 2.6 mM MgSO₄, 10 mM glucose, 5 mM HEPES, pH 7.2). Cells were fixed with 4% paraformaldehyde for 20 minutes, washed with PBS, permeabilized with 0.5% Triton X-100 in PBS for 5 minutes and blocked with 5% BSA (Sigma-Aldrich) in PBS for 1 hour at room temperature. Coverslips were incubated with antibodies against γ -tubulin (1:500; Abcam) and amyloid- β (6E10, 1:350; Covance) overnight at 4 °C. γ -tubulin and amyloid- β were detected by subsequent incubation with secondary Alexa Fluor-488 and Alexa Fluor-633-conjugated antibodies (Invitrogen), respectively, for 1 hour at room temperature. Immunofluorescence was detected on an LSM510 confocal microscope equipped with a 63x/1.4NA oil-immersion objective lens. The resultant fluorescence from neurites was integrated using NIH ImageJ software.

3.3 Results

3.3.1 Mapping of A β O interface on PrP

Previous studies have revealed that residues 95-110 of PrP^C play a pivotal role in mediating the interaction with A β O [6, 13, 16]. To refine the A β O binding-site on PrP in a residue specific basis, we performed ¹H-¹⁵N-HSQC experiments on ¹⁵N-labelled PrP (90-231) in the absence and presence of preformed A β O at a 1:1 molar ratio (Figure 3.1A). A significant decrease in signal intensity was observed for amide resonances spanning residues 90-110 of the disordered N-terminal of PrP (Figure 3.1C), while no new NMR peaks were observed in the PrP spectrum upon the addition of A β O. This loss in signal intensity is likely due to peak broadening resultant from residues 90-110 binding a large molecular weight species of A β O. No significant systematic changes in intensity were observed for C-terminal resonances, suggesting the A β O binding site is highly localized to the region spanning residues 90-110 of PrP (90-231) (Figures 3.1B and

3.1C). The greatest decreases in peak intensity were observed in a glycine-rich region N-terminal of the sequence (residues 91-100). Interestingly, small but notable chemical shifts were observed for C-terminal residues Leu125, His140, Gly142, Asn174 Val180, Asn181, His187, Thr188 and Val189. These changes are likely due to weak transient interactions with A β O or moderate conformational changes in PrP upon A β O binding. Unfortunately, we were unable to assign the N-terminal of PrP, residues 23-95, due to the high sequence redundancy and signal overlap of the spectrum. However, no significant intensity changes or chemical shift perturbations were seen in the visible peaks of the disordered N-terminal fragment PrP (23-95) in the presence of A β O (Figure 3.1D), which stresses the importance of residues 90-110 in PrP-A β O complex formation.

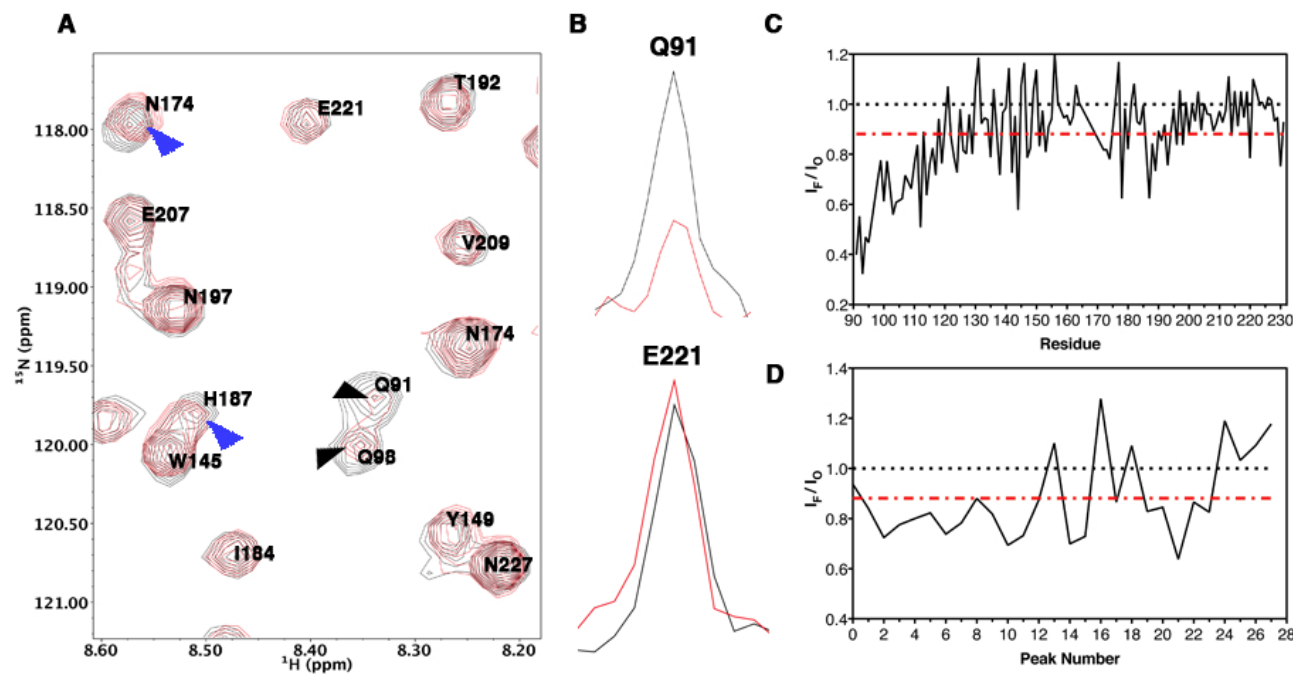


Figure 3.1. NMR reveals A β O associate with PrP residues 90-110.

(A) ^1H - ^{15}N HSQC spectra of PrP (90-231) in the absence (black) and presence (red) of mature A β_{1-42} oligomers at a 1:1 ratio. Residues that demonstrate a change in intensity (*black arrows*) or chemical shift changes (*blue arrows*) are noted. (B) Sample of one-dimensional traces of peak intensity presented in (A). Residues 90-231 show a loss in signal intensity (Q91) while C-terminal residues remain unchanged (E221). (C) Normalized peak intensity of PrP (90-231) plotted against residue number. (*black line*) Normalized peak intensity level expected if no interaction took place between PrP (90-231) and A β_{1-42} oligomers. (*red line*) Average normalized intensity decrease for all residues of PrP (90-231). (D) Normalized peak intensity of N-terminal PrP (23-95) peaks resolved in the ^1H - ^{15}N HSQC spectra in the presence of A β O. Due to signal overlap and sequence redundancy, the identity of the residues represented by each peak could not be determined and the thus were assigned an arbitrary number. (*black line*) Normalized peak intensity level expected if no interaction took place between PrP (23-95) and A β_{1-42} oligomers. (*red line*) Average normalized intensity decrease for all peaks of PrP (23-95).

3.3.2 Identification of STIP1 binding domains of PrP

We next sought to identify domains of STIP1 that bind PrP and the respective regions of PrP that mediate the interactions. Previous studies have identified the TPR2A domain of STIP1 as the major interaction site for PrP [19, 26, 36]. However, additional regions of STIP1 may be involved in PrP binding due to the modular structure of STIP1 and the structural similarity shared between its TPR domains. Of particular interest were STIP1 domains that specifically bind to PrP (90-231), since they may impair PrP-A β O complex and provide a mechanistic basis for STIP1 neuroprotective properties against A β O insult [19]. We tested binding of STIP1 and its domains using a multi-well protein-binding assay. The domain boundaries of STIP1 are shown in Figure 2A. We confirmed that STIP1 specifically bound PrP with high affinity (Figure 3.2B), $K_d = 186 \pm 15$ nM), which is in agreement with previous studies [26]. Probing full-length PrP with individual domains of STIP1 revealed that TPR1 ($K_d = 1.2 \pm 0.2$ μ M) and DP1 ($K_d = 600 \pm 50$ nM), in addition to the previously reported TPR2A ($K_d = 800 \pm 130$ nM) domain, can also interact with PrP with comparable affinity, albeit lower than the affinity of full length STIP1 (Figure 3.2C). The DP1 domain of STIP1 was capable of interacting in a specific and saturable manner with an N-terminal fragment of PrP (23-95), whereas the other domains (TPR1 and TPR2A) did not (Figure 3.2D). The results strongly suggest that DP1 interacts with the disordered N-terminal fragment of PrP (23-95), while PrP (90-231) binds TPR1 and TPR2A. The result is consistent with finding of previous studies showing that residues 113-128 of mouse PrP is responsible for mediating the interaction with the TPR2A domain of STI1P [26].

Since TPR1 and TPR2A both bind the C-terminal fragment of PrP (90-231), we investigated whether these domains can bind simultaneously or compete for binding to PrP. TPR2A was capable of displacing fluorescently labeled TPR1 from its complex with PrP in a concentration-dependent manner suggesting that binding of TPR1 and TPR2A to PrP is mutually exclusive (i.e. the TPR1 and TPR2A binding sites on PrP are either overlapping or in close proximity) (Figure 3.2E).

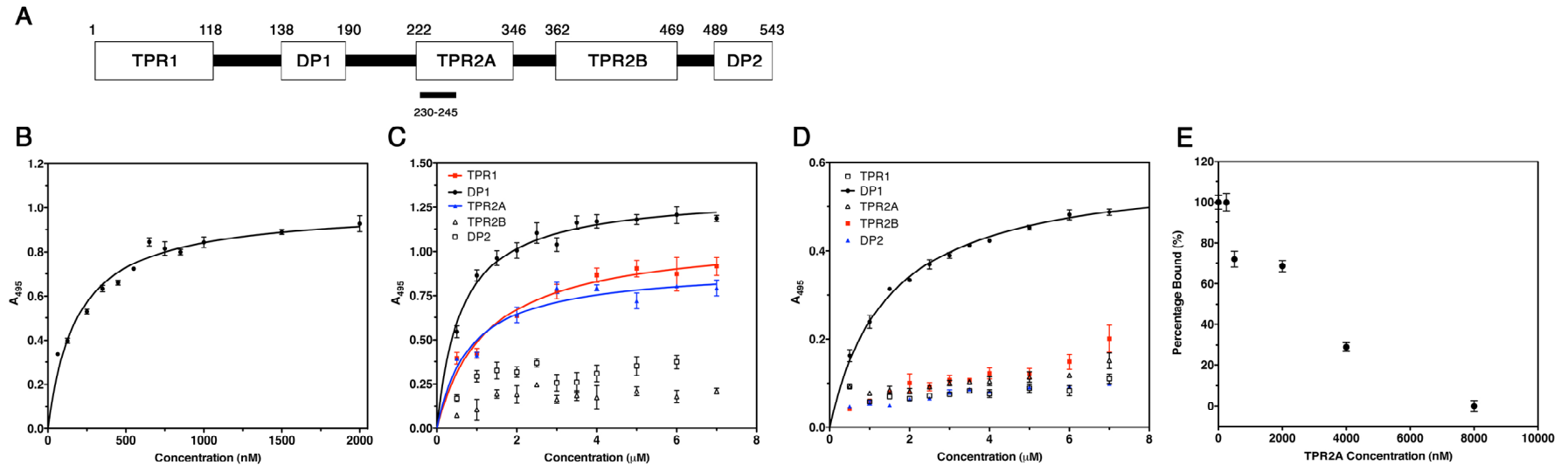


Figure 3.2. DP1, TPR1 and TPR2A associate with PrP.

(A) Domain structure of STIP1 illustrating domain boundaries of three TPR (TPR1, TPR2A and TPR2B) and two DP (DP1 and DP2) domains. (B) Polystyrene plates were pre-coated with 10 μ g of PrP (23-231). Wells were probed with various concentrations of STIP1 (B) or STIP1 domains (C). STIP1 or domain immunoreactivity was detected using polyclonal anti-STIP1 antibodies and binding is presented as OD₄₉₅ values. (D) N-terminal PrP (23-95) was incubated with increasing concentrations of STIP1 domains. Binding of the domains was detected as in (B and C) ($n=3$). (E) Immobilized PrP (23-231) was incubated with 1 μ M fluorescein-labeled TPR1 in the presence of various concentrations of TPR2A ($n=4$). Fluorescence of bound TPR1 was measured at excitation and emission wavelengths of 485/535 nm, respectively.

3.3.3 TPR1 and TPR2A prevent A β O binding to PrP

We have previously demonstrated that the TPR2A domain of STIP1 is able to inhibit A β O binding to PrP, albeit with lower potency than full length STIP1 [19]. Given that TPR1 and TPR2A can both bind to the C-terminal part of PrP (residues 90-231), we investigated whether TPR1 can modulate A β O-PrP binding by surface plasmon resonance (SPR). A β O injections showed a dose-dependent increase in response monitored by SPR indicating binding (Figure 3.3A). Co-injection of STIP1 (62.5 nM) with a constant concentration of A β O showed an appreciable decrease in the response signal, suggesting inhibition of A β O binding to PrP. When co-injected with 125 nM STIP1, the response from A β O was equal to that of an injection of 125 nM STIP1 alone, suggesting complete inhibition of A β O binding (Figure 3.3B). Injections of TPR1 or TPR2A domains also inhibited A β O binding to PrP in a dose-dependent manner, albeit at higher concentrations than full-length STIP1 (Figures 3.3C and 3.3D, respectively). DP1, which binds the N-terminal region of PrP (residues 23-95), did not have any effect on A β O signals, consistent with this region being dispensable for A β O binding to PrP (Figure 3.3E). Injection of each domain individually produced no detectable signal likely due to their small size and sensitivity of the instrument (data not shown). These results suggest that both the TPR1 and the TPR2A domains of STIP1 contribute to the direct inhibition of A β O binding to PrP through interactions with PrP (90-231).

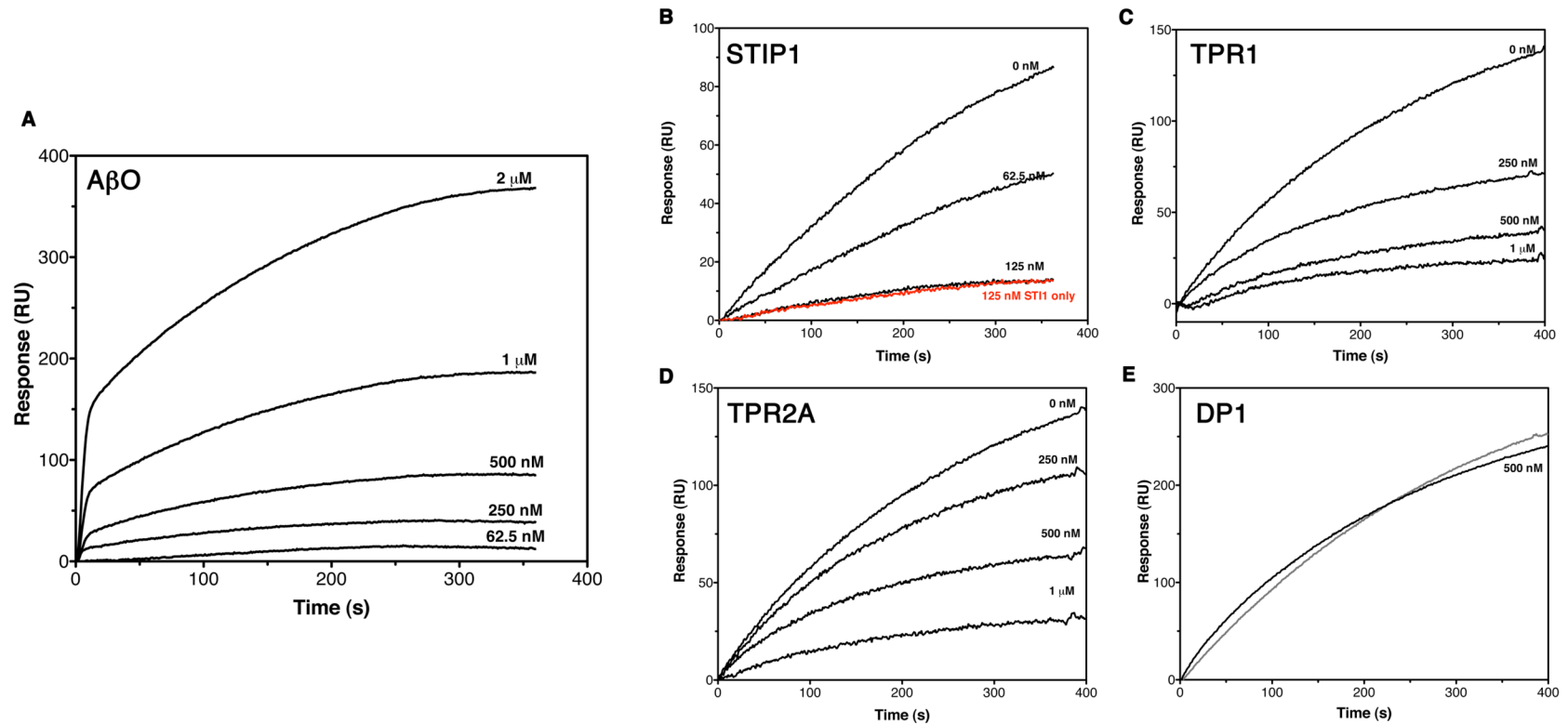


Figure 3.3. TPR1 and TPR2A, but not DP1, inhibit AβO binding to PrP(23-231) in vitro.

PrP (23-231) was covalently immobilized on to a CM5 sensor chip. (A) Sensograms were collected for various AβO concentrations binding to PrP (23-231). (B-E) Binding of AβO (2 μM) in the presence of increasing concentrations of STIP1 (B), TPR1 (C), TPR2A (D) or DP1 (E).

3.3.4 TPR1 and TPR2A inhibit A β O binding and toxicity in neurons

STIP1 is a neuroprotective regulator of A β O toxicity in hippocampal neurons and TPR2A domain by itself can reproduce this effect [19]. We therefore investigated whether *in vitro* inhibition of A β O binding to PrP by TPR1 can also translate to a beneficiary response in cultured primary mouse hippocampal neurons. Ectopic treatment of neurons with recombinant STIP1, TPR1 or TPR2A domains in the presence of A β O significantly decreased A β O binding to neuronal cell bodies compared to treatment with A β O alone (Figures 3.4A and 3.4B). Co-treatment of neuronal cultures with A β O and DP1 resulted in no visible effect on the amount of A β O bound to neurites. These observations reflected our *in vitro* SPR results where only the TPR1 and TPR2A domains, but not DP1, were able to inhibit A β O binding to PrP in a concentration-dependent manner. To assess if the decrease in A β O binding translated to inhibition of A β O cytotoxicity, primary hippocampal neurons were treated with A β O in the presence or absence of STIP1, TPR1, TPR2A or DP1 and incubated for 48 hours before assessing the number of dead cells. A β O treatment alone increased cell death by ~15% compared to basal levels. Co-treatment with STIP1, TPR1 or TPR2A rescued neuronal death from A β O induced toxicity (Figure 3.4C). No discernible effect on cell viability was seen in cells co-treated with DP1 and A β O compared to A β O treatment alone.

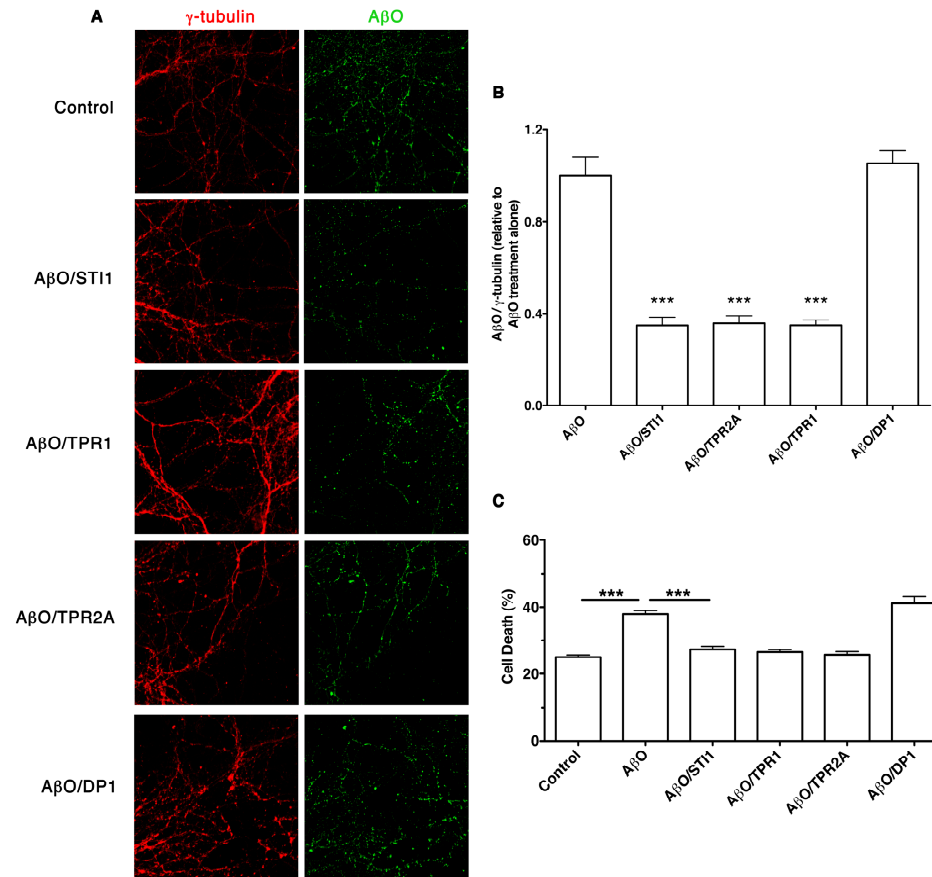


Figure 3.4. STIP1, TPR1 and TPR2A inhibit A β O binding and toxicity in primary mouse hippocampal neurons.

(A) Representative images of 13 DIV neurons stained for γ -tubulin (red) and β -amyloid (green) after treatment with A β O in the presence of STIP1, TPR1, TPR2A or DP1. (B) Quantification of A. (C) Comparison of neuronal cell death after 48 hours treatment with A β O (1 μ M) alone or in the presence of STIP1 (1 μ M), TPR1 (2 μ M), TPR2A (2 μ M) or DP1 (2 μ M). Experiments were analyzed by one-way ANOVA, followed by Tukey's *post hoc* test. *** $P < 0.001$, (n=3).

3.3.5 Mapping of TPR1 and TPR2A interfaces mediating PrP binding

To gain molecular understanding of the STIP1-PrP interactions, NMR spectroscopy was used to map the binding interfaces of PrP on TPR1 and TPR2A on a residue-specific manner. ^1H - ^{15}N HSQC spectra of TPR1 and TPR2A showed comparable amplitude of chemical shift perturbations upon addition of PrP (Figures 3.5A and 3.5C). Resonances undergoing fast exchange (i.e. chemical shift difference between the free and bound states is small compared to the rate of exchange between these two states) were traced upon titration of PrP and were mapped onto the crystal structures of TPR1 and TPR2A (Figures 3.5B and 3.5D). Notable chemical shift changes were observed for residues Asp70, Trp71, Gly98, Lys100, His101 and Ala103 of TPR1, which form a contiguous patch on the surface of the C-terminal part of the TPR1 structure (Figure 3.5B). In contrast, the TPR2A binding interface for PrP is more extensive, extending diagonally across a hydrophobic cradle-shaped groove on one side of the TPR2A molecule. Interestingly, this cradle-shaped groove is reserved for binding of the C-terminal peptide of Hsp90 to fulfill STIP1 cochaperone function during protein client folding [30]. While critical contacts between TPR2A and Hsp90 C-terminal peptide made by the carboxylate clamp (Lys229, Asn233, Asn264, Lys301, Arg305) of TPR2A did not show the largest chemical shift changes upon binding of PrP, the partial overlap between the Hsp90 and PrP binding interfaces suggests that Hsp90 and PrP may regulate each other's binding to STIP1 (Figure 3.6A). Therefore, we examined the potential for cooperative binding and complex formation for STIP1, PrP and Hsp90.

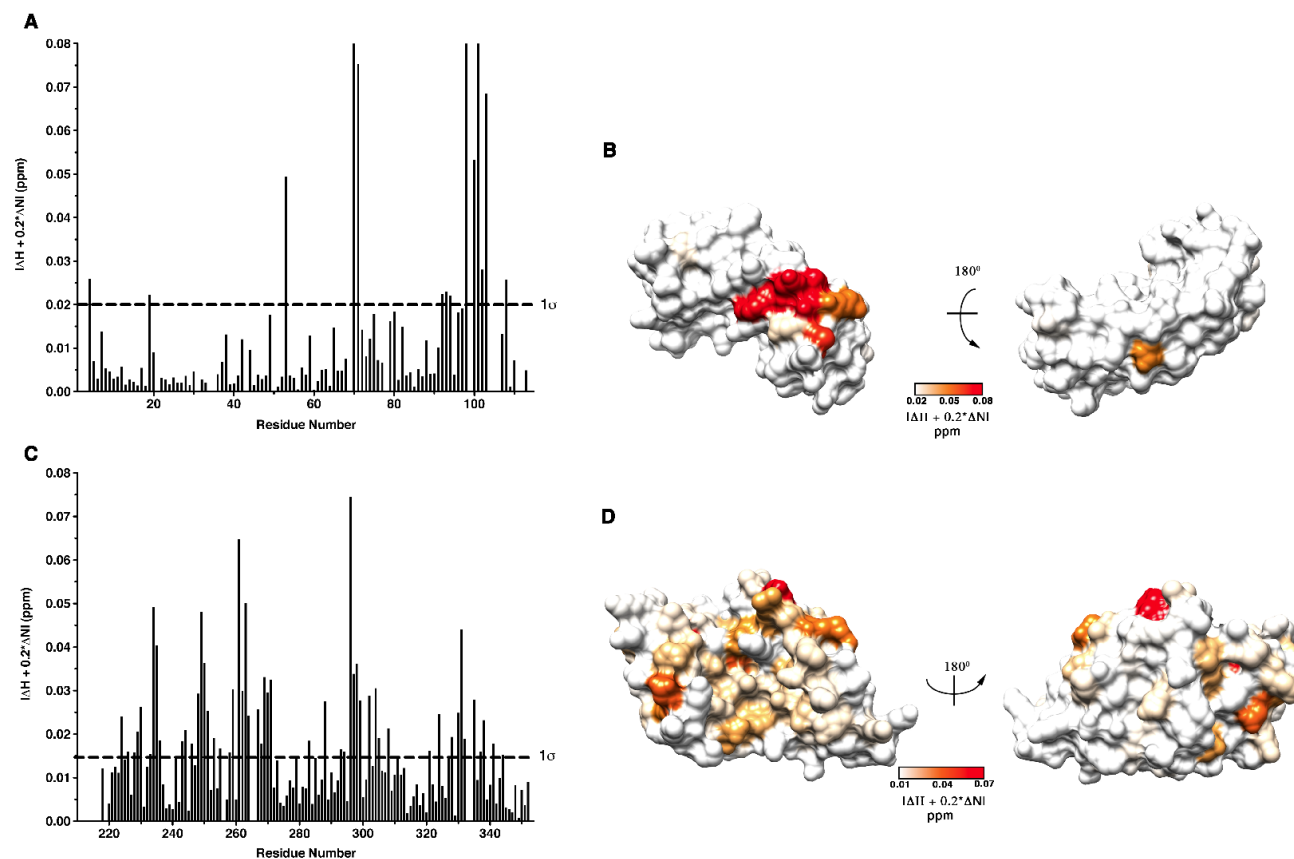


Figure 3.5. NMR indicates distinct regions of TPR1 and TPR2A interact with PrP(23-231).

(A) Graphical representations of chemical shift changes observed in ^1H - ^{15}N spectra of ^{15}N -labelled TPR1 or (C) TPR2A in the presence of PrP(23-231). (B) Combined chemical shift changes mapped on to the crystal structure of TPR1 (PDB:1ELW) or (D) TPR2A (PDB:1ELR). The protein structure images are generated using the Chimera molecular graphics software [54].

STIP1 was adsorbed onto polystyrene plates and probed with PrP. Following thorough washing of the complex; plates were incubated with a constant amount of Hsp90 (4 μM) and bound Hsp90 was detected using antibodies directed against Hsp90. Intriguingly, by increasing the concentration of PrP we achieved a saturable increase in Hsp90 binding to the plate (Figure 3.6B). In contrast, no Hsp90 binding was detected to PrP immobilized onto a polystyrene plate in the absence of STIP1 (Figure 3.6C). These data suggest that PrP binding to STIP1 may induce conformational changes in the complex, which in turn may increase the recruitment of Hsp90.

To investigate the potential relevance for the ternary complex formation of STIP1, Hsp90 and PrP in A β O toxicity, primary mouse hippocampal neurons were incubated in the presence of A β O (1 μM) and sub-optimal concentrations of STIP1. STIP1 caused a dose-dependent decrease of A β O-induced cell death (Figure 3.6D). However, addition of excess recombinant Hsp90 (2 μM) prevented STIP1 neuroprotection against A β O (Figure 3.6D). These results suggest that excess Hsp90 is able to block STIP1 neuroprotective signaling, potentially by sequestering the protein or by interfering with signaling events through PrP at the cellular membrane.

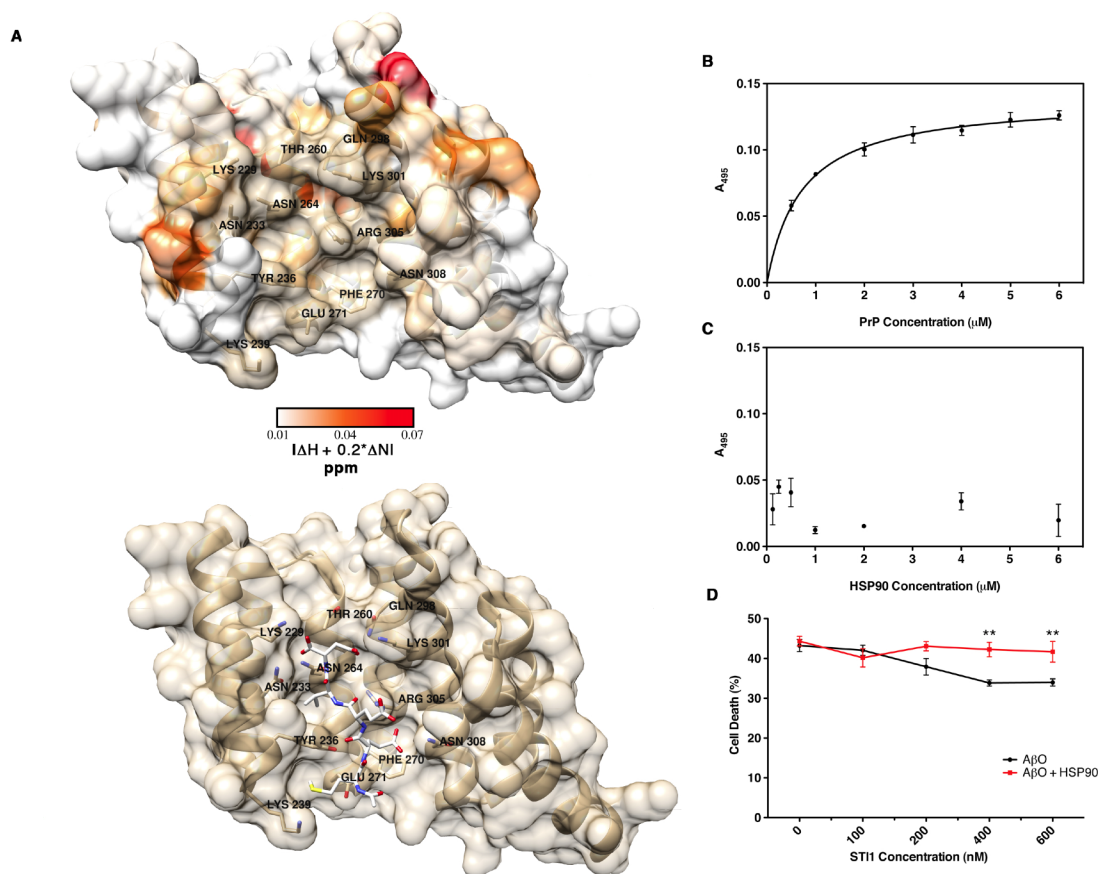


Figure 3.6. Hsp90 inhibits STIP1 rescue of primary mouse hippocampal neurons against A β O induced cell death.

(A) Chemical shift changes of PrP binding site on TPR2A (top) compared to the solved crystal structure of Hsp90 C-terminal MEEVD peptide bound to TPR2A (bottom) (PDB:1ELR). Residues of TPR2A involved in electrostatic interactions, hydrogen bonding or Van der Waals interactions with Hsp90 peptide are labeled (black). The protein structure images are generated using the Chimera molecular graphics software [54]. (B) Polystyrene plates pre-coated with 10 μg of STI1P were first incubated with increasing concentration of PrP, followed by incubation with Hsp90 (2 μM). Bound Hsp90 was detected using polyclonal anti-Hsp90 antibodies. Binding is presented as OD₄₉₅ values ($n=3$). (C) Polystyrene plates were pre-coated with 10 μg of full-length PrP (23-231). Wells were probed with various concentrations of Hsp90, followed by detection of bound Hsp90 using polyclonal anti-Hsp90 antibodies. Binding is presented as OD₄₉₅ values ($n=3$). (D) Comparison of cell death of 13 d neurons after 48 hour treatment with A β O (1 μM) and various concentrations of STI1P (0-600 nM) in the presence (red) or absence of HSP90 (2 μM) (black) ($n=7$). Experiments in the presence or absence of Hsp90 were analyzed by two-way ANOVA, followed by Bonferroni's *post hoc* test. ** $P<0.01$.

3.4 Discussion

A β O_s have been demonstrated to trigger synaptic dysfunction through interactions with several neuronal receptors [3-5, 41]. Numerous studies have identified PrP^C as a high affinity receptor for A β O_s and implicated the interaction in the transmission of neurotoxic signaling [6, 15, 17]. Disruption of the PrP^C-A β O complex has shown therapeutic merit in the reduction of A β O toxicity [7, 19]. We have recently determined that the cellular cochaperone and physiological PrP^C ligand STIP1 is able to directly inhibit A β O binding to PrP^C and alleviate synaptic loss, depression of long-term potentiation and neuronal cell death [19]. Therefore, understanding how this complex is modulated is of importance.

The studies reported here provide molecular insights regarding the functional modules of STIP1 that directly contribute to its recently described protective role against A β O neurotoxicity and structural details of regions involved in binding to PrP. Our NMR studies revealed significant resonance attenuations in the N-terminal unstructured region of PrP encompassing residues 90-110 upon binding of mature preformed A β O_s, suggesting these residues mediate complex formation. These results are consistent with previous observations, which indicated residues centered around 95-110 are essential and sufficient for A β O binding to PrP [6, 7, 13, 14]. No significant chemical shift changes were observed upon the addition of A β O to N-terminal PrP (23-95). A short highly basic charge cluster 'KKRPK' located in the far N-terminal of PrP (residues 23-27) has been suggested as a secondary A β O binding; however, other groups have reported near identical A β O binding levels to PrP (90-231) as wild-type PrP [13, 42]. It is possible the charge cluster acts as a secondary binding event following initial association of A β O to

the primary binding site (residues 90-110). Thus, residues 23-95 may not participate in binding in the absence of the high affinity site, which could explain the lack of large chemical shift perturbations of PrP (23-95). Unfortunately, due to high sequence redundancy and peak overlap problems owing to its disordered properties, we were unable to assign residues 23-95 of PrP constructs. Thus, we cannot rule out the possibility of minor, but localized chemical shift changes in residues 23-95 upon A β O titration.

Small chemical shift changes were noted for C-terminal PrP residues mapping to α -helices 1 and 2. These changes were much smaller in magnitude than those observed for the primary A β O binding site. These findings are unexpected, since the globular part of C-terminal portion of PrP is thought to be dispensable in its interaction with A β O. These changes may result from conformational alterations in helix 1-helix 2 of PrP upon A β O interaction. Alternatively, transient contacts between PrP molecules may be induced upon binding to A β aggregates, stabilizing these complexes. Indeed, competition experiments targeting an epitope spanning residues 131-153 effectively disrupted A β O binding to PrP [7].

Our protein-protein binding assay results showed that full-length STIP1 binds to PrP (23-231) with high affinity ($K_d \sim 186$ nM), which is in agreement with previous finding [26, 36]. Surprisingly, binding of different domains of STIP1 to PrP (23-231) indicated that not only previously identified TPR2A, but also the structurally related TPR1 domain and the DP1 domain bind PrP with high affinity. TPR2A was capable of displacing TPR1 binding to PrP suggesting that they have overlapping binding sites or TPR2A is capable of occluding the TPR1 binding site on PrP. Interestingly, DP1 domain bound to the N-

terminal of PrP (residues 23-95), while the TPR domains did not, suggesting their binding-site on PrP lies within residues 90-231. The recently solved NMR structures of the DP1 and DP2 domains of yeast STIP1 reveal a novel α -helical fold composed of 6 and 5 helices, respectively [35]. Electrostatic potentials of DP1 illustrate a slightly positive groove containing an additional α -helix absent in DP2, which stabilizes secondary structure elements in DP1. Consequently, while both DP1 and DP2 share a common tertiary structure, these distinct structural differences may indicate the inability of DP2 to bind to the N-terminal of PrP.

Even though the function of the DP domains remains uncertain, the length of the linker between TPR1 and TPR2A, which includes the DP1 domain, has recently been proposed to facilitate transfer of Hsp90 from TPR1 to TPR2B during protein client folding [33]. This is the first study to identify a direct ligand of DP1, suggesting the domain may influence STIP1 binding to physiological ligands outside of its cochaperone role in client protein refolding.

We confirmed by SPR the dose-dependent specific interaction between immobilized PrP and A β O. Due to the abnormally long dissociation kinetics, consistent with other studies, we were unable to quantitatively determine a binding constant for the interaction [13, 19, 43]. Thus, the effects of STIP1 and individual domains on A β O were assessed qualitatively based on the absolute magnitude of the response change. STIP1 effectively inhibited A β O binding to PrP, abolishing the interaction at low nanomolar concentrations, as demonstrated previously [19]. TPR2A and TPR1 domains were also capable of inhibiting A β O binding to PrP albeit at much greater concentrations than

STIP1, in agreement with our previous observations of STIP1 having a greater binding affinity than the individual domains alone, supporting the notion of multiple binding sites. DP1, the N-terminal PrP-binding domain of STIP1, had no discernible effect on A β O binding with full-length PrP, which agrees with C-terminal PrP being the primary A β O binding site. While DP1 may not actively disrupt A β O interaction with PrP, it may contribute to the greater binding affinity of full length STIP1 binding to PrP and thus its efficacy as an A β O inhibitor. Further investigation will be needed to determine the molecular basis by which DP1, TPR1, and TPR2A domains inhibit PrP-A β O binding in the full-length context.

A β O binding to neurons leads to cell death and impaired synaptic plasticity through multiple signaling pathways [10, 44, 45]. Activation of aberrant NMDAR signaling by A β O interaction to PrP^C resulting in hyper excitability and activation of Fyn kinase has been implicated in dendritic spine loss and neuronal cell death. We found that treatment of primary mouse hippocampal neurons with STIP1, TPR1 or TPR2A reduced the amount of A β O bound to the neuronal surface. Importantly, decrease in A β O binding translated to rescue of neuronal cell death. Consistent with the inability of DP1 to inhibit A β O binding *in vitro*, DP1 had no notable effect on binding of A β O to neurons or on cell death. These results suggest that the TPR1 and TPR2A domains of STIP1 may cooperate for the neuroprotective effects of STIP1 against A β O insult through PrP^C.

Tetratricopeptide repeat motifs are highly degenerate 34 amino acids sequences arranged into helix-loop helix structures forming adjacent anti-parallel helices [46]. The high structural similarity between the TPR1 and TPR2A domains and their similar

properties in inhibition of A β O binding to PrP led us to investigate whether these two regions bind similarly to PrP at the structural level using NMR. Intriguingly, the binding interfaces of TPR1 and TPR2A with PrP differ significantly. PrP bound TPR1 in a short region encompassing the C-terminus of helix 6 and its respective interconnecting loop region with helix 7. This region is far removed from the traditional TPR binding site involved in protein-protein interactions.

The TPR2A interface extends diagonally across a hydrophobic cradle-shaped groove on a single face of the TPR2A molecule [30]. Notably, this region overlaps with the Hsp90 binding site of TPR2A, which is formed by electrostatic interactions with highly conserved carboxylate clamp residues of TPR2A and the C-terminal EEVD motif of Hsp90 [30]. Significant chemical shift changes were observed in residues corresponding to the carboxylate clamp, as well as in additional residues occupying the cradle-shaped groove that binds Hsp90.

While Hsp90 plays an important role in assisting and maintaining the proper folding of many non-natively structured proteins, it has been implicated as detrimental in the clearance of hyper-phosphorylated tau and A β , the pathological species in AD [47-49]. Along with this, Hsp90 inhibitors have been shown to be effective in facilitating tau clearance and inhibiting A β neurotoxicity in mice [50]. In addition, actively secreted Hsp90 also contributes to the regulation of extracellular client proteins [24, 51]. Given that both STIP1 and Hsp90 are secreted, it is plausible that extracellular Hsp90 may influence STIP1 interaction with PrP in the extracellular matrix or on the cell membrane. Interestingly, while the TPR2A interfaces for Hsp90 and PrP binding show large overlapping regions, PrP binding to STIP1 appears to promote ternary complex formation

with Hsp90. PrP binding to STIP1 has been suggested to induce conformational changes in PrP resulting in loss of helical structure [36]. The STIP1 induced unfolding may reveal previously buried hydrophobic pockets on PrP, thus mimicking a misfolded protein and resulting in the recruitment of Hsp90. Alternatively, Hsp90 binding to TPR2A domain of STIP1 may induce structural rearrangements in both proteins, which may hinder STIP1 signaling through PrP. However; the relationship and potential interplay between STIP1, Hsp90 and the PrP is poorly understood and will require further study regarding their roles in the extracellular environment and implications in AD.

STIP1 has traditionally been considered as a cochaperone in the regulation of Hsp70 and Hsp90 client protein folding, however; strong evidence has revealed its importance as a signaling molecule through PrP in neuroprotection [27, 29-31, 35, 52, 53]. The modular structure of STIP1 allows for multiple domains to contribute to complex formation with PrP, which have a direct influence on its protective role against A β O insult. In addition, our studies indicate the possibility of ternary complex formation composed of PrP, STIP1 and Hsp90, which may influence STIP1 neuroprotective signaling against A β O toxicity in AD.

3.5 References

- 1 Cleary, J. P., Walsh, D. M., Hofmeister, J. J., Shankar, G. M., Kuskowski, M. A., Selkoe, D. J. and Ashe, K. H. (2005) Natural oligomers of the amyloid-beta protein specifically disrupt cognitive function. *Nat Neurosci.* **8**, 79-84
- 2 Mucke, L. and Selkoe, D. J. (2012) Neurotoxicity of amyloid beta-protein: synaptic and network dysfunction. *Cold Spring Harb Perspect Med.* **2**, a006338
- 3 Lambert, M. P., Barlow, A. K., Chromy, B. A., Edwards, C., Freed, R., Liosatos, M., Morgan, T. E., Rozovsky, I., Trommer, B., Viola, K. L., Wals, P., Zhang, C., Finch, C. E., Krafft, G. A. and Klein, W. L. (1998) Diffusible, nonfibrillar ligands derived from Abeta1-42 are potent central nervous system neurotoxins. *Proc Natl Acad Sci U S A.* **95**, 6448-6453
- 4 Walsh, D. M., Klyubin, I., Fadeeva, J. V., Cullen, W. K., Anwyl, R., Wolfe, M. S., Rowan, M. J. and Selkoe, D. J. (2002) Naturally secreted oligomers of amyloid beta protein potently inhibit hippocampal long-term potentiation in vivo. *Nature.* **416**, 535-539
- 5 Takuma, K., Fang, F., Zhang, W., Yan, S., Fukuzaki, E., Du, H., Sosunov, A., McKhann, G., Funatsu, Y., Nakamichi, N., Nagai, T., Mizoguchi, H., Ibi, D., Hori, O., Ogawa, S., Stern, D. M., Yamada, K. and Yan, S. S. (2009) RAGE-mediated signaling contributes to intraneuronal transport of amyloid-beta and neuronal dysfunction. *Proc Natl Acad Sci U S A.* **106**, 20021-20026
- 6 Lauren, J., Gimbel, D. A., Nygaard, H. B., Gilbert, J. W. and Strittmatter, S. M. (2009) Cellular prion protein mediates impairment of synaptic plasticity by amyloid-beta oligomers. *Nature.* **457**, 1128-1132
- 7 Freir, D. B., Nicoll, A. J., Klyubin, I., Panico, S., Mc Donald, J. M., Risse, E., Asante, E. A., Farrow, M. A., Sessions, R. B., Saibil, H. R., Clarke, A. R., Rowan, M. J., Walsh, D. M. and Collinge, J. (2011) Interaction between prion protein and toxic amyloid beta assemblies can be therapeutically targeted at multiple sites. *Nat Commun.* **2**, 336
- 8 Calella, A. M., Farinelli, M., Nuvolone, M., Mirante, O., Moos, R., Falsig, J., Mansuy, I. M. and Aguzzi, A. (2010) Prion protein and Abeta-related synaptic toxicity impairment. *EMBO Mol Med.* **2**, 306-314
- 9 Linden, R., Martins, V. R., Prado, M. A., Cammarota, M., Izquierdo, I. and Brentani, R. R. (2008) Physiology of the prion protein. *Physiol Rev.* **88**, 673-728
- 10 Um, J. W., Kaufman, A. C., Kostylev, M., Heiss, J. K., Stagi, M., Takahashi, H., Kerrisk, M. E., Vortmeyer, A., Wisniewski, T., Koleske, A. J., Gunther, E. C., Nygaard, H. B. and Strittmatter, S. M. (2013) Metabotropic glutamate receptor 5 is a coreceptor for Alzheimer abeta oligomer bound to cellular prion protein. *Neuron.* **79**, 887-902

- 11 Venkitaramani, D. V., Chin, J., Netzer, W. J., Gouras, G. K., Lesne, S., Malinow, R. and Lombroso, P. J. (2007) Beta-amyloid modulation of synaptic transmission and plasticity. *J Neurosci.* **27**, 11832-11837
- 12 Rammes, G., Hasenjager, A., Sroka-Saidi, K., Deussing, J. M. and Parsons, C. G. (2011) Therapeutic significance of NR2B-containing NMDA receptors and mGluR5 metabotropic glutamate receptors in mediating the synaptotoxic effects of beta-amyloid oligomers on long-term potentiation (LTP) in murine hippocampal slices. *Neuropharmacology.* **60**, 982-990
- 13 Chen, S., Yadav, S. P. and Surewicz, W. K. (2010) Interaction between human prion protein and amyloid-beta (A β) oligomers: role OF N-terminal residues. *J Biol Chem.* **285**, 26377-26383
- 14 Younan, N. D., Sarell, C. J., Davies, P., Brown, D. R. and Viles, J. H. (2013) The cellular prion protein traps Alzheimer's A β in an oligomeric form and disassembles amyloid fibers. *FASEB J.* **27**, 1847-1858
- 15 Gimbel, D. A., Nygaard, H. B., Coffey, E. E., Gunther, E. C., Lauren, J., Gimbel, Z. A. and Strittmatter, S. M. (2010) Memory impairment in transgenic Alzheimer mice requires cellular prion protein. *J Neurosci.* **30**, 6367-6374
- 16 Chung, E., Ji, Y., Sun, Y., Kascsak, R. J., Kascsak, R. B., Mehta, P. D., Strittmatter, S. M. and Wisniewski, T. (2010) Anti-PrPC monoclonal antibody infusion as a novel treatment for cognitive deficits in an Alzheimer's disease model mouse. *BMC Neurosci.* **11**, 130
- 17 Barry, A. E., Klyubin, I., Mc Donald, J. M., Mably, A. J., Farrell, M. A., Scott, M., Walsh, D. M. and Rowan, M. J. (2011) Alzheimer's disease brain-derived amyloid-beta-mediated inhibition of LTP in vivo is prevented by immunotargeting cellular prion protein. *J Neurosci.* **31**, 7259-7263
- 18 Haas, L. T., Kostylev, M. A. and Strittmatter, S. M. (2014) Therapeutic molecules and endogenous ligands regulate the interaction between brain cellular prion protein (PrPC) and metabotropic glutamate receptor 5 (mGluR5). *J Biol Chem.* **289**, 28460-28477
- 19 Ostapchenko, V. G., Beraldo, F. H., Mohammad, A. H., Xie, Y. F., Hirata, P. H., Magalhaes, A. C., Lamour, G., Li, H., Maciejewski, A., Belrose, J. C., Teixeira, B. L., Fahnestock, M., Ferreira, S. T., Cashman, N. R., Hajj, G. N., Jackson, M. F., Choy, W. Y., MacDonald, J. F., Martins, V. R., Prado, V. F. and Prado, M. A. (2013) The prion protein ligand, stress-inducible phosphoprotein 1, regulates amyloid-beta oligomer toxicity. *J Neurosci.* **33**, 16552-16564
- 20 Brehme, M., Voisine, C., Rolland, T., Wachi, S., Soper, J. H., Zhu, Y., Orton, K., Vilella, A., Garza, D., Vidal, M., Ge, H. and Morimoto, R. I. (2014) A chaperome subnetwork safeguards proteostasis in aging and neurodegenerative disease. *Cell Rep.* **9**, 1135-1150

- 21 Chen, S. and Smith, D. F. (1998) Hop as an adaptor in the heat shock protein 70 (Hsp70) and hsp90 chaperone machinery. *J Biol Chem.* **273**, 35194-35200
- 22 Hajj, G. N., Arantes, C. P., Dias, M. V., Roffe, M., Costa-Silva, B., Lopes, M. H., Porto-Carreiro, I., Rabachini, T., Lima, F. R., Beraldo, F. H., Prado, M. A., Linden, R. and Martins, V. R. (2013) The unconventional secretion of stress-inducible protein 1 by a heterogeneous population of extracellular vesicles. *Cell Mol Life Sci.* **70**, 3211-3227
- 23 McCready, J., Sims, J. D., Chan, D. and Jay, D. G. (2010) Secretion of extracellular hsp90alpha via exosomes increases cancer cell motility: a role for plasminogen activation. *BMC Cancer.* **10**, 294
- 24 Li, W., Sahu, D. and Tsen, F. (2011) Secreted heat shock protein-90 (Hsp90) in wound healing and cancer. *Biochim Biophys Acta.* **1823**, 730-741
- 25 Hegmans, J. P., Bard, M. P., Hemmes, A., Luijck, T. M., Kleijmeer, M. J., Prins, J. B., Zitvogel, L., Burgers, S. A., Hoogsteden, H. C. and Lambrecht, B. N. (2004) Proteomic analysis of exosomes secreted by human mesothelioma cells. *Am J Pathol.* **164**, 1807-1815
- 26 Zanata, S. M., Lopes, M. H., Mercadante, A. F., Hajj, G. N., Chiarini, L. B., Nomizo, R., Freitas, A. R., Cabral, A. L., Lee, K. S., Juliano, M. A., de Oliveira, E., Jachieri, S. G., Burlingame, A., Huang, L., Linden, R., Brentani, R. R. and Martins, V. R. (2002) Stress-inducible protein 1 is a cell surface ligand for cellular prion that triggers neuroprotection. *EMBO J.* **21**, 3307-3316
- 27 Caetano, F. A., Lopes, M. H., Hajj, G. N., Machado, C. F., Pinto Arantes, C., Magalhaes, A. C., Vieira Mde, P., Americo, T. A., Massensini, A. R., Priola, S. A., Vorberg, I., Gomez, M. V., Linden, R., Prado, V. F., Martins, V. R. and Prado, M. A. (2008) Endocytosis of prion protein is required for ERK1/2 signaling induced by stress-inducible protein 1. *J Neurosci.* **28**, 6691-6702
- 28 Lopes, M. H., Hajj, G. N., Muras, A. G., Mancini, G. L., Castro, R. M., Ribeiro, K. C., Brentani, R. R., Linden, R. and Martins, V. R. (2005) Interaction of cellular prion and stress-inducible protein 1 promotes neuritogenesis and neuroprotection by distinct signaling pathways. *J Neurosci.* **25**, 11330-11339
- 29 Beraldo, F. H., Arantes, C. P., Santos, T. G., Queiroz, N. G., Young, K., Rylett, R. J., Markus, R. P., Prado, M. A. and Martins, V. R. (2010) Role of alpha7 nicotinic acetylcholine receptor in calcium signaling induced by prion protein interaction with stress-inducible protein 1. *J Biol Chem.* **285**, 36542-36550
- 30 Scheufler, C., Brinker, A., Bourenkov, G., Pegoraro, S., Moroder, L., Bartunik, H., Hartl, F. U. and Moarefi, I. (2000) Structure of TPR domain-peptide complexes: critical elements in the assembly of the Hsp70-Hsp90 multichaperone machine. *Cell.* **101**, 199-210

- 31 Onuoha, S. C., Coulstock, E. T., Grossmann, J. G. and Jackson, S. E. (2008) Structural studies on the co-chaperone Hop and its complexes with Hsp90. *J Mol Biol.* **379**, 732-744
- 32 Lee, C. T., Graf, C., Mayer, F. J., Richter, S. M. and Mayer, M. P. (2012) Dynamics of the regulation of Hsp90 by the co-chaperone Sti1. *EMBO J.* **31**, 1518-1528
- 33 Rohl, A., Wengler, D., Madl, T., Lagleder, S., Tippel, F., Herrmann, M., Hendrix, J., Richter, K., Hack, G., Schmid, A. B., Kessler, H., Lamb, D. C. and Buchner, J. (2015) Hsp90 regulates the dynamics of its cochaperone Sti1 and the transfer of Hsp70 between modules. *Nat Commun.* **6**, 6655
- 34 Southworth, D. R. and Agard, D. A. (2011) Client-loading conformation of the Hsp90 molecular chaperone revealed in the cryo-EM structure of the human Hsp90:Hop complex. *Mol Cell.* **42**, 771-781
- 35 Schmid, A. B., Lagleder, S., Grawert, M. A., Rohl, A., Hagn, F., Wandinger, S. K., Cox, M. B., Demmer, O., Richter, K., Groll, M., Kessler, H. and Buchner, J. (2012) The architecture of functional modules in the Hsp90 co-chaperone Sti1/Hop. *EMBO J.* **31**, 1506-1517
- 36 Romano, S. A., Cordeiro, Y., Lima, L. M., Lopes, M. H., Silva, J. L., Foguel, D. and Linden, R. (2009) Reciprocal remodeling upon binding of the prion protein to its signaling partner hop/STI1. *FASEB J.* **23**, 4308-4316
- 37 Maciejewski, A., Prado, M. A. and Choy, W. Y. (2012) (1)H, (1)(5)N and (1)(3)C backbone resonance assignments of the TPR1 and TPR2A domains of mouse STI1. *Biomol NMR Assign.* **7**, 305-310
- 38 Delaglio, F., Grzesiek, S., Vuister, G. W., Zhu, G., Pfeifer, J. and Bax, A. (1995) NMRPipe: a multidimensional spectral processing system based on UNIX pipes. *J Biomol NMR.* **6**, 277-293
- 39 Johnson, B. A. and Blevins, R. A. (1994) NMR View: A computer program for the visualization and analysis of NMR data. *J Biomol NMR.* **4**, 603-614
- 40 Hornemann, S., von Schroetter, C., Damberger, F. F. and Wuthrich, K. (2009) Prion protein-detergent micelle interactions studied by NMR in solution. *J Biol Chem.* **284**, 22713-22721
- 41 Lacor, P. N., Buniel, M. C., Furlow, P. W., Clemente, A. S., Velasco, P. T., Wood, M., Viola, K. L. and Klein, W. L. (2007) Abeta oligomer-induced aberrations in synapse composition, shape, and density provide a molecular basis for loss of connectivity in Alzheimer's disease. *J Neurosci.* **27**, 796-807
- 42 Fluharty, B. R., Biasini, E., Stravalaci, M., Scip, A., Diomede, L., Balducci, C., La Vitola, P., Messa, M., Colombo, L., Forloni, G., Borsello, T., Gobbi, M. and Harris,

- D. A. (2013) An N-terminal fragment of the prion protein binds to amyloid-beta oligomers and inhibits their neurotoxicity in vivo. *J Biol Chem.* **288**, 7857-7866
- 43 Balducci, C., Beeg, M., Stravalaci, M., Bastone, A., Scip, A., Biasini, E., Tapella, L., Colombo, L., Manzoni, C., Borsello, T., Chiesa, R., Gobbi, M., Salmona, M. and Forloni, G. (2010) Synthetic amyloid-beta oligomers impair long-term memory independently of cellular prion protein. *Proc Natl Acad Sci U S A.* **107**, 2295-2300
- 44 Um, J. W. and Strittmatter, S. M. (2012) Amyloid-beta induced signaling by cellular prion protein and Fyn kinase in Alzheimer disease. *Prion.* **7**, 37-41
- 45 Khan, G. M., Tong, M., Jhun, M., Arora, K. and Nichols, R. A. (2010) beta-Amyloid activates presynaptic alpha7 nicotinic acetylcholine receptors reconstituted into a model nerve cell system: involvement of lipid rafts. *Eur J Neurosci.* **31**, 788-796
- 46 Cortajarena, A. L. and Regan, L. (2006) Ligand binding by TPR domains. *Protein Sci.* **15**, 1193-1198
- 47 Blair, L. J., Nordhues, B. A., Hill, S. E., Scaglione, K. M., O'Leary, J. C., 3rd, Fontaine, S. N., Breydo, L., Zhang, B., Li, P., Wang, L., Cotman, C., Paulson, H. L., Muschol, M., Uversky, V. N., Klengel, T., Binder, E. B., Kaye, R., Golde, T. E., Berchtold, N. and Dickey, C. A. (2013) Accelerated neurodegeneration through chaperone-mediated oligomerization of tau. *J Clin Invest.* **123**, 4158-4169
- 48 Ansar, S., Burlison, J. A., Hadden, M. K., Yu, X. M., Desino, K. E., Bean, J., Neckers, L., Audus, K. L., Michaelis, M. L. and Blagg, B. S. (2007) A non-toxic Hsp90 inhibitor protects neurons from Abeta-induced toxicity. *Bioorg Med Chem Lett.* **17**, 1984-1990
- 49 Dickey, C. A., Kamal, A., Lundgren, K., Klosak, N., Bailey, R. M., Dunmore, J., Ash, P., Shoraka, S., Zlatkovic, J., Eckman, C. B., Patterson, C., Dickson, D. W., Nahman, N. S., Jr., Hutton, M., Burrows, F. and Petrucelli, L. (2007) The high-affinity HSP90-CHIP complex recognizes and selectively degrades phosphorylated tau client proteins. *J Clin Invest.* **117**, 648-658
- 50 Luo, W., Dou, F., Rodina, A., Chip, S., Kim, J., Zhao, Q., Moulick, K., Aguirre, J., Wu, N., Greengard, P. and Chiosis, G. (2007) Roles of heat-shock protein 90 in maintaining and facilitating the neurodegenerative phenotype in tauopathies. *Proc Natl Acad Sci U S A.* **104**, 9511-9516
- 51 Liao, D. F., Jin, Z. G., Baas, A. S., Daum, G., Gygi, S. P., Aebersold, R. and Berk, B. C. (2000) Purification and identification of secreted oxidative stress-induced factors from vascular smooth muscle cells. *J Biol Chem.* **275**, 189-196
- 52 Coitinho, A. S., Lopes, M. H., Hajj, G. N., Rossato, J. I., Freitas, A. R., Castro, C. C., Cammarota, M., Brentani, R. R., Izquierdo, I. and Martins, V. R. (2007) Short-term memory formation and long-term memory consolidation are enhanced by cellular prion association to stress-inducible protein 1. *Neurobiol Dis.* **26**, 282-290

53 Roffe, M., Beraldo, F. H., Bester, R., Nunziante, M., Bach, C., Mancini, G., Gilch, S., Vorberg, I., Castilho, B. A., Martins, V. R. and Hajj, G. N. (2010) Prion protein interaction with stress-inducible protein 1 enhances neuronal protein synthesis via mTOR. *Proc Natl Acad Sci U S A.* **107**, 13147-13152

54 Pettersen, E. F., Goddard, T. D., Hung, C. C., Couch, G. S., Greenblatt, D. M., Meng, E. C., Ferrin, T. E. (2004) *J Comput Chem* **25**, 1605-1612.

4 Structural details of STIP1 complex with S100A1

4.1 Introduction

The S100-family of proteins comprises approximately 25 members involved in several crucial biological processes including calcium (Ca^{2+}) homeostasis, proliferation, differentiation, inflammation and apoptosis [1-3]. These proteins are tissue and cell-specific homo/hetero dimers composed of two EF-hand helix motifs capable of Ca^{2+} ion coordination [4]. Typically upon Ca^{2+} -binding, α -helices III of each subunit undergo a significant conformational change exposing a hydrophobic cleft, which represents the binding site to various ligands [5]. Thus, S100-family is considered as Ca^{2+} -dependent regulators of several cellular pathways through multiple documented protein-protein interactions [4]. Altered expression patterns of unique S100 proteins have been noted in several disease states including different forms of cancer, cardiomyopathy and neurodegenerative diseases such as Alzheimer's disease (AD) and serve as clinical diagnostic biomarkers [6-9].

Calcium serves as a ubiquitous signaling molecule in neuronal activation whose deregulation is a common hallmark in AD causing synaptic dysfunction[10]. Ca^{2+} -binding proteins play an important role in regulating Ca^{2+} homeostasis and modulating protein-protein interactions. Consistent in this capacity, a number of S100-family members have been implicated in aberrant AD signaling [6, 11, 12]. S100A1 is abundantly expressed in skeletal muscle, cardiomyocytes and neurons [6, 8, 13]. S100A1 has been found to regulate amyloid precursor protein (APP) processing, tau

phosphorylation and A β oligomer induced neuronal cell death [14]. In addition, studies have revealed roles for S100A1 in the heat-shock protein response, regulating Hsp70 and Hsp90 binding to stress-inducible phosphoprotein 1 (STIP1) during client protein refolding [15, 16].

STIP1 is a cellular co-chaperone, which coordinates client protein transfer from Hsp70 to Hsp90 during protein folding of various cellular ligands including numerous oncogenic kinases and transcription factors [17]. STIP1 is composed of three structurally related tetratricopeptide repeat (TPR1, TPR2A and TPR2B) domains and two aspartate and proline rich DP (DP1 and DP2) domains. TPR domains are 34-amino acid degenerate consensus motifs arranged in tandem forming a series of anti-parallel amphipathic α -helices [18]. They are common protein-protein interaction modules involved in numerous cellular processes including cell cycle regulation, transcription and protein folding [19]. TPR2A and TPR2B mediate interactions between the C-terminal EEVD motif of Hsp90 and through a series of contacts located in the middle domain of Hsp90 [17, 18, 20, 21]. Hsp70 coordination involves binding to the TPR1 and TPR2B domains of STIP1.

S100A1, S100A2 and S100A6 family members have been identified as STIP1 ligands, forming molecular complexes through interactions with the TPR domains of STIP1 [15, 16]. S100A2 and S100A6 association has also been shown to inhibit Hsp70 and Hsp90 binding to STIP1 *in vitro* and in cell culture upon Ca²⁺ stimulation, implicating their function in the STIP1-directed protein-folding relay. However, the molecular details of S100 binding to STIP1 remain largely unknown.

The present study employed NMR, analytical ultracentrifugation and isothermal titration calorimetry (ITC) to define the molecular details of S100A1 binding to STIP1. Our results reveal that each TPR domain is capable of simultaneous binding to a single S100A1 dimer with varying affinities and thermodynamic parameters in the full-length STIP1 molecule. Each TPR domain associates with S100A1 through a common binding site, spanning α -helices III and IV of S100A1 in a Ca^{2+} -dependent manner. While nuclear magnetic resonance (NMR) studies for each TPR domain noted binding, a global loss in peak intensity due to line broadening prevented chemical-shift mapping of the S100A1 binding site on each TPR domain of STIP1.

4.2 Materials and methods

4.2.1 Protein purification

Recombinant STIP1 or individual TPR domains (TPR1 (residues 1-118), TPR2A (residues 217-352) and TPR2B (residues 353-480)) were cloned into pDEST17 expression vectors (Invitrogen-ThermoFisher Scientific). Each construct contained an additional N-terminal 6xHis-tag joined by a cleavable tobacco etch virus (TEV) recognition site to facilitate tag removal. Individual constructs were transformed into *Escherichia coli* (*E. coli*) BL21 (DE3) pLysS strain and grown in standard M9 minimal media at 37 °C to an OD_{600} of 0.9. Expression was induced with 1 mM isopropyl β -D-1-thiogalactopyranoside (IPTG) and cultures were grown at 22 °C overnight. Protein samples for NMR spectroscopy were expressed in standard M9 media supplemented with 1 g/L ^{15}N -labeled ammonium chloride.

Recombinant STIP1 proteins were purified by Ni²⁺-affinity chromatography using Ni Sepharose 6 Fast Flow beads (GE Healthcare Life Sciences). 6xHis-tag cleavage was achieved by incubation with 6xHis tagged TEV overnight at 22°C. TEV and 6xHis tag were subsequently removed by additional Ni²⁺-affinity chromatography.

pETDuet vector encoding S100A1 (kindly provided by Dr. Gary Shaw) was transformed into *E. coli* BL21(DE3)-RIL and cultures were grown in standard M9 minimal medium or in M9 supplemented with 1g/L ¹⁵N-labeled ammonium chloride for NMR spectroscopy studies. Cultures were grown to an OD₆₀₀ of 0.9 and induced with 1 mM IPTG and grown overnight at 22°C. The bacterial pellet was resuspended in 50 mM Tris-HCl, 5mM MgCl₂, pH 8.0 and lysed by French press at 10,000 psi. Cellular debris were pelleted by centrifugation at 40,000 x g for 30 minutes. Supernatant was filtered through a 0.45 µm syringe filter (Thermo Scientific) and loaded onto a 2 mL HiTrap Q anion exchange column (GE Healthcare) equilibrated in Buffer A (25mM Tris-HCl, 1 mM EDTA, 1 mM DTT, pH 8.0) using a AKTA FPLC (GE Healthcare) at a flow rate 1 mL/min. The column was washed with 10 column volumes of Buffer A and subsequently eluted by a 20-column volume linear gradient of Buffer A with 1 M NaCl. Fractions containing S100A1 were pooled and the CaCl₂ concentration was adjusted to 5 mM. Fractions were incubated with phenyl-Sepharose resin (Amersham Bioscience) for 1 hour at room temperature and washed with 25 mM Tris-HCl, 100 mM NaCl, 1 mM DTT, 1mM CaCl₂, pH 8.0. Bound S100A1 was eluted with 25 mM Tris-HCl, 100 mM NaCl, 1 mM DTT, 5 mM EGTA, pH 8.0 and all proteins were dialyzed into 10 mM HEPES, 100mM NaCl, 1 mM DTT, pH 8.0 with 5 mM CaCl₂ or 5 mM EGTA for further studies.

4.2.2 Analytical ultracentrifugation – sedimentation equilibrium

Analytical ultracentrifugation (AUC) experiments were performed at 20 °C on STIP1 (18 µM) and S100A1 (30 µM), or STIP1 and S100A1 mixtures containing 8 µM and 48 µM of each protein, respectively, using a Beckman Optima XL-A Analytical Ultracentrifuge equipped with an An-60Ti rotor containing six-channel Epon-charcoal centerpieces and 1.2 cm path length (Biomolecular Interactions and Conformations Facility, University of Western Ontario). Absorbance measurements were collected at 250 nm in 0.002 cm radial steps and averaged over 10 scans. Sedimentation equilibrium measurements were collected at rotor speeds of 12 000, 15 000 and 18 000 rpm (STIP1) or 20 000, 24 000 and 28 000 rpm (S100A1) or 7 000 and 10 000 rpm (STIP1-STIP1 complex). Data was fit to the following global single-ideal species model equation using GraphPad Prism

$$C = C_0 \exp\left(\frac{\omega^2}{2RT} M_{obs}(1 - \bar{v}\rho)(x^2 - x_0^2)\right) + I_0$$

(Equation 1) where C is the concentration of protein at radius x , C_0 is the concentration at initial radius x_0 , ω is the angular velocity, \bar{v}_{bar} is the partial specific volume of the protein, ρ is the solvent density, R is the ideal gas constant, T is the absolute temperature, I_0 is the baseline offset and M_{obs} is the fit of the molecular weight based on sedimentation data.

4.2.3 Isothermal titration calorimetry (ITC)

Binding of STIP1 and TPR domains to S100A1 was measured using a MicroCal™ VP-ITC calorimeter or Nano-ITC (TA Instruments) at 25°C. All protein concentrations for S100A1 correspond to dimer concentrations. Twenty-five to 30 aliquots of 5 μ L STIP1 (60 μ M) or individual TPR domains (\sim 150 μ M) were titrated to S100A1 (\sim 30-70 μ M). Buffer blank or ligand into buffer titrations demonstrated negligible heats of binding and heats of dilution, respectively. Each titration was replicated in duplicate. Isotherms were fit to a single-site binding model using Origin or NanoAnalyze software provided by the manufacturer, where K_d is the dissociation constant, n is the stoichiometry of binding and ΔH and ΔS represent the change in enthalpy and entropy of binding, respectively.

4.2.4 Nuclear magnetic resonance (NMR) spectroscopy

Nuclear Magnetic Resonance (NMR) Spectroscopy experiments were performed on a Varian Inova 600 MHz NMR spectrometer equipped with xyz-gradient triple resonance cryogenic probe at 25 °C. Backbone resonance assignments for TPR2B (\sim 400 μ M) were obtained from HNCACB and CBCA(CO)NH experiments prepared in 50 mM sodium phosphate, 50 mM NaCl, 1 mM DTT, pH 7. Backbone amide resonance assignments for TPR1, TPR2A and S100A1 were obtained from the BioMagResBank under accession numbers 18691, 18689 and 18231, respectively. NMR spectra were processed with NMRPipe and analyzed by NMRViewJ or CARRA [22-24]. ^1H - ^{15}N HSQC spectra of ^{15}N -labeled S100A1 (\sim 200 μ M) were collected in the presence of increasing TPR domains (\sim 0-200 μ M). The reciprocal of the binding experiments were collected with ^{15}N -labeled TPR domains (TPR1, TPR2A and TPR2B) at identical concentrations.

4.3 Results

4.3.1 Multiple S100A1 dimers bind to STIP1 with different affinities

Previous studies have demonstrated that S100-family of proteins complex with STIP1 through its structurally related TPR domains; however, the biochemical details of S100 binding to STIP1 to date are poorly understood [16, 25]. We have used isothermal titration calorimetry (ITC) to measure the binding affinities and characterize the thermodynamic details of the STIP1-S100A1 complex.

S100A1 bound to full-length STIP1 with high affinity in the presence of Ca^{2+} . No heat change was detected upon Ca^{2+} chelation, suggesting STIP1-S100A1 complex formation is Ca^{2+} dependent (Figure 4.1A and 4.1B). The change in enthalpy (ΔH) upon STIP1 titration to S100A1 is highly endothermic indicating complex formation is entropically driven and likely involving a large number of hydrophobic contacts (Figure 1.A). Consistent with this hypothesis, Ca^{2+} binding to S100-family of proteins results in structural rearrangement of the EF-hand α -helical motifs resulting in the exposure of a hydrophobic interface involved in numerous S100-family ligand interactions [7]. The stoichiometry of binding of STIP1 to S100A1 deviated dramatically from a single-site binding model, suggesting multiple S100A1 dimers bind a single molecule of STIP1. This agrees with previous studies demonstrating the S100 family members S100A2 and S100A6 bind to multiple individual TPR domains (TPR1, TPR2A and TPR2B) of STIP1 [16]. Interestingly, only a single inflection point is seen in the binding isotherm and it was not possible to distinguish the different binding equilibria.

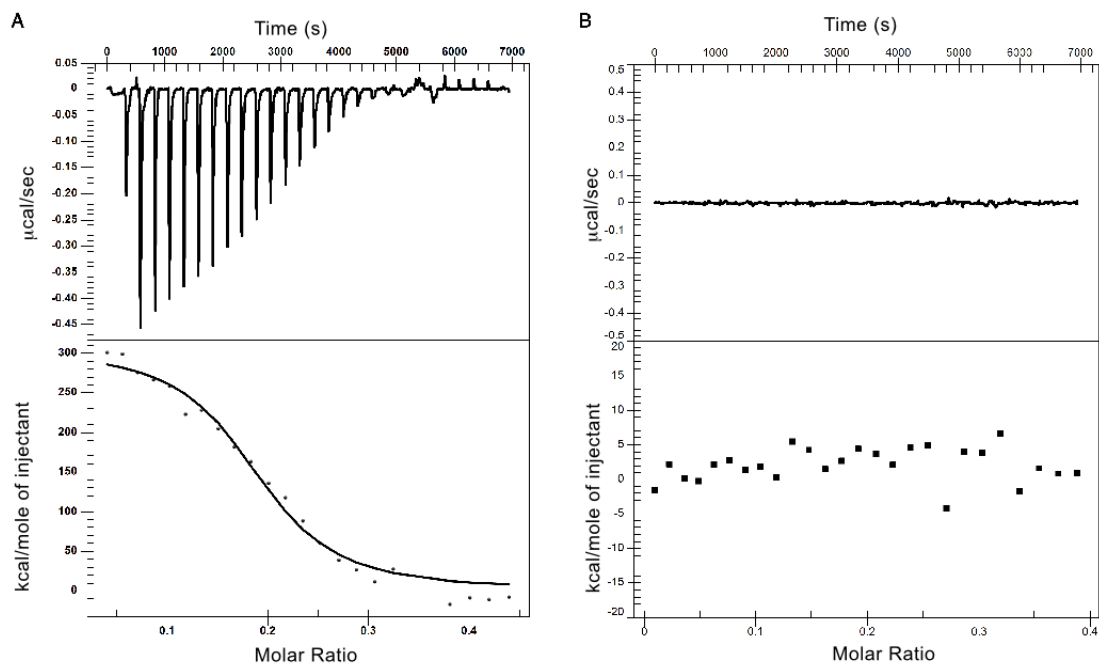


Figure 4.1. STIP1 binds multiple S100A1 dimers in a Ca^{2+} -dependent manner. Isothermal titration calorimetry thermogram of STIP1 binding to S100A1 in the presence (A) of 5mM CaCl_2 or (B) 5 mM EGTA.

Due to the potential complexity of STIP1 binding to S100A1, measurements were conducted on individual TPR (TPR1, TPR2A and TPR2B) domains of STIP1 to obtain greater insight into complex formation. Binding affinities between the individual TPR domains and S100A1 differed significantly, approximately 15-fold range between the strongest and weakest interaction (Figure 4.2A, 4.2B, and 4.2C) (Table 1). Due to the relatively weak binding of the TPR2A domain compared to the other TPR domains (TPR1, TPR2B), the enthalpy and binding affinity could not be accurately determined for this interaction ($K_d = \sim 15 \mu\text{M}$). TPR2B bound to S100A1 with the highest affinity ($K_d = 0.76 \pm 0.01 \mu\text{M}$), approximately 6 folds greater than TPR1 ($K_d = 4.37 \pm 0.1 \mu\text{M}$). The enthalpies of binding to each TPR domain were endothermic in agreement with the values seen for full-length STIP1 and confirm S100A1 complex formation to each TPR domain is entropically driven.

Table 1. Thermodynamic parameters of TPR domains of STIP1 binding to S100A1.

TPR domain	n^a	K_d (μM)^b	ΔH^b (kcal/mol)	TΔS^b (kcal/mol)	ΔG^b (kcal/mol)
STIP1	0.19	0.59 ± 1.2	72.9 ± 5.8	81.4	-8.5 ± 6.0
TPR1	0.95	4.37 ± 0.1	55.4 ± 1.0	62.6	-7.2 ± 1.0
TPR2A	-	-	-	-	-
TPR2B	0.96	0.76 ± 0.1	20.8 ± 0.3	29.1	-8.3 ± 0.3

^aBinding stoichiometry of dimeric S100A1 and the TPR domains of STIP1

^bK_d is the dissociation constant and ΔH, ΔS and ΔG are the change in enthalpy, entropy and Gibbs free energy upon binding at T=298.15 K, respectively.

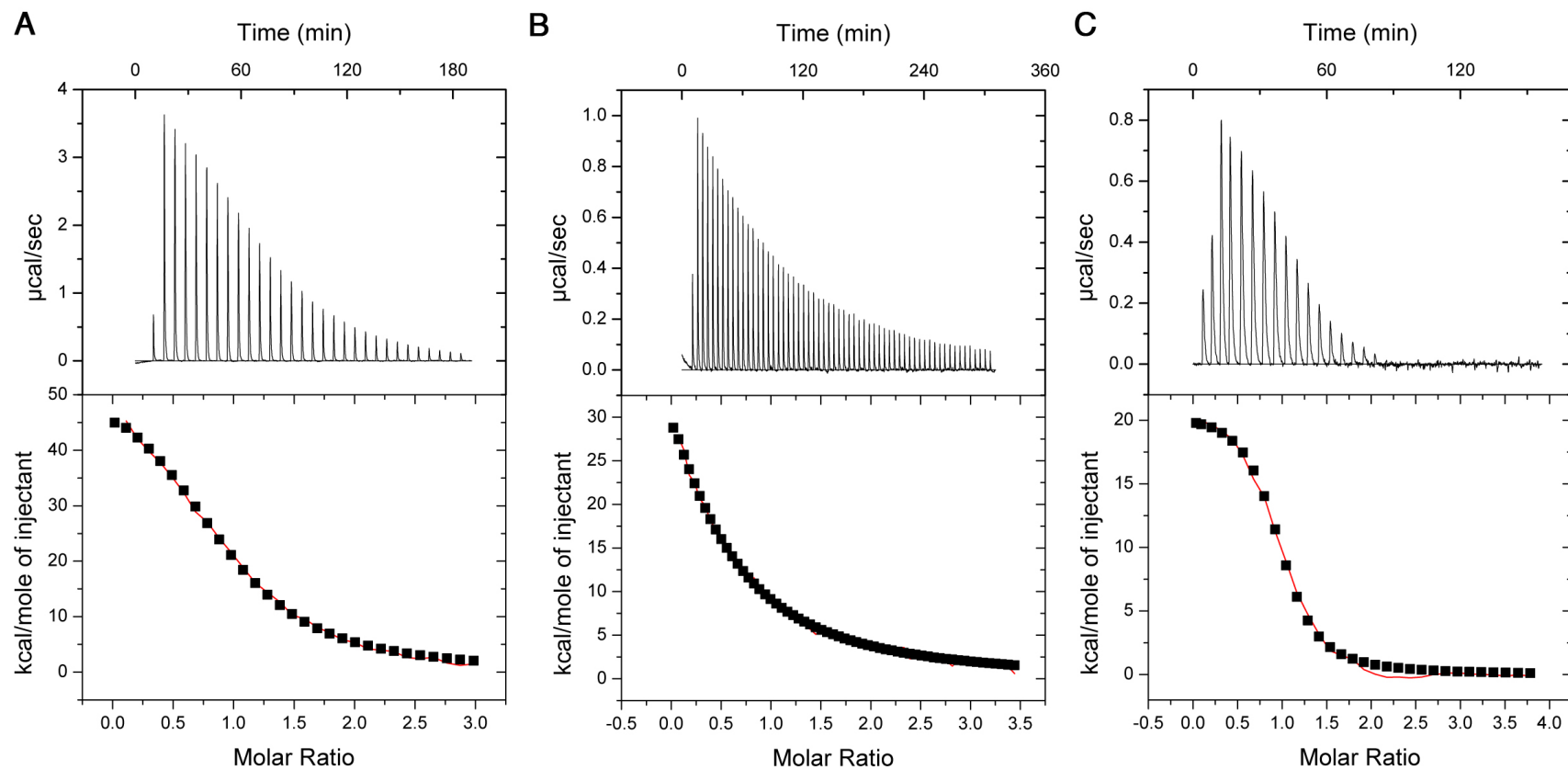


Figure 4.2. The TPR domains of STIP1 bind a single S100A1 dimer with various affinities.

Isothermal titration calorimetry thermogram of S100A1 binding to (A) TPR1, (B) TPR2A or (C) TPR2B domains of STIP1.

4.3.2 STIP1 binds to three S100A1 dimers

Studies have indicated additional S100 proteins complex with STIP1 through TPR-motif interactions in each domain through pulldown experiments [16]. These include S100A2 and S100A6, but not S100B, S100A4, S100A10, S100A11, S100A12 or S100A13 [13]. Thus, this is not a property shared by all S100 family members. The S100 proteins identified to bind STIP1 differed in the number of S100 dimers that bind a single molecule of STIP1. Our ITC results did not fit perfectly to a single-site model, thus we could not say for certain the stoichiometry of binding of S100A1 to STIP1. Thus, AUC experiments were conducted to gain additional insights into the stoichiometry of binding of S100A1 to full-length STIP1. S100A1 exhibited a M_{obs} value of 24.2 ± 0.2 kDa, consistent with previous studies suggesting S100A1 exists as a homodimer in solution of a calculated molecular weight of 21.1 kDa based on the amino acid sequence (Figure 4.3A). Alternatively, STIP1 presented a M_{obs} value of 55.3 ± 0.9 kDa, reasonably close to the predicted molecular weight of 62.6 kDa and consistent with current monomeric models of STIP1 function in solution during Hsp70 and Hsp90 client protein transfer (Figure 4.4B). AUC of STIP1 at saturating concentrations of S100A1 revealed the formation of a larger molecular weight species with a M_{obs} of 126.1 ± 1.2 kDa (Figure 4.4C). These results are in agreement with a single S100A1 dimer binding to each of the three TPR domains of STIP1, which would have an inferred molecular weight of 125.9 kDa.

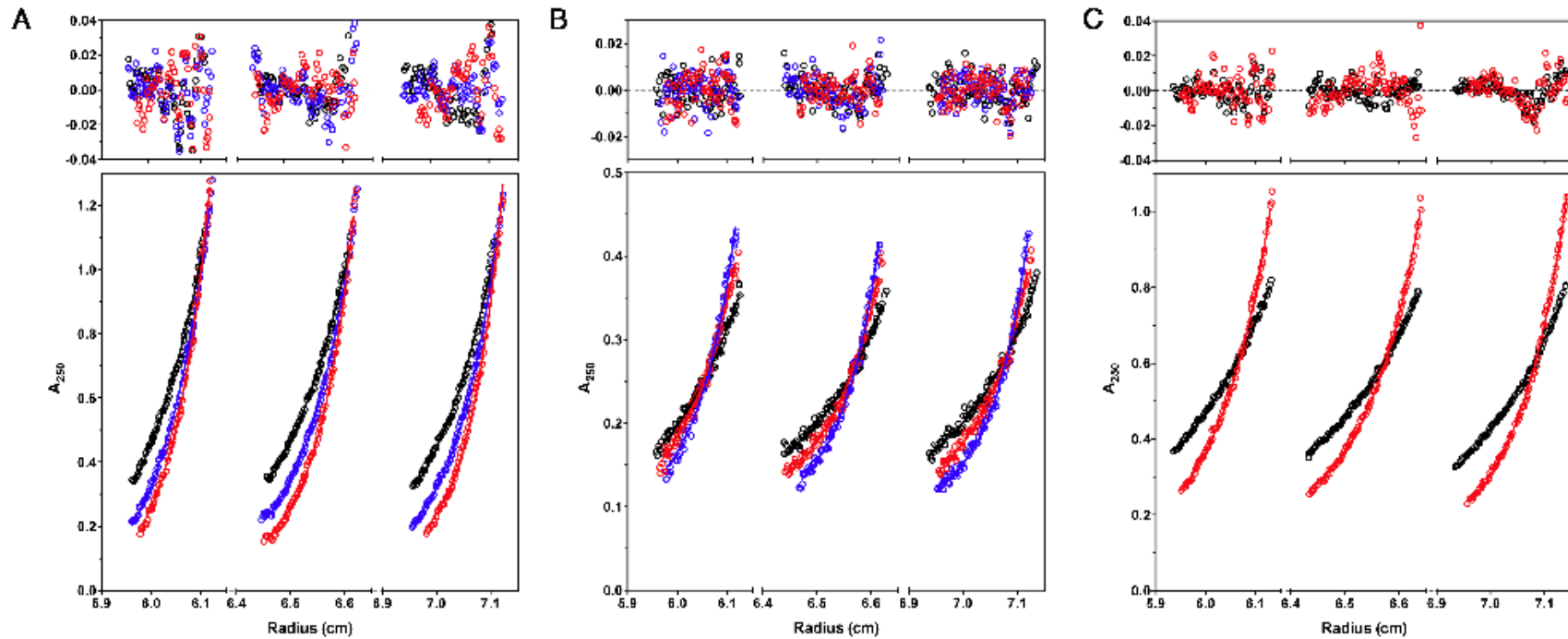


Figure 4.3. A single STIP1 molecule binds three S100A1 dimers simultaneously.

Sedimentation equilibrium of AUC (A) S100A1 obtained at rotor speeds 20 000, 24 000 and 28 000 rpm (black, blue and red, respectively), (B) STIP1 measured at 12 000, 15 000 and 18 000 rpm (black, red, blue, respectively) or (C) STIP1-S100A1 complex collected at 7 000 and 10 000 rpm (black and red, respectively). Lines represent global fits to a single species model as described in Equation 1.

4.3.3 S100A1 shares a common interface when binding each TPR domain

The disparity in affinities and significant differences in thermodynamic properties of S100A1-TPR interactions suggests there are differences in the binding interfaces between these interactions. Thus, we used nuclear magnetic resonance (NMR) spectroscopy to define residues involved in complex formation at the molecular level. Titration of ^{15}N -isotopically labeled S100A1 with increasing concentrations of each TPR domain (TPR1, TPR2A and TPR2B) resulted in a systematic global reduction in peak intensity (Figure 4.4). The loss in signal is likely the result of line broadening through enhanced relaxation, the consequence of increased molecular weight of the S100A1-TPR complex (37.4 kDa) in relation to the unbound S100A1 spectrum (21.1 kDa). Interestingly, a significantly greater loss in peak intensity was observed in residues localized to a continuous region spanning α -helices III and IV of S100A1 (Figure 4.4A, B and C). Residues of S100A1 showing the largest peak intensity attenuations upon addition of each TPR domain were mapped to an identical region suggesting that they share a common binding site on S100A1.

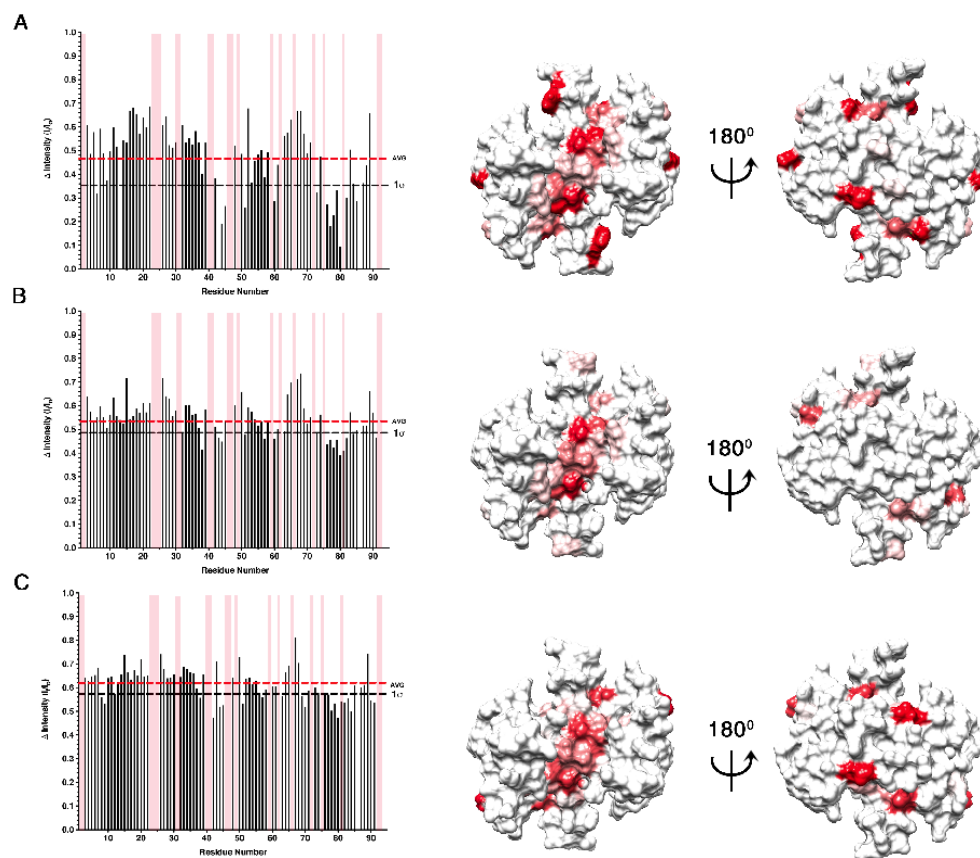


Figure 4.4. TPR domains of STIP1 share a common binding interface on S100A1.

Graphical representations of chemical shift changes observed in ^1H - ^{15}N spectra of ^{15}N -labelled S100A1 in the presence of (A) TPR1, (B) TPR2A or (C) TPR2B (*left*) (*red line*: average decrease in signal intensity upon TPR titration; black line: one standard deviation from the mean decrease in signal intensity) Chemical shift changes mapped on to S100A1 structure (PDB:2LP3)[33] (*right*). Regions of S100A1 that demonstrated a greater than one standard deviation from the mean average decrease in signal intensity are colored in red.

The similarity of the S100A1-TPR binding regions suggests differences in affinity and thermodynamics are likely due to differences in amino acid composition on the individual TPR domains. To determine the regions of each TPR domain involved in S100A1 complex formation, the reciprocal experiment was conducted where ^{15}N -labeled TPR domains were titrated with S100A1. A global decrease in signal intensity was observed for each TPR spectrum consistent with the results obtained in the S100A1 spectra (Figure 4.5A, B and C). Unfortunately, no significant localized deviation from the global decrease in signal intensity was observed for each TPR titration. This result prevented accurate mapping of the S100A1 binding site on each TPR domain. Further study is required to identify the S100A1 binding site in each TPR domain of STIP1 by complementary techniques.

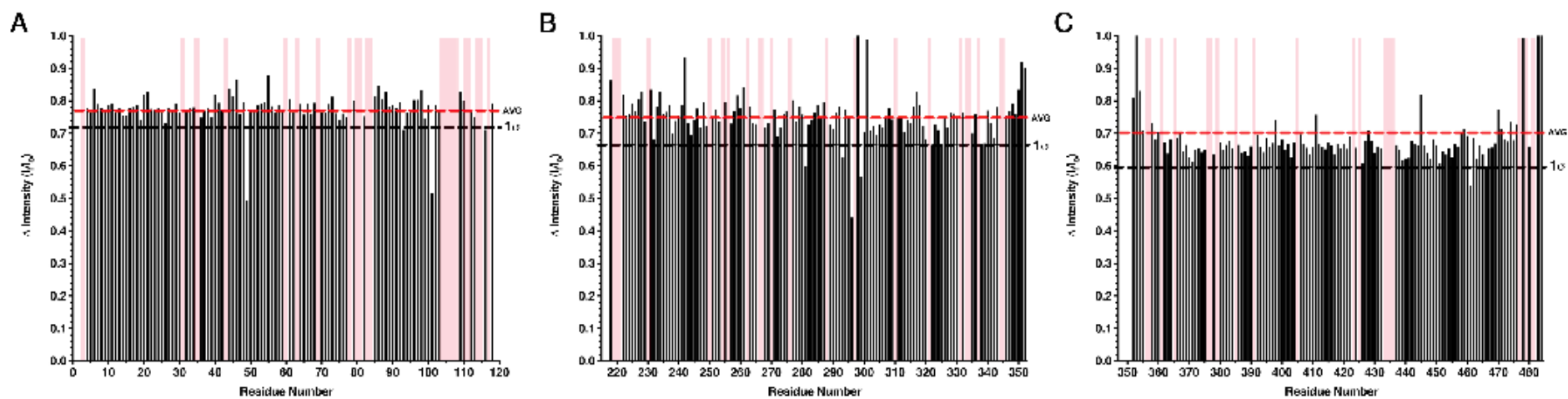


Figure 4.5. Graphical representations of chemical shift changes observed in ^1H - ^{15}N spectra of ^{15}N -labelled (A)TPR1, (B) TPR2A or (C) TPR2B in the presence of S100A1.

(red line: average decrease in signal intensity upon TPR titration; black line: one standard deviation from the mean decrease in signal intensity)

4.4 Discussion

The studies presented here provide molecular details of the interactions between S100A1 and STIP1. ITC thermograms indicated a high affinity interaction between S100A1 and full-length STIP1. The stoichiometry of binding (n) differed dramatically from a single one-site model; however, only a single inflection point was evident in the thermograms, suggesting multiple binding sites with similar thermodynamic properties. The possibility of multiple binding sites complicated fitting the isotherm to a single binding model, thus we investigated binding to individual TPR domains. Previous studies have demonstrated that each individual TPR domain of STIP1 is capable of binding related S100 family members (S100A2 and S100A6) [16]. However, these studies were limited to affinity pull down experiments and the thermodynamic details of S100 binding to each TPR domain and S100 proteins were lacking. Though similar in structure, S100A2 and S100A6 dimers have been shown to bind STIP1 at stoichiometric ratios of 4:1 and 2:1 by pull-down experiments, respectively [16]. Steric hindrance or conformational rearrangements in STIP1's modular structure may alter the binding capacity of STIP1 for S100 proteins, even though individually each TPR domain possesses the capacity to bind S100 proteins.

ITC binding experiments of each TPR domain titrated to S100A1 revealed significantly different binding properties. Binding affinities differed approximately 20 fold between the tightest bindings TPR2B ($K_d = 0.8 \mu\text{M}$) and weakest, TPR2A (K_d estimated to be $\sim 15 \mu\text{M}$). While representative of TPR affinities to S100A1, we cannot rule out potential cooperatively in binding in the context of the full-length protein. TPR domains are believed to function as ancient protein-protein interaction modules and are

often seen in tandem across multiple TPR containing proteins [26]. It is therefore not uncommon for a single ligand to interface with multiple TPR domains, as is seen with the prototypical and best characterized STIP1 binding partners, Hsp70 and Hsp90 [21, 27, 28]. Interestingly, in the case of Hsp70 and Hsp90 coordination, while each TPR domain is capable of recognizing C-terminal region ‘EEVD’ motifs of Hsp70 and Hsp90, the individual TPR domains take on different roles to regulate binding properties of the full-length molecule [18]. TPR1 and TPR2B show preference for Hsp70 binding, while Hsp90 interacts with TPR2A-TPR2B. In addition, it appears that Hsp70 and Hsp90 are not capable of binding each TPR domain concurrently due to steric hindrance or conformational changes in full-length STIP1. The binding model for S100A1 differs in that each TPR domain is occupied by an S100A1 dimer.

Sedimentation equilibrium AUC experiments confirmed the dimeric and monomeric native states of S100A1 and STIP1, respectively. There has been some disagreement as to the native state of STIP1 in solution as studies have suggested monomeric and dimeric forms [21, 29-31]. The most detailed and recent model of STIP1 suggests a large elongated structure in the free state and attributing previous dimeric models as the result of an atypical elongated structure and large hydrodynamic radius of the full-length protein [29, 32].

To date numerous TPR interactions have been described between S100A1 and additional S100 family members. Coincidentally, a large number of the TPR-motif interactions identified thus far segregate into additional co-chaperones and members of the heat shock protein complex, such as FKBP52, Cyp40, PP5, CHIP [15, 25]. These co-chaperones utilize TPR motifs to associate with Hsp70 and Hsp90 influencing many

cellular processes. Thus, these studies implicate S100A1 and additional S100 proteins in a regulatory network of heat shock protein machinery in protein client refolding.

S100 interactions with chaperone and co-chaperone proteins vary on their dependence on Ca^{2+} for protein binding, suggesting differing modes of interaction, though structural details involving these interactions are scarce. Therefore, we used NMR chemical shift perturbation mapping to determine the binding interfaces between S100A1 and the individual TPR domains (TPR1, TPR2A and TPR2B) of STIP1. Titrations of ^{15}N -labeled S100A1 with each TPR domain lead to a systematic decrease in signal intensity. Chemical shift mapping revealed a significant decrease in intensity for residues localized to α -helices III and IV of EF-hand motifs. Each S100A1 subunit is composed of a 14-residue N and 12-residue C-terminal calcium-binding loop [33]. The latter is situated between helices III and IV. NMR solution structures of the apo- and Ca^{2+} bound forms indicate Ca^{2+} binding triggers a large conformational change resulting in the reorientation of α -helix III by approximately 100° and exposing a large hydrophobic region in α -helix IV[5]. The Ca^{2+} -dependant binding of STIP1 presented by ITC and the significant NMR peak intensity changes in α -helix IV upon TPR binding agrees with the interaction localizing to an interface spanning α -helix IV and provides rationale for the interaction being Ca^{2+} dependant. The mapped hydrophobic interface on S100A1 for TPR binding is consistent with a variety of S100-family member ligands that associate in a Ca^{2+} -dependant manner [4]. Interestingly, the stoichiometry of complex formation determined by ITC and AUC suggest a single TPR domain binds a single S100A1 homodimer. This differs from many S100-target peptide complexes solved to date which display symmetric binding [34-36]. However; these studies involved short peptides

corresponding to ligand binding regions, which may not be representative of full-length proteins, where alternate structural elements may occlude binding to both S100 monomers.

While NMR spectra of each TPR domain did show a global peak intensity change upon S100A1 titration, the binding interface could not be mapped to a particular region. The local effects of binding may be masked due to intermediate exchange rates or the large size of the complex. However, comments on particular regions of the TPR domains that may potentially be involved in binding to S100A1 can be made using the structural information available. Crystal structures of the TPR1 and TPR2A domains reveal a hydrophobic cradle shaped groove extending on one side of each TPR domain [18]. This site serves as the binding interface of the disordered C-terminal 'EEVD' motifs of Hsp70 and Hsp90, respectively, and is the canonical binding site for other TPR-motif ligands. However, due to the concave nature of the mapped S100A1 binding interface and this canonical TPR binding site, it is unlikely the binding site of S100A1. Steric clashing generated by α -helices III of S100A1 subunits and the N and C terminal α -helices of each TPR domain would likely prevent binding to α -helices IV of S100A1 unless significant conformational deviations occur in the bound state of the complex. As well, the similarity of the binding site on S100A1 for each TPR domain suggests that differences in binding and thermodynamic properties in the interactions is likely due to the amino acid compositions and residue contacts formed by each TPR domain on the shared S100A1 binding site. Further, study of the TPR domain-binding site for S100A1 is needed to identify regions involved in complex formation.

The S100 families of binding proteins have been shown to demonstrate unique and characteristic expression profiles in multiple human diseases including different forms of cancer and neurodegenerative disorders such as ALS and AD [6, 7, 12]. Multiple interactions have been documented between S100A1 and other S100-family members with TPR containing proteins, with a large number S100A1 ligands identified to be involved in the Hsp complex machinery, though the molecular details of these interactions has not previously been described. Our studies describe the molecular details of STIP1 interaction with S100A1 and its TPR domains, which may influence STIP1 function upon S100A1 deregulation in multiple disease states.

4.5 References

- 1 Donato, R., Cannon, B. R., Sorci, G., Riuzzi, F., Hsu, K., Weber, D. J. and Geczy, C. L. (2013) Functions of S100 proteins. *Curr Mol Med.* **13**, 24-57
- 2 Lesniak, W., Slomnicki, L. P. and Filipek, A. (2009) S100A6 - new facts and features. *Biochem Biophys Res Commun.* **390**, 1087-1092
- 3 Wolf, S., Haase-Kohn, C. and Pietzsch, J. S100A2 in cancerogenesis: a friend or a foe? *Amino Acids.* **41**, 849-861
- 4 Santamaria-Kisiel, L., Rintala-Dempsey, A. C. and Shaw, G. S. (2006) Calcium-dependent and -independent interactions of the S100 protein family. *Biochem J.* **396**, 201-214
- 5 Wright, N. T., Varney, K. M., Ellis, K. C., Markowitz, J., Gitti, R. K., Zimmer, D. B. and Weber, D. J. (2005) The three-dimensional solution structure of Ca(2+)-bound S100A1 as determined by NMR spectroscopy. *J Mol Biol.* **353**, 410-426
- 6 Zimmer, D. B., Chaplin, J., Baldwin, A. and Rast, M. (2005) S100-mediated signal transduction in the nervous system and neurological diseases. *Cell Mol Biol (Noisy-le-grand).* **51**, 201-214
- 7 Heizmann, C. W., Fritz, G. and Schafer, B. W. (2002) S100 proteins: structure, functions and pathology. *Front Biosci.* **7**, d1356-1368
- 8 Afanador, L., Roltsch, E. A., Holcomb, L., Campbell, K. S., Keeling, D. A., Zhang, Y. and Zimmer, D. B. (2014) The Ca²⁺ sensor S100A1 modulates neuroinflammation, histopathology and Akt activity in the PSAPP Alzheimer's disease mouse model. *Cell Calcium.* **56**, 68-80
- 9 Wright, N. T., Cannon, B. R., Zimmer, D. B. and Weber, D. J. (2009) S100A1: Structure, Function, and Therapeutic Potential. *Curr Chem Biol.* **3**, 138-145
- 10 LaFerla, F. M. (2002) Calcium dyshomeostasis and intracellular signalling in Alzheimer's disease. *Nat Rev Neurosci.* **3**, 862-872
- 11 Van Eldik, L. J. and Wainwright, M. S. (2003) The Janus face of glial-derived S100B: beneficial and detrimental functions in the brain. *Restor Neurol Neurosci.* **21**, 97-108
- 12 Boom, A., Pochet, R., Authelet, M., Pradier, L., Borghgraef, P., Van Leuven, F., Heizmann, C. W. and Brion, J. P. (2004) Astrocytic calcium/zinc binding protein S100A6 over expression in Alzheimer's disease and in PS1/APP transgenic mice models. *Biochim Biophys Acta.* **1742**, 161-168

- 13 Remppis, A., Greten, T., Schafer, B. W., Hunziker, P., Erne, P., Katus, H. A. and Heizmann, C. W. (1996) Altered expression of the Ca(2+)-binding protein S100A1 in human cardiomyopathy. *Biochim Biophys Acta*. **1313**, 253-257
- 14 Roltsch, E., Holcomb, L., Young, K. A., Marks, A. and Zimmer, D. B. (2010) PSAPP mice exhibit regionally selective reductions in gliosis and plaque deposition in response to S100B ablation. *J Neuroinflammation*. **7**, 78
- 15 Okada, M., Hatakeyama, T., Itoh, H., Tokuta, N., Tokumitsu, H. and Kobayashi, R. (2004) S100A1 is a novel molecular chaperone and a member of the Hsp70/Hsp90 multichaperone complex. *J Biol Chem*. **279**, 4221-4233
- 16 Shimamoto, S., Takata, M., Tokuda, M., Oohira, F., Tokumitsu, H. and Kobayashi, R. (2008) Interactions of S100A2 and S100A6 with the tetratricopeptide repeat proteins, Hsp90/Hsp70-organizing protein and kinesin light chain. *J Biol Chem*. **283**, 28246-28258
- 17 Chen, S. and Smith, D. F. (1998) Hop as an adaptor in the heat shock protein 70 (Hsp70) and hsp90 chaperone machinery. *J Biol Chem*. **273**, 35194-35200
- 18 Scheufler, C., Brinker, A., Bourenkov, G., Pegoraro, S., Moroder, L., Bartunik, H., Hartl, F. U. and Moarefi, I. (2000) Structure of TPR domain-peptide complexes: critical elements in the assembly of the Hsp70-Hsp90 multichaperone machine. *Cell*. **101**, 199-210
- 19 Allan, R. K. and Ratajczak, T. (2011) Versatile TPR domains accommodate different modes of target protein recognition and function. *Cell Stress Chaperones*. **16**, 353-367
- 20 Onuoha, S. C., Coulstock, E. T., Grossmann, J. G. and Jackson, S. E. (2008) Structural studies on the co-chaperone Hop and its complexes with Hsp90. *J Mol Biol*. **379**, 732-744
- 21 Rohl, A., Wengler, D., Madl, T., Lagleder, S., Toppel, F., Herrmann, M., Hendrix, J., Richter, K., Hack, G., Schmid, A. B., Kessler, H., Lamb, D. C. and Buchner, J. (2015) Hsp90 regulates the dynamics of its cochaperone Sti1 and the transfer of Hsp70 between modules. *Nat Commun*. **6**, 6655
- 22 Keller, R. (2005) *Optimizing the Process of Nuclear Magnetic Spectrum Analysis and Computer Aided Resonance Assignment*. ed.)^{eds.}), Swiss Federal Institute of Technology: Zurich
- 23 Delaglio, F., Grzesiek, S., Vuister, G. W., Zhu, G., Pfeifer, J. and Bax, A. (1995) NMRPipe: a multidimensional spectral processing system based on UNIX pipes. *J Biomol NMR*. **6**, 277-293
- 24 Johnson, B. A. and Blevins, R. A. (1994) NMR View: A computer program for the visualization and analysis of NMR data. *J Biomol NMR*. **4**, 603-614

- 25 Shimamoto, S., Kubota, Y., Tokumitsu, H. and Kobayashi, R. (2010) S100 proteins regulate the interaction of Hsp90 with Cyclophilin 40 and FKBP52 through their tetratricopeptide repeats. *FEBS Lett.* **584**, 1119-1125
- 26 D'Andrea, L. D. and Regan, L. (2003) TPR proteins: the versatile helix. *Trends Biochem Sci.* **28**, 655-662
- 27 Rohl, A., Toppel, F., Bender, E., Schmid, A. B., Richter, K., Madl, T. and Buchner, J. (2014) Hop/Sti1 phosphorylation inhibits its co-chaperone function. *EMBO Rep.* **16**, 240-249
- 28 Schmid, A. B., Lagleder, S., Grawert, M. A., Rohl, A., Hagn, F., Wandinger, S. K., Cox, M. B., Demmer, O., Richter, K., Groll, M., Kessler, H. and Buchner, J. (2012) The architecture of functional modules in the Hsp90 co-chaperone Sti1/Hop. *EMBO J.* **31**, 1506-1517
- 29 Flom, G., Behal, R. H., Rosen, L., Cole, D. G. and Johnson, J. L. (2007) Definition of the minimal fragments of Sti1 required for dimerization, interaction with Hsp70 and Hsp90 and in vivo functions. *Biochem J.* **404**, 159-167
- 30 Romano, S. A., Cordeiro, Y., Lima, L. M., Lopes, M. H., Silva, J. L., Foguel, D. and Linden, R. (2009) Reciprocal remodeling upon binding of the prion protein to its signaling partner hop/STI1. *FASEB J.* **23**, 4308-4316
- 31 Prodromou, C., Siligardi, G., O'Brien, R., Woolfson, D. N., Regan, L., Panaretou, B., Ladbury, J. E., Piper, P. W. and Pearl, L. H. (1999) Regulation of Hsp90 ATPase activity by tetratricopeptide repeat (TPR)-domain co-chaperones. *EMBO J.* **18**, 754-762
- 32 Southworth, D. R. and Agard, D. A. (2011) Client-loading conformation of the Hsp90 molecular chaperone revealed in the cryo-EM structure of the human Hsp90:Hop complex. *Mol Cell.* **42**, 771-781
- 33 Nowakowski, M., Ruszczyńska-Bartnik, K., Budzinska, M., Jaremko, L., Jaremko, M., Zdanowski, K., Bierzynski, A. and Ejchart, A. (2013) Impact of calcium binding and thionylation of S100A1 protein on its nuclear magnetic resonance-derived structure and backbone dynamics. *Biochemistry.* **52**, 1149-1159
- 34 Penumutchu, S. R., Chou, R. H. and Yu, C. (2014) Structural insights into calcium-bound S100P and the V domain of the RAGE complex. *PLoS One.* **9**, e103947
- 35 Rustandi, R. R., Baldisseri, D. M. and Weber, D. J. (2000) Structure of the negative regulatory domain of p53 bound to S100B(beta-beta). *Nat Struct Biol.* **7**, 570-574
- 36 Wright, N. T., Prosser, B. L., Varney, K. M., Zimmer, D. B., Schneider, M. F. and Weber, D. J. (2008) S100A1 and calmodulin compete for the same binding site on ryanodine receptor. *J Biol Chem.* **283**, 26676-26683

5 Summary

Stress-inducible phosphoprotein 1 (STIP1) has been extensively studied as a cochaperone of the Hsp70/Hsp90 protein client folding machinery [1-4]. STIP1 couples transfer of immature or abnormally folded proteins from Hsp70 to Hsp90 during the client folding cycle [5]. It is now accepted that extracellular STIP1 can function as a potent neuroprotective and neuroproliferative signaling molecule through complex formation with the cellular prion protein (PrP^C) [6-10]. The resultant signaling cascade rescues neurons from various cellular stressors including staurosporine-induced programmed cell death and ischemia [6, 11]. This neuroprotection has recently been extended to A β oligomer (A β O) toxicity, suggesting STIP1 signaling as an endogenous protective mechanism in Alzheimer's disease (AD) [12]. In addition, recent studies have identified particular members of the S100- family of Ca²⁺ sensors as STIP1 ligands [13]. S100 proteins altered expression has been implicated in several diseases including cardiomyopathy, cancer and AD [14].

Detailed structural studies have been conducted to dissect STIP1 co-chaperone interactions with Hsp machinery [1-3, 15]. In contrast, few details are available concerning STIP1 interaction with PrP^C and the S100-family of proteins [13, 16]. The work presented in this thesis addressed the molecular details of STIP1 interactions with PrP^C and S100A1 proteins in order to provide a better understanding of alternate STIP1 complexes beyond Hsp interactions and their role in AD.

5.1 Structural characterization of STIP1 domains

The majority of NMR studies to date involving STIP1 have focused on the yeast homologue [2, 3, 15]. Where as complementary x-ray crystallographic data and other biophysical techniques suggest a conserved structure, the sequence identity between mouse and yeast STIP1 is approximately 40% [1]. Thus, we characterized mouse STIP1 by NMR to facilitate future ligand studies. We confirmed the less than expected number of observable STIP1 NMR amide resonances was not due to dimer formation of STIP1 or the TPR2A domain, confirming a monomeric model of STIP1 in solution, which has been challenged in previous studies [17, 18]. Rather, the lack of amide resonance signals is likely reflective of STIP1's large molecular weight (62.6 kDa) and predicted elongated tertiary structure [15, 16]. Therefore, we assigned the amide proton resonances of the structured domains of STIP1 (TPR1, TPR2A, TPR2B and DP2). Only a partial assignment of DP1 could be obtained due to low signal strength (chapter 2).

The amide backbone resonance assignments lay the foundation for determining the molecular details of PrP^C (chapter 3) and S100A1 (chapter 4) complexes. These studies can be extended to other STIP1 ligands, such as inhibitors of Hsp90 complex formation with STIP1. Hsp90 client proteins include numerous oncogenic kinases, receptors and transcription factors including Her2/neu, Bcr-Abl, vascular endothelial growth factor (VEGF) and Raf-1 [19]. Inhibition of Hsp90 results in rapid proteasomal degradation of these targets. Traditional Hsp90 inhibitors target the ATPase activity of Hsp90, which have the undesired effect of Hsp70 induction resulting in resistance to apoptosis [20]. An alternate approach has been proposed by Regan and co-workers, which targeted STIP1-Hsp90 complexes, thus indirectly interrupting stabilization of oncogenic targets [21].

Importantly, these small molecules demonstrated anti-tumorigenic effects without inducing Hsp70 overexpression suggesting they may escape the positive feedback mechanism of Hsp70 induction inherent to traditional Hsp90 ATPase inhibitors [22].

5.2 Mapping of A β O interface on PrP

PrP^C is a high affinity receptor for A β O whose complex induces synaptic dysfunction, inhibition of long term potentiation (LTP), loss of dendritic spines and, ultimately, neuronal cell death [12, 23, 24]. A β O binding to PrP^C is thought to be mediated by two distinct regions in the disordered N-terminal of PrP^C. These include a highly basic cluster 'KKRPK' spanning residues 23-27 and residues 95-110 of PrP^C [23, 25]. Our NMR studies of ¹⁵N-labelled PrP (90-231) titrated with preformed A β O revealed a short, highly localized region involved in A β O binding spanning residues 90-110 of PrP. These results are consistent with the literature that implicates residues 95-110 in A β O binding [23, 25]. In addition, we noted small but notable chemical shift changes of C-terminal residues of the globular domain of PrP. These may arise due to conformational changes in PrP upon A β O or from transient contacts between PrP or A β O species. No chemical shift changes or changes in peak intensity were noted for the N-terminal residues of PrP (23-95). High sequence redundancy and peak overlap prevented the assignment of residues 23-95. Thus, we cannot rule out the possibility of minor, but localized chemical shift changes in residues 23-95 upon A β O titration. However, antibodies directed against residues 90-110 of PrP were sufficient to block A β O binding to PrP, inhibit A β O neurotoxicity and improved cognitive deficits in AD transgenic mouse models [24, 26, 27]. Thus, targeting residues of PrP 90-110 appears sufficient to disrupt A β O induced deficits and may be a viable therapeutic approach in AD.

5.3 Domains of STIP1 participating in PrP binding

The interaction between STIP1 with PrP^C has been well documented to elicit neuroprotective signaling in response to cellular stressors [6, 7, 11, 12]. Complex formation has been suggested to be mediated between the TPR2A domain of STIP1 and the disordered N-terminal of PrP^C [6]. In the present study, we confirmed a high affinity (1×10^{-7} M K_d) complex between STIP1 and PrP^C, while demonstrating that additional domains of STIP1 are involved in binding. The structurally related TPR1 and TPR2A domains, but not TPR2B, bound PrP. TPR1 and TPR2A binding were mutually exclusive; suggesting binding of either domain to PrP^C occludes the binding site of the other. In addition, the DP1 domain was found to interact with the N-terminal (residues 23-95) of PrP^C. This is the first reported instance of a binding partner for the DP1 domain of STIP1.

The involvement of multiple domains of STIP1 in ligand binding is reminiscent of STIP1 cochaperone interactions. Hsp70 binding to STIP1 is shared between the TPR1 and TPR2B domains and has functional consequences in for the proposed mechanism of Hsp client transfer [3]. Upon Hsp90 recruitment, the high affinity Hsp70 site shifts from TPR1 to TPR2B to presumably to spatially orient the client protein for efficient transfer to Hsp90 at the TPR2A site [3]. Due to the modular structure of STIP1 and structural homology of individual TPR domains, multi-domain STIP1 ligand interactions may be a common feature of STIP1 complexes [1].

5.4 Domains of STIP1 that inhibit PrP-A β O toxicity

We have previously demonstrated ectopic STIP1 treatment is capable of efficiently inhibit A β oligomer toxicity in a PrP^C dependent manner [12]. The identification of novel domains participating in PrP complex formation led us to investigate the regions of STIP1 responsible for its neuroprotection from A β O insult. Surface plasmon resonance (SPR) was utilized to assess A β O binding to PrP (23-231) and the influence of STIP1 and its individual domains *in vitro*. Our findings indicated that TPR1 and TPR2A domain of STIP1, but not DP1, could inhibit A β O binding in a concentration dependant manner.

While DP1 may not directly participate in STIP1 inhibition of A β O binding, it likely contributes to the greater binding affinity of STIP1 for PrP compared to the individual domains alone. Considering TPR1 and TPR2A bind residues 90-231 of PrP, they may physically occlude or induce conformational changes in PrP that inhibit A β O binding. STIP1 binding to PrP has been suggested to induce significant conformational changes in PrP [16]. Importantly, inhibition of A β O binding to PrP by TPR1 and TPR2A translated to primary mouse hippocampal neurons and rescued them from A β O induced cell death.

STIP1-PrP^C induces Ca²⁺ influx resulting in downstream neuroprotective signaling events through the alpha 7 nicotinic acetylcholine receptor (α 7nAChR) [10]. Therefore, we cannot rule out that TPR1 and TPR2A inhibition of A β O neuronal cell death is not due to activation of a neuroprotective signaling cascade. Indeed, genetic deletion of α 7nAChR resulted in enhanced memory deficits and A β O accumulation in young 5-month old APP transgenic mice [28]. Alternatively, STIP1 induced neuroprotective

signaling events and direct inhibition of A β O binding to PrP^C may act in concert to protect primary hippocampal neurons against A β O neurotoxicity.

STIP1 upregulation has been noted in APP^{swe}/PS1^{dE9} mouse model of AD and in AD-afflicted brain homogenates [12]. Additionally, decreased levels of STIP1 in mammalian neurons or knockdown of STIP1 in *C. elegans* increases the toxicity of amyloid peptides [29][12]. Thus, extracellular STIP1 may serve as an endogenous protective mechanism against neurotoxic A β O in early stages of AD.

5.5 Regions of TPR1 and TPR2A involved in PrP binding

While previous studies have suggested residues 230-245 of STIP1 and 113-128 of PrP are involved in complex formation, molecular details at the residue level were absent [6, 16]. The high structural similarity of TPR1 and TPR2A and their competitive binding to PrP led us to investigate if complementary interfaces on each domain are involved. Similar interfaces have been described for TPR1 and TPR2A binding to the C-terminal of Hsp70 and Hsp90, respectively, as they both utilize conserved carboxylate clamp residues to coordinate the acidic Hsp C-terminal tail [1]. Interestingly, NMR studies revealed TPR1 and TPR2A binding interfaces for PrP are significantly different. TPR1 residues spanning the C-terminal of α -helix 6 and the interconnecting loop region connecting it to α -helix 7 showed significant chemical shift changes. In contrast, the TPR2A binding interface extended diagonally across the concave TPR2A surface which overlaps with the Hsp90 binding site [1].

Hsp90 chaperone function is critical for assuring proper folding of client proteins, solubilizing protein aggregates or facilitating their targeting for proteasomal degradation [19]. Hsp70 and Hsp90 have been shown to block A β ₁₋₄₂ aggregation *in vitro* [30]. Hsp90 and other Hsps also promote A β clearance by the stimulation of phagocytosis in microglia [32]. Thus, modulation of Hsp proteins has gained traction as a possible therapeutic pathway in AD [33].

Given both Hsp90 and STIP1 are secreted through an exosomal non-canonical pathway and the TPR2A domain is involved in both PrP and Hsp90 binding, we investigated the influence of PrP on Hsp90 binding to STIP1 [34, 35]. Interestingly, PrP-STIP1 complex formation promoted Hsp90 binding, suggesting they form a ternary complex at the cellular membrane. STIP1 binding may induce structural conformational changes in PrP, which may in turn recruit Hsp90 [16]. Hsp90 has been localized to the cellular membrane, thus PrP-STIP1-Hsp90 complexes may form on the cellular surface and influence STIP1 signaling events [36].

5.6 Molecular details of STIP1 interaction with S100A1

S100A1 is a Ca²⁺-binding protein sensor that modulates protein-protein interactions in the cell [14]. S100A1 along with S100B and S100A6 are overexpressed in AD and are considered as disease biomarkers [37]. S100A1 has been found to interact with various co-chaperones through TPR domain interactions [13, 38]. TPR domains are common structural elements shared by many Hsp70 and Hsp90 co-chaperones as they coordinate binding to the highly conserved C-terminal Hsp ‘EEVD’ motifs [39]. Thus, S100A1 and

other S100 family members may function as regulators of Hsp client refolding by influencing which co-chaperones are involved.

We have shown that S100A1 dimer bound each of the single TPR domains of STIP1 with various affinities in a Ca^{2+} -dependent manner. Interestingly, this differs from many S100A1 binding partners, which bind symmetrically to each S100 monomer, although asymmetric interactions have been described for other S100 family members [40, 41]. However; it is important to note many studies displaying symmetrical binding utilize short peptide sequences. In the full-length proteins, additional structural elements of the S100 ligand may occlude the binding pocket of the S100 proteins, preventing symmetric binding to each S100 monomer.

Our NMR studies indicated each TPR domain (TPR1, TPR2A and TPR2B) bound identical hydrophobic region composed of α -helices III of each S100 monomer. This observation agrees with these interactions being Ca^{2+} -dependant. In the absence of Ca^{2+} , this region is inaccessible as it blocked by helix IV of each S100A1 subunit [42]. Upon Ca^{2+} binding, helices IV of each S100 monomer undergo a large conformational change by rotating approximately 100° and exposing the hydrophobic interface.

Unfortunately, the S100A1 binding interface on each TPR could not be determined due to line broadening likely due to the large molecular weight or intermediate exchange rates of the complex. However, due to the concave nature of the S100A1 binding site and each TPR domain, binding likely involves the N or C-terminal helices of each TPR domain to minimize steric clashing [1, 42]. Further study is required to determine TPR site for S100A1 binding.

S100A1 and STIP1 are both found in the cytoplasm as well as the extracellular space [34, 43]. S100A1 may modulate STIP1 ligand interactions influencing critical cellular processes such as protein folding or cell signaling events through Hsp proteins or PrP^C, respectively. Thus, S100A1 over-expression in AD may alter the processing of A β and tau aggregates by STIP1 or regulate formation of neuroprotective complexes through PrP^C.

5.7 Future directions

Our results suggest a ternary complex may form between STIP1, PrP and Hsp90; however, the details of the regions of PrP involved and the stoichiometry of the interaction are unknown. Different length PrP constructs can be used to determine if Hsp90 recognizes the globular C-terminal or N-terminal of PrP. The solid support assay developed here can be used with PrP (90-231) to rule out Hsp90 binding to the N-terminal of PrP. As well, sedimentation equilibrium or gel filtration experiments of STIP1-PrP-Hsp90 can be performed to determine the stoichiometry of the complex, as larger species will change the elution profile or the rate the protein sediments.

Our results suggest the formation of a STIP1-Hsp90-PrP ternary complex *in vitro*, however; it is unclear if the complex occurs on the cell surface or its effect on STIP1 signaling. Endogenously expressed GPI-anchored PrP^C may behave differently than when immobilized on to the polystyrene surface used in our solid support assays. Immunohistochemistry and confocal microscopy studies may reveal if the proteins colocalize on the cellular surface or if they are internalized together in intracellular

compartments. Co-immunoprecipitation of isolated membrane fractions may also reveal if ternary complexes occur in cell culture.

The significant global loss in signal intensity prevented the determination of the S100A1 binding interface on the individual TPR domains of STIP1. This is potentially due to the increased size of the complex in relation to the individual proteins alone. A common strategy for signal enhancement involves deuteration of the protein samples. Due to their large size, larger proteins experience slower tumbling and thus enhanced relaxation and decay resulting in loss of signal. Deuteration removes most ^1H protons improving relaxation rates thus resulting in a greater signal strength and resolution.

Alternatively, cross-saturation experiments can be used to identify the TPR binding interface and have been used for protein-protein complexes >50 kDa. This technique relies on uniformly labeling the target protein for which the interface is to be determined with ^2H and ^{15}N (TPR domain). The aliphatic proton resonances of the unlabeled binding partner (S100A1) is non-selectively irradiated and transferred to the target through cross relaxation by protons located at the interface. Thus, only residues at the interface are affected and can be identified.

5.8 Conclusions

The work presented provides novel molecular details regarding STIP1 complexes implicated in AD. STIP1's modular structure and inter-domain homology, implicate extensive multi-domain interactions in PrP and S100A1 binding. Additional domain interactions were found to influence STIP1 binding to PrP and influence PrP^C dependant

A β O neurotoxicity. As well, structural studies of STIP1-S100A1 provided molecular insights into their complex formation.

5.9 References

- 1 Scheufler, C., Brinker, A., Bourenkov, G., Pegoraro, S., Moroder, L., Bartunik, H., Hartl, F. U. and Moarefi, I. (2000) Structure of TPR domain-peptide complexes: critical elements in the assembly of the Hsp70-Hsp90 multichaperone machine. *Cell*. **101**, 199-210
- 2 Schmid, A. B., Lagleder, S., Grawert, M. A., Rohl, A., Hagn, F., Wandinger, S. K., Cox, M. B., Demmer, O., Richter, K., Groll, M., Kessler, H. and Buchner, J. (2012) The architecture of functional modules in the Hsp90 co-chaperone Sti1/Hop. *EMBO J*. **31**, 1506-1517
- 3 Rohl, A., Wengler, D., Madl, T., Lagleder, S., Toppel, F., Herrmann, M., Hendrix, J., Richter, K., Hack, G., Schmid, A. B., Kessler, H., Lamb, D. C. and Buchner, J. (2015) Hsp90 regulates the dynamics of its cochaperone Sti1 and the transfer of Hsp70 between modules. *Nat Commun*. **6**, 6655
- 4 Southworth, D. R. and Agard, D. A. (2011) Client-loading conformation of the Hsp90 molecular chaperone revealed in the cryo-EM structure of the human Hsp90:Hop complex. *Mol Cell*. **42**, 771-781
- 5 Chen, S. and Smith, D. F. (1998) Hop as an adaptor in the heat shock protein 70 (Hsp70) and hsp90 chaperone machinery. *J Biol Chem*. **273**, 35194-35200
- 6 Zanata, S. M., Lopes, M. H., Mercadante, A. F., Hajj, G. N., Chiarini, L. B., Nomizo, R., Freitas, A. R., Cabral, A. L., Lee, K. S., Juliano, M. A., de Oliveira, E., Jachieri, S. G., Burlingame, A., Huang, L., Linden, R., Brentani, R. R. and Martins, V. R. (2002) Stress-inducible protein 1 is a cell surface ligand for cellular prion that triggers neuroprotection. *EMBO J*. **21**, 3307-3316
- 7 Roffe, M., Beraldo, F. H., Bester, R., Nunziante, M., Bach, C., Mancini, G., Gilch, S., Vorberg, I., Castilho, B. A., Martins, V. R. and Hajj, G. N. (2010) Prion protein interaction with stress-inducible protein 1 enhances neuronal protein synthesis via mTOR. *Proc Natl Acad Sci U S A*. **107**, 13147-13152
- 8 Lopes, M. H., Hajj, G. N., Muras, A. G., Mancini, G. L., Castro, R. M., Ribeiro, K. C., Brentani, R. R., Linden, R. and Martins, V. R. (2005) Interaction of cellular prion and stress-inducible protein 1 promotes neuritogenesis and neuroprotection by distinct signaling pathways. *J Neurosci*. **25**, 11330-11339
- 9 Caetano, F. A., Lopes, M. H., Hajj, G. N., Machado, C. F., Pinto Arantes, C., Magalhaes, A. C., Vieira Mde, P., Americo, T. A., Massensini, A. R., Priola, S. A., Vorberg, I., Gomez, M. V., Linden, R., Prado, V. F., Martins, V. R. and Prado, M. A. (2008) Endocytosis of prion protein is required for ERK1/2 signaling induced by stress-inducible protein 1. *J Neurosci*. **28**, 6691-6702

- 10 Beraldo, F. H., Arantes, C. P., Santos, T. G., Queiroz, N. G., Young, K., Rylett, R. J., Markus, R. P., Prado, M. A. and Martins, V. R. (2010) Role of alpha7 nicotinic acetylcholine receptor in calcium signaling induced by prion protein interaction with stress-inducible protein 1. *J Biol Chem.* **285**, 36542-36550
- 11 Beraldo, F. H., Soares, I. N., Goncalves, D. F., Fan, J., Thomas, A. A., Santos, T. G., Mohammad, A. H., Roffe, M., Calder, M. D., Nikolova, S., Hajj, G. N., Guimaraes, A. L., Massensini, A. R., Welch, I., Betts, D. H., Gros, R., Drangova, M., Watson, A. J., Bartha, R., Prado, V. F., Martins, V. R. and Prado, M. A. (2013) Stress-inducible phosphoprotein 1 has unique cochaperone activity during development and regulates cellular response to ischemia via the prion protein. *FASEB J.* **27**, 3594-3607
- 12 Ostapchenko, V. G., Beraldo, F. H., Mohammad, A. H., Xie, Y. F., Hirata, P. H., Magalhaes, A. C., Lamour, G., Li, H., Maciejewski, A., Belrose, J. C., Teixeira, B. L., Fahnestock, M., Ferreira, S. T., Cashman, N. R., Hajj, G. N., Jackson, M. F., Choy, W. Y., MacDonald, J. F., Martins, V. R., Prado, V. F. and Prado, M. A. (2013) The prion protein ligand, stress-inducible phosphoprotein 1, regulates amyloid-beta oligomer toxicity. *J Neurosci.* **33**, 16552-16564
- 13 Shimamoto, S., Takata, M., Tokuda, M., Oohira, F., Tokumitsu, H. and Kobayashi, R. (2008) Interactions of S100A2 and S100A6 with the tetratricopeptide repeat proteins, Hsp90/Hsp70-organizing protein and kinesin light chain. *J Biol Chem.* **283**, 28246-28258
- 14 Wright, N. T., Cannon, B. R., Zimmer, D. B. and Weber, D. J. (2009) S100A1: Structure, Function, and Therapeutic Potential. *Curr Chem Biol.* **3**, 138-145
- 15 Rohl, A., Toppel, F., Bender, E., Schmid, A. B., Richter, K., Madl, T. and Buchner, J. (2014) Hop/Sti1 phosphorylation inhibits its co-chaperone function. *EMBO Rep.* **16**, 240-249
- 16 Romano, S. A., Cordeiro, Y., Lima, L. M., Lopes, M. H., Silva, J. L., Foguel, D. and Linden, R. (2009) Reciprocal remodeling upon binding of the prion protein to its signaling partner hop/STI1. *FASEB J.* **23**, 4308-4316
- 17 Flom, G., Behal, R. H., Rosen, L., Cole, D. G. and Johnson, J. L. (2007) Definition of the minimal fragments of Sti1 required for dimerization, interaction with Hsp70 and Hsp90 and in vivo functions. *Biochem J.* **404**, 159-167
- 18 Prodromou, C., Siligardi, G., O'Brien, R., Woolfson, D. N., Regan, L., Panaretou, B., Ladbury, J. E., Piper, P. W. and Pearl, L. H. (1999) Regulation of Hsp90 ATPase activity by tetratricopeptide repeat (TPR)-domain co-chaperones. *EMBO J.* **18**, 754-762
- 19 Whitesell, L. and Lindquist, S. L. (2005) HSP90 and the chaperoning of cancer. *Nat Rev Cancer.* **5**, 761-772

- 20 Garrido, C., Schmitt, E., Cande, C., Vahsen, N., Parcellier, A. and Kroemer, G. (2003) HSP27 and HSP70: potentially oncogenic apoptosis inhibitors. *Cell Cycle*. **2**, 579-584
- 21 Yi, F. and Regan, L. (2008) A novel class of small molecule inhibitors of Hsp90. *ACS Chem Biol*. **3**, 645-654
- 22 Pimienta, G., Herbert, K. M. and Regan, L. (2011) A compound that inhibits the HOP-Hsp90 complex formation and has unique killing effects in breast cancer cell lines. *Mol Pharm*. **8**, 2252-2261
- 23 Lauren, J., Gimbel, D. A., Nygaard, H. B., Gilbert, J. W. and Strittmatter, S. M. (2009) Cellular prion protein mediates impairment of synaptic plasticity by amyloid-beta oligomers. *Nature*. **457**, 1128-1132
- 24 Freir, D. B., Nicoll, A. J., Klyubin, I., Panico, S., Mc Donald, J. M., Risse, E., Asante, E. A., Farrow, M. A., Sessions, R. B., Saibil, H. R., Clarke, A. R., Rowan, M. J., Walsh, D. M. and Collinge, J. (2011) Interaction between prion protein and toxic amyloid beta assemblies can be therapeutically targeted at multiple sites. *Nat Commun*. **2**, 336
- 25 Chen, S., Yadav, S. P. and Surewicz, W. K. (2010) Interaction between human prion protein and amyloid-beta (Abeta) oligomers: role OF N-terminal residues. *J Biol Chem*. **285**, 26377-26383
- 26 Kudo, W., Lee, H. P., Zou, W. Q., Wang, X., Perry, G., Zhu, X., Smith, M. A., Petersen, R. B. and Lee, H. G. (2012) Cellular prion protein is essential for oligomeric amyloid-beta-induced neuronal cell death. *Hum Mol Genet*. **21**, 1138-1144
- 27 Chung, E., Ji, Y., Sun, Y., Kascsak, R. J., Kascsak, R. B., Mehta, P. D., Strittmatter, S. M. and Wisniewski, T. (2010) Anti-PrPC monoclonal antibody infusion as a novel treatment for cognitive deficits in an Alzheimer's disease model mouse. *BMC Neurosci*. **11**, 130
- 28 Hernandez, C. M., Kaye, R., Zheng, H., Sweatt, J. D. and Dineley, K. T. (2010) Loss of alpha7 nicotinic receptors enhances beta-amyloid oligomer accumulation, exacerbating early-stage cognitive decline and septohippocampal pathology in a mouse model of Alzheimer's disease. *J Neurosci*. **30**, 2442-2453
- 29 Brehme, M., Voisine, C., Rolland, T., Wachi, S., Soper, J. H., Zhu, Y., Orton, K., Villeda, A., Garza, D., Vidal, M., Ge, H. and Morimoto, R. I. (2014) A chaperome subnetwork safeguards proteostasis in aging and neurodegenerative disease. *Cell Rep*. **9**, 1135-1150
- 30 Evans, C. G., Wisen, S. and Gestwicki, J. E. (2006) Heat shock proteins 70 and 90 inhibit early stages of amyloid beta-(1-42) aggregation in vitro. *J Biol Chem*. **281**, 33182-33191

- 31 Dou, F., Netzer, W. J., Tanemura, K., Li, F., Hartl, F. U., Takashima, A., Gouras, G. K., Greengard, P. and Xu, H. (2003) Chaperones increase association of tau protein with microtubules. *Proc Natl Acad Sci U S A.* **100**, 721-726
- 32 Kakimura, J., Kitamura, Y., Takata, K., Umeki, M., Suzuki, S., Shibagaki, K., Taniguchi, T., Nomura, Y., Gebicke-Haerter, P. J., Smith, M. A., Perry, G. and Shimohama, S. (2002) Microglial activation and amyloid-beta clearance induced by exogenous heat-shock proteins. *FASEB J.* **16**, 601-603
- 33 Luo, W., Rodina, A. and Chiosis, G. (2008) Heat shock protein 90: translation from cancer to Alzheimer's disease treatment? *BMC Neurosci.* **9 Suppl 2**, S7
- 34 Hajj, G. N., Arantes, C. P., Dias, M. V., Roffe, M., Costa-Silva, B., Lopes, M. H., Porto-Carreiro, I., Rabachini, T., Lima, F. R., Beraldo, F. H., Prado, M. A., Linden, R. and Martins, V. R. (2013) The unconventional secretion of stress-inducible protein 1 by a heterogeneous population of extracellular vesicles. *Cell Mol Life Sci.* **70**, 3211-3227
- 35 McCready, J., Sims, J. D., Chan, D. and Jay, D. G. (2010) Secretion of extracellular hsp90alpha via exosomes increases cancer cell motility: a role for plasminogen activation. *BMC Cancer.* **10**, 294
- 36 Sidera, K., Samiotaki, M., Yfanti, E., Panayotou, G. and Patsavoudi, E. (2004) Involvement of cell surface HSP90 in cell migration reveals a novel role in the developing nervous system. *J Biol Chem.* **279**, 45379-45388
- 37 Zimmer, D. B., Chaplin, J., Baldwin, A. and Rast, M. (2005) S100-mediated signal transduction in the nervous system and neurological diseases. *Cell Mol Biol (Noisy-le-grand).* **51**, 201-214
- 38 Shimamoto, S., Kubota, Y., Tokumitsu, H. and Kobayashi, R. (2010) S100 proteins regulate the interaction of Hsp90 with Cyclophilin 40 and FKBP52 through their tetratricopeptide repeats. *FEBS Lett.* **584**, 1119-1125
- 39 Allan, R. K. and Ratajczak, T. (2011) Versatile TPR domains accommodate different modes of target protein recognition and function. *Cell Stress Chaperones.* **16**, 353-367
- 40 Rezvanpour, A., Santamaria-Kisiel, L. and Shaw, G. S. (2011) The S100A10-annexin A2 complex provides a novel asymmetric platform for membrane repair. *J Biol Chem.* **286**, 40174-40183
- 41 Wright, N. T., Prosser, B. L., Varney, K. M., Zimmer, D. B., Schneider, M. F. and Weber, D. J. (2008) S100A1 and calmodulin compete for the same binding site on ryanodine receptor. *J Biol Chem.* **283**, 26676-26683
- 42 Wright, N. T., Varney, K. M., Ellis, K. C., Markowitz, J., Gitti, R. K., Zimmer, D. B. and Weber, D. J. (2005) The three-dimensional solution structure of Ca(2+)-bound S100A1 as determined by NMR spectroscopy. *J Mol Biol.* **353**, 410-426

43 Most, P., Boerries, M., Eicher, C., Schweda, C., Ehlermann, P., Pleger, S. T., Loeffler, E., Koch, W. J., Katus, H. A., Schoenenberger, C. A. and Remppis, A. (2003) Extracellular S100A1 protein inhibits apoptosis in ventricular cardiomyocytes via activation of the extracellular signal-regulated protein kinase 1/2 (ERK1/2). *J Biol Chem.* **278**, 48404-48412

Curriculum Vitae

Name: Andrzej Maciejewski

Post-secondary Education and Degrees: University of Western Ontario
London, Ontario, Canada
2006-2010 B.M.Sc Honors Biochemistry

The University of Western Ontario
London, Ontario, Canada
2010-2016 Ph.D. Candidate Biochemistry

Honours and Awards: Province of Ontario Graduate Scholarship
2010-2011, 2011-2012 (declined), 2013-2014, 2014-2015

CIHR Fredrick Banting and Charles Best Canada Graduate Scholarship
2011-2012

Western Scholarship of Excellence
2006-2007

Related Work Experience Teaching Assistant
The University of Western Ontario
2014-2015

Publications:

Maciejewski, A., Ostapchenko, V. G., Beraldo, F. H., Prado, V. F., Prado, M. A. and Choy, W. Y. (2016) Domains of STIP1 responsible for regulating the PrPC-dependent amyloid-beta oligomer toxicity. *Biochem J*, in press

Ostapchenko, V. G., Beraldo, F. H., Mohammad, A. H., Xie, Y. F., Hirata, P. H., Magalhaes, A. C., Lamour, G., Li, H., Maciejewski, A., Belrose, J. C., Teixeira, B. L., Fahnestock, M., Ferreira, S. T., Cashman, N. R., Hajj, G. N., Jackson, M. F., Choy, W. Y., MacDonald, J. F., Martins, V. R., Prado, V. F. and Prado, M. A. (2013) The prion protein ligand, stress-inducible phosphoprotein 1, regulates amyloid-beta oligomer toxicity. *J Neurosci.* **33**, 16552-16564

Maciejewski, A., Prado, M. A. and Choy, W. Y. (2012) (1)H, (1)(5)N and (1)(3)C backbone resonance assignments of the TPR1 and TPR2A domains of mouse STI1. *Biomol NMR Assign.* **7**, 305-310